

# **The Synthesis of Novel Comb Shaped and Chiral Amphiphilic Polymers**

**Nura Ageel**

Submitted to the  
Institute of Graduate Studies and Research  
in partial fulfillment of the requirement for the degree of

Master of Science  
in  
Chemistry

Eastren Mediterranean University  
February 2017  
Gazimağusa, North Cyprus

Approval of the Institute of Graduate Studies and Research

---

Prof. Dr. Mustafa Tümer  
Director

I certify that this thesis satisfies the requirement as a thesis for the degree of Master of Science in Chemistry

---

Assoc. Prof Dr. Izzet Sakalli  
Chair, Department of Chemistry

We certify that we have read this thesis and that in our opinion, it is fully adequate in scope and quality as a thesis for degree of Master of Science in Chemistry.

---

Prof. Dr. Huriye İcil  
Supervisor

---

Examining Committee

1. Prof. Dr. Huriye İcil

---

2. Asst. Prof. Dr. Süleyman Aşır

---

3. Dr. Duygu Uzun

---

## ABSTRACT

In recent years, intensive research efforts have been committed to studying Amphiphilic polymers, particularly in the pharmaceutical applications. These polymers have ability to form a different macromolecular architecture in the aqueous solution such as polymeric micelles.

Novel comb-shaped, chiral and fluorescent amphiphilic polymers are important for pharmaceutical applications including hydrophobic drug solubilization.

In this thesis, four chiral, comb-shaped and fluorescent novel amphiphilic polymers were synthesized from chitosan and perylene diimide. The compounds were analyzed using FTIR, UV-vis and Emission spectroscopy.

**Keywords:** Amphiphilic polymer, comb shaped, fluorescent chitosan

## ÖZ

Son yıllarda, özellikle farmasötik uygulamalarda, amfifilik polimerler ile ilgili yoğun arařtırmalar yapılmaktadır. Bu polimerler, polimerik miseller gibi sulu çözeltilerde farklı bir makromoleküler yapı oluşturabilme özelliğine sahiptirler.

Yeni tarak şeklinde ve kiral amfifilik polimerler, hidrofobik ilaç çözünürlüğü bakımından farmasötik uygulamalarda önemlidirler.

Bu tez çalışmasında, kiral ve tarak yapısı özellikleriyle dört yeni amfifilik polimerler sentezlenmiştir. Bileşikler, FTIR, UV-vis ve Emisyon spektroskopisi kullanılarak analiz edilmiştir.

**Anahtar Kelimeler:** Amfifilik polimer, tarak yapısında, floresan kitosan

# *To My Parents*

## ACKNOWLEDGEMENT

I gratefully express all praise to the almighty **Allah**, on whom we completely count for guidance, assistance and sustenance.

I would like to express my deepest respect and heartfelt gratitude to my supervisor, Prof. Dr. Huriye İcil for the opportunity given to me to work in her research group. Her understanding, determination, honesty, motivation, valuable, contribution were matchless during every step my Ms. Program. It was indeed a great honor and privilege to work under her guidance.

My special thanks go to Dr. Duygu Uzun, who has been always there to listening, give practical advice, support and spending precious time with me along my master study.

I would like to express my sincere feeling to all other members of the İcil organic research group family. Melika Mostafanejed, Basma Basil, Selin Temürlü, Meltem Dinleyeci and Arwa Abourajab.

My deepest gratitude goes to my beloved parents: Mr. Husin Ageel and Mrs. Najmia Kalif for their endless encouragement and love. Thank to my husband Mr. Ezziddin Naieli for his sacrifice, endless support and priceless love.

# TABLE OF CONTENTS

ABSTRACT.....	iii
ÖZ.....	iv
ACKNOWLEDGEMENT.....	vi
LIST OF TABLES.....	x
LIST OF FIGURES.....	xi
LIST OF SCHEMES.....	xiv
LIST OF ABBREVIATIONS.....	xv
1 INTRODUCTION.....	1
1.1 Perylene Diimides and Polymers.....	1
1.2 Chitosan polymer.....	3
1.3 Amphiphilic polymers.....	5
2 THEORETICAL.....	8
2.1 Synthesis and Application of perylene Diimides and Polymers.....	8
2.1.1 Synthesis.....	8
2.1.2 Applications.....	10
2.2 Synthesis and Application of Chitosan polymers.....	11
2.2.1 Synthesis.....	11
2.2.2 Applications.....	14
2.3 Comb Shaped Amphiphilic Polymers.....	15
2.4 Polymer Hydrophobicity and Aggregation.....	17
2.5 Drug Delivery.....	18
3 EXPERIMENTAL.....	20
3.1 Materials.....	20
3.2 Instruments.....	20

3.3 Methods of Synthesis	21
3.4 Synthesis of N-((2S)-amino hexanoic acid)-3,4,9,10- perylene tetracarboxylic- 3,4-anhydride-9,10-imide conjugated chitosan (LCP1)....	23
3.5 Synthesis of N-((2S)-amino hexanoic acid)-3,4,9,10- perylene tetracarboxylic- 3,4- anhydride-9,10-imide conjugated chitosan (LCP2).....	24
3.6 Synthesis of N-((2S)-amino hexanoic acid)-3,4,9,10- perylene tetracarboxylic- 3,4-anhydride-9,10-imide conjugated chitosan (LCP3).....	25
3.7 Synthesis of N-((2S)-amino hexanoic acid)-3,4,9,10- perylene tetracarboxylic- 3,4-anhydride-9,10-imide conjugated chitosan (LCP4).....	26
3.8 General Reaction Mechanism of PDI .....	27
4 DATA AND CALCULATION .....	30
4.1 Optical and Photochemical Properties .....	30
4.1.1 Fluorescence Quantum Yield ( $\Phi_f$ ).....	30
4.1.2 Half-Width of Selected Absorption Band ( $\Delta\bar{\nu}_{1/2}$ ) .....	33
4.1.3 Singlet Energies ( $E_S$ ).....	36
4.1.4 Optical Band Gap Energies ( $E_g$ ).....	38
4.1.5 Absorption Intensity Ratios .....	41
4.1.6 Stokes Shifts.....	42
5 RESULTS AND DISCUSSIONS .....	93
5.1 Synthesis and Characterization .....	93
5.2 Solubility of LCPs.....	93
5.3 Analysis of FTIR Spectra.....	97
5.4. Absorption and Fluorescence Properties .....	99
5.4.1 Optical properties of LCP1 .....	100
5.4.2 Optical properties of LCP2 .....	101
5.4.3 Optical properties of LCP3 .....	102



5.4.4 Optical Properties of LCP4 .....	104
6 CONCLUSION .....	107
REFERENCES .....	109
APPENDIX .....	117
Appendix A: Curriculum Vitae .....	118

## LIST OF TABLES

Table 4.1: Fluorescence Quantum Yield Data of LCPs.....	33
Table 4.2: The half-widths of LCPs in Different Solvents .....	36
Table 4.3: The Singlet Energy Values for All LCPs in Different Solvents.....	38
Table 4.4: Optical Band Gap Energies of LCPs in Different Solvent .....	41
Table 4.5: Intensity Ratios of LCPs in Different Solvents .....	42
Table 4.6: Stokes Shifts of LCPs in Different Solvents.....	43
Table 5.1: Solubility properties of LPMI and CH .....	92
Table 5.2: Solubility Test of LCP1, LCP2, LCP3 and LCP4 .....	93
Table 5.3: The UV-vis Absorption and Fluorescence Wavelengths LCP1.....	96
Table 5.4: The UV-vis Absorption and Fluorescence Wavelengths LCP2.....	97
Table 5.5: The UV-vis Absorption and Fluorescence Wavelengths LCP3.....	98
Table 5.6: The UV-vis Absorption and Fluorescence Wavelengths LCP4.....	100
Table 5.7: Optical and Photochemical Properties of LCP1 .....	101
Table 5.8: Optical and Photochemical Properties of LCP2 .....	102
Table 5.9: Optical and Photochemical Properties of LCP3 .....	102
Table 5.10: Optical and Photochemical Properties of LCP4 .....	102

# LIST OF FIGURES

Figure 1.1: The Chemical Structure of PDI.....	2
Figure 1.2: Chemical Structure of Chitin and Chitosan.....	3
Figure 1.3: Schematic Illustration of.....	6
Figure 1.4: The Structure of Lysine Perlene Diimide Conjugated Chitosan .....	7
Figure 2.1: Chemical Structure of PTCDA and PDIs.....	8
Figure 2.2.A: Conversion of Chitin to Chitosan by Deacetylation.....	12
Figure 2.2.B: Schematic representations of Chitosan preparation from raw materials.....	13
Figure 2.3: The Structure Comb Shaped Amphiphilic polymer .....	17
Figure 4.1: possible Deactivation Pathways of Excited Molecules.....	30
Figure 4.2: Representantative plot to Calculate the Half-width of the LCP in DMSO ..	34
Figure 4.3: Representantative plot to Calculate the Gap energies of the LCP in DMSO	39
Figure 4.4: Representantative plot to calculate the Stokes Shifts of The LCP in DMSO.....	42
Figure 4.5:LPMI, FT-IR Spectrum .....	43
Figure 4.6:Chitosan, FT-IR Spectrum .....	44
Figure 4.7: LCP1, FT-IR Spectrum .....	45
Figure 4.8: LCP2, FT-IR Spectrum .....	46
Figure 4.9: LCP3, FT-IR Spectrum .....	47
Figure 4.10: LCP4, FT-IR Spectrum .....	48
Figure 4.11: LPMI, Absorption Spectrum (DMSO).....	49
Figure 4.12: LPMI, Emission Spectrum (DMSO).....	50
Figure 4.13: CH, Absorption Spectrum (1 % CH <sub>3</sub> COOH ).....	51

Figure 4.14: CH, Emission Spectrum (1% CH <sub>3</sub> COOH).....	52
Figure 4.15: LCP1, Absorption Spectrum (NMP) .....	53
Figure 4.16: LCP1, Absorption Spectrum (DMF) .....	54
Figure 4.17: LCP1 Absorption Spectrum (DMAc).....	55
Figure 4.18: LCP1, Absorption Spectrum (DMSO) .....	56
Figure 4.19: LCP1, Absorption Spectra (NMP, DMF, DMAc, DMSO) .....	57
Figure 4.20: LCP1, Emission Spectrum (NMP) .....	58
Figure 4.21: LCP1, Emission Spectrum (DMF) .....	59
Figure 4.22: LCP1, Emission Spectrum (DMAc).....	60
Figure 4.23: LCP1, Emission Spectrum (DMSO) .....	61
Figure 4.24: LCP1, Emission Spectrum (NMP, DMF, DMAc, DMSO).....	62
Figure 4.25: LCP2, Absorption Spectrum (NMP) .....	63
Figure 4.26: LCP2, Absorption Spectrum (DMF) .....	64
Figure 4.27: LCP2, Absorption Spectrum (DMAc).....	65
Figure 4.28: LCP2, Absorption Spectrum (DMSO) .....	66
Figure 4.29: LCP2, Absorption Spectra (NMP, DMF, DMAc and DMSO) .....	67
Figure 4.30: LCP2, Emission Spectrum (NMP) .....	68
Figure 4.31: LCP2, Emission Spectrum (DMF) .....	69
Figure 4.32: LCP2, Emission Spectrum (DMAc).....	70
Figure 4.33: LCP2, Emission Spectrum (DMSO) .....	71
Figure 4.34: LCP2, Emission Spectrum (NMP, DMF, DMAc, DMSO).....	72
Figure 4.35: LCP3, Absorption Spectrum (NMP) .....	73
Figure 4.36: LCP3, Absorption Spectrum (DMF) .....	74
Figure 4.37: LCP3, Absorption Spectrum (DMAc).....	75
Figure 4.38: LCP3, Absorption Spectrum (DMSO) .....	76

Figure 4.39: LCP3, Absorption Spectra (NMP, DMF, DMAc, DMSO) .....	77
Figure 4.40: LCP3, Emission Spectrum (NMP) .....	78
Figure 4.41: LCP3, Emission Spectrum (DMF) .....	79
Figure 4.42: LCP3, Emission Spectrum (DMAc).....	80
Figure 4.43: LCP3, Emission Spectrum (DMSO) .....	81
Figure 4.44: LCP3, Emission Spectrum (NMP, DMF, DMAc and DMSO) .....	82
Figure 4.45: LCP4, Absorption Spectra (NMP) .....	83
Figure 4.46: LCP4, Absorption Spectra (DMF) .....	84
Figure 4.47: LCP4, Absorption Spectra (DMAc) .....	85
Figure 4.48: LCP4, Absorption Spectra (DMSO).....	86
Figure 4.49: LCP4, Absorption Spectra (NMP, DMF, DMAc and DMSO) .....	87
Figure 4.50: LCP4, Emission Spectra (NMP) .....	88
Figure 4.51: LCP4, Emission Spectra (DMF) .....	89
Figure 4.52: LCP4, Emission Spectra (DMAc) .....	90
Figure 4.53: LCP4, Emission Spectra (DMSO).....	91
Figure 4.54: LCP4, Emission Spectra (NMP, DMF, DMAc and DMSO) .....	92

## LIST OF SCHEMES

Scheme 2.1: Synthetic Method of Perylene Dyes.....	9
Scheme 3.1: General Synthesis LCP.....	22

## LIST OF ABBREVIATIONS

Å	Armstrong
A	Absorption
AP <sub>s</sub>	Amphiphilic Polymers
CAC	Critical aggregation concentration
CHL	Chloroform
CMC	Critical micelle concentration
CP	Comb polymer
CH	Chitosan
DD	Deacetylation degree
DMF	Dimethylformamide
DMSO	Dimethyl sulfoxide
Eqn.	Equation
E <sub>s</sub>	Singlet energy
FT-IR	Fourier Transform Infrared Spectroscopy
IR	Infrared Spectrum/Spectroscopy
LCP	Lysine Perylene Diimide Conjugated Chitosan
M	Molar concentration
M <sub>w</sub>	Molecular Weight
max	Maximum
min	Minimum
mmol	Millimole
mol	Mol
OLED	Organic light emitting diodes

OFETs	Organic field effect transistors
$\Phi_f$	Fluorescence quantum yield
PDA	Perylene-3,4,9,10-tetracarboxylic dianhydride
PDI	Perylene Diimide
Std.	Standard
UV	Ultraviolet
UV-Vis	Ultraviolet, visible light absorption
$\Delta\tilde{\nu}_{1/2}$	Half-width (of the selected absorption)
$\nu_{\max}$	Maximum wavenumber
$\lambda_{\text{exc}}$	Excitation wavelength



# Chapter 1

## INTRODUCTION

### 1.1 Perylene Diimides and Polymers

Perylene-3,4,9,10-tetracarboxylic acid dianhydride, PDA and its derivatives have been widely utilized in a spacious range of various applications as pigments [1], Opto-electronic nano devices [2], solar cell and the formation of supramolecular architectures [3]. Perylene diimides which also known as perylene-3,4,9,10-tetracarboxylic acid diimides are one of the most stable PDA derivatives. In the beginning of 1910s, perylene diimides were synthesized by Kardos. In recent years, perylene diimides, PDIs has been employed as a substantial category of performance pigments [4], and as fluorescent dyes. PDIs also have been investigated widely of optical and optoelectrical applications [5].

Perylene diimides and polymers are extensively studied because of their outstanding thermal and photochemical stabilization and high optical absorption and fluorescence characteristics. On the other hand, PDIs suffer from some disadvantages, the restricted processability owing to low solubility and aggregates in common organic solvents. As well as self quenching which leads to low fluorescence quantum efficiency in the solid state [6, 7].

To overcome PDIs limited solubility in aqueous medium and extend their application for bio-imaging purposes, it is compulsory to improve the solubility of PDI in aque-

ous medium [8]. Highly water soluble PDI can be achieved by lowering or prevent its  $\pi$ - $\pi$  interactions, it is reported that grafting sterically hindered substituents to the core of the perylene chemical structure at imide or bay position increase their solubility in aqueous environments Figure 1.1 [8]. Icil and her co-workers reported a set of highly water soluble PDI derivatives, which simply and easily synthesized [9].

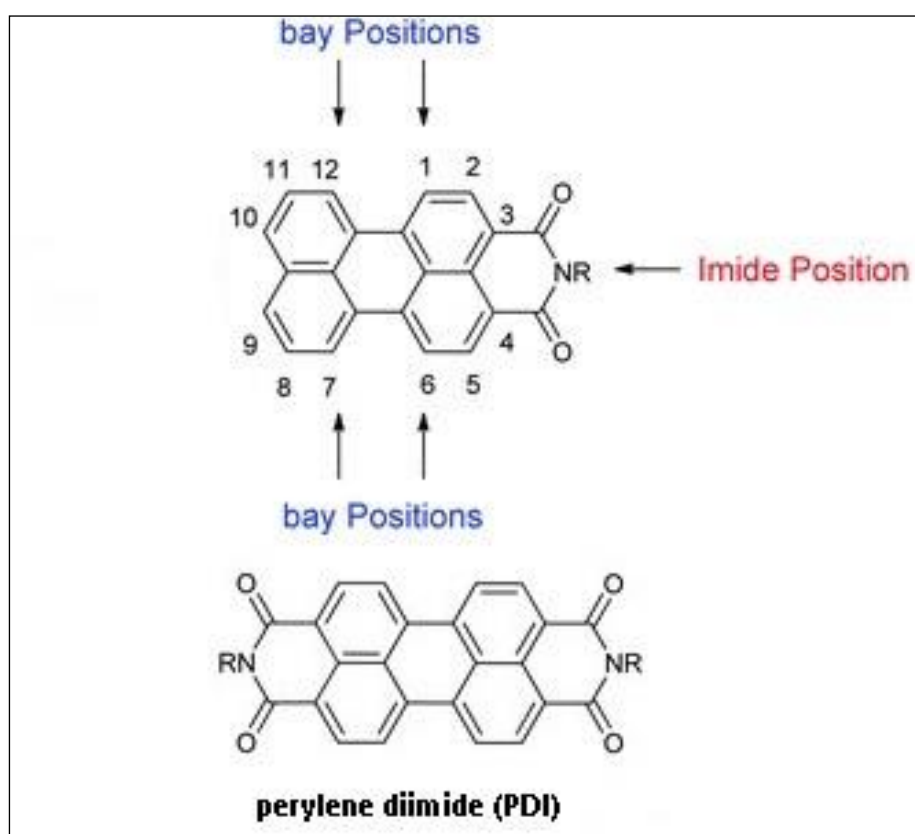


Figure 1.1: The Chemical Structure of PDI

Most perylene diimide based polymers display high optical absorption in the visible to near-infrared spectral and irradiate emissions above 500nm that made them suitable molecules as acceptors chromophores in organic solar cell devices. Furthermore, some perylene derivatives have been assured to be cell permeable which may be useful in living cell imaging [10].

## 1.2 Chitosan polymer

Chitosan (CH) is a biopolymer composed of 2-acetamide-2-deoxy-D-glucopyranose and 2-amino-2-deoxy-D-glucopyranose repeat units with  $\beta$  (1 $\rightarrow$ 4) linkages. This polysaccharide is mainly obtained from chitin by alkaline deacetylation. The chemical structures of chitin and chitosan are illustrated below Figure 1.2. Chitin is widely found in nature and existent in the crustacean shells and the cells of fungi and yeast. However, chitosan (CH) is more attractive than chitin as a poly cationic polymer for biomedical applications owing to its physicochemical and biological properties. [11, 12]. CH and its derivatives have positive characteristics of excellent biodegradability, nontoxic with environmental safety, thus giving opportunities for future development in various fields [13].

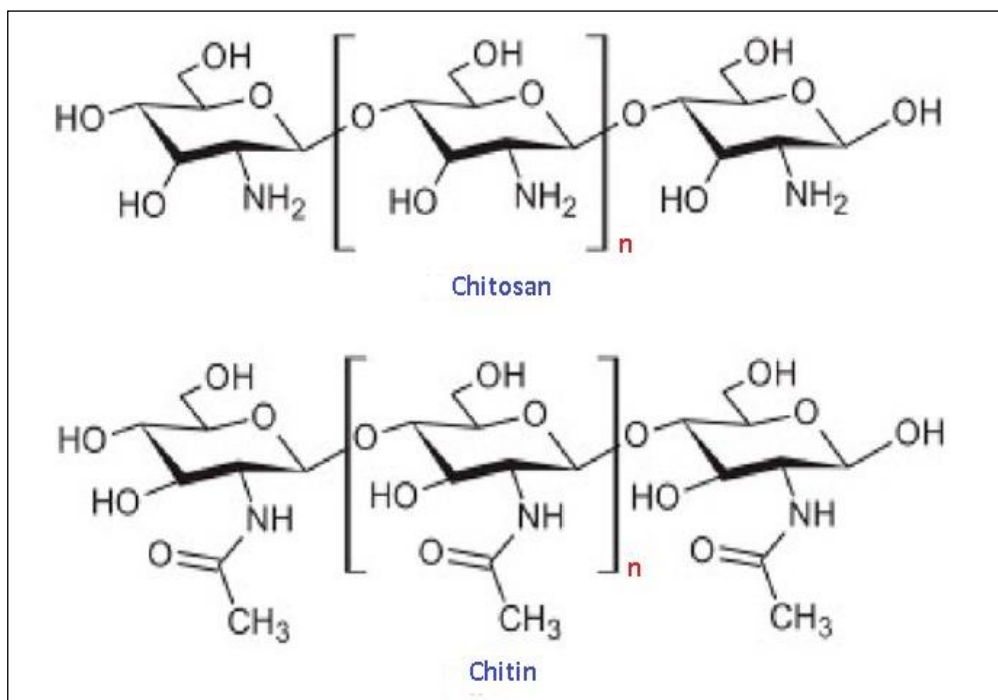


Figure 1.2: Chemical Structure of Chitin and Chitosan

The characteristics of chitosan depend extremely on the molecular weight (Mw) and the degree of deacetylation (DD), which are substantial factors in specifying chi-

tosan. In fact, CH is mainly acquired at synthetic scale with different deacetylation degrees, therefore high quality products need a well characterized by chitosan properties for interesting applications [15, 16].

On the other hand, chitosan suffer from some disadvantages, the limited solubility of CH in water or organic solvents due to intermolecular hydrogen bonding and rigid crystallinity of its structure. However, CH is a polyamine and show solubility in aqueous dilute acids like formic, oxalic, lactic and acetic acids. The presence of amino groups on the CH backbone ( $-NH_2$ ) determine its solubility in dilute acids. The amino groups of chitosan could be protonated and turn into positively charged amino groups ( $-NH_3^+$ ) at PH values below 6. When the PH increases to values above than 6, amino groups become unprotected. As a result, CH loses its charge and become insoluble [17].

Many researchers have been made to overcome the drawbacks of CH. Several chemical modifications are carried out to convert chitosan to become water or organic solvent soluble derivatives for biological applications. The molecular structure of chitosan could modify by introducing some hydrophobic or hydrophilic agents into chitosan, such as cholesterol, deoxycholic acid, poly ( $\epsilon$ -caprolactone), methoxy poly (ethylene glycol). As a consequence chitosan nanoparticles can be obtained by simple self-assembly that have been studied for biomedical applications such as drug delivery system [18 ,19].

### **13 Amphiphilic polymers**

Amphiphilic polymers (APs) are able to form macromolecule structures in the hydrous medium. APs are consisted of two parts hydrophobic and hydrophilic regions within their structure by covalent bonds. The hydrophobic parts, authorise the formation of self-organize interface in hydrous medium (hydrophobic interaction), whereas the hydrophilic parts make the polymer soluble in the water (hydrophilic interaction). In recent years, intensive research efforts have been committed to studying Amphiphilic polymers, particularly in the pharmaceutical application [20].

Block copolymer is one of the most prevalent molecular structures of amphiphilic polymers which are invented by copolymerization of hydrophilic and hydrophobic segments. Carbohydrate polymers such as starch, hydroxypropyl cellulose, and chitosan has been utilized to build comb shaped amphiphilic polymers by polymerization of hydrophilic and hydrophobic monomers. It is reported that, water-soluble homopolymers grafted with hydrophobic segments have attracted considerable regard in the biomedical applications. These comb polymers enable to form a variant macromolecular architecture in the hydrous medium like polymeric micelles, dense nano particles and vesicles [21].

Polymeric micelles fabricated from supramolecular species have generated growing attention, particularly in the biomedical application, including drug delivery and catalysis [22], due to their superb ability to self-assembly at interfaces and in aqueous surrounding (Figure 1.3).

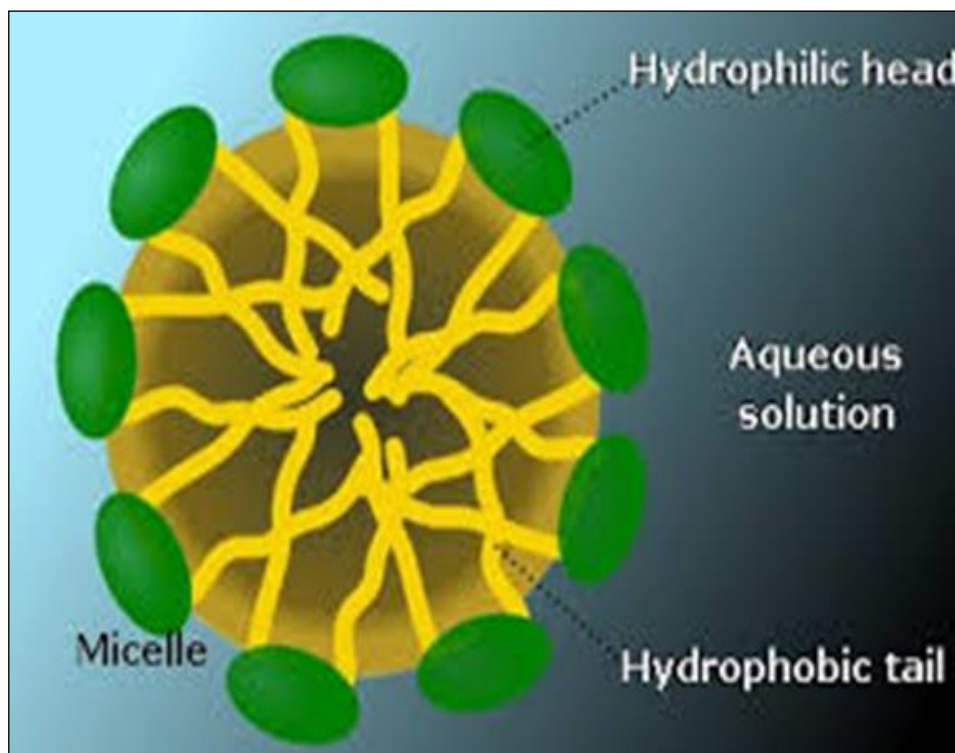


Figure 1.3: Schematic Illustration of Micelle Formation

The hydrophilic outer shell of the micelles exposed into the aqueous environment compose of components that are rarely reactive with blood or tissue components. As a result polymeric micelles allows to stay long time in the blood or tissues without being known by phagocytic cells or\and certain proteins. This property is an attractive feature of micelles as drug delivery, sensing, imaging and catalysis [20].

The cardinal aim of this study is to synthesize a chiral amphiphilic chitosan polymer having a comb shaped fluorescent perylene imide chromophores for pharmaceutical applications including hydrophobic drug solubilization Figure 1.4. The synthesized products were assigned by FTIR, UV-Visible, emission spectrum techniques. As well as the photophysical and optical properties were examined.

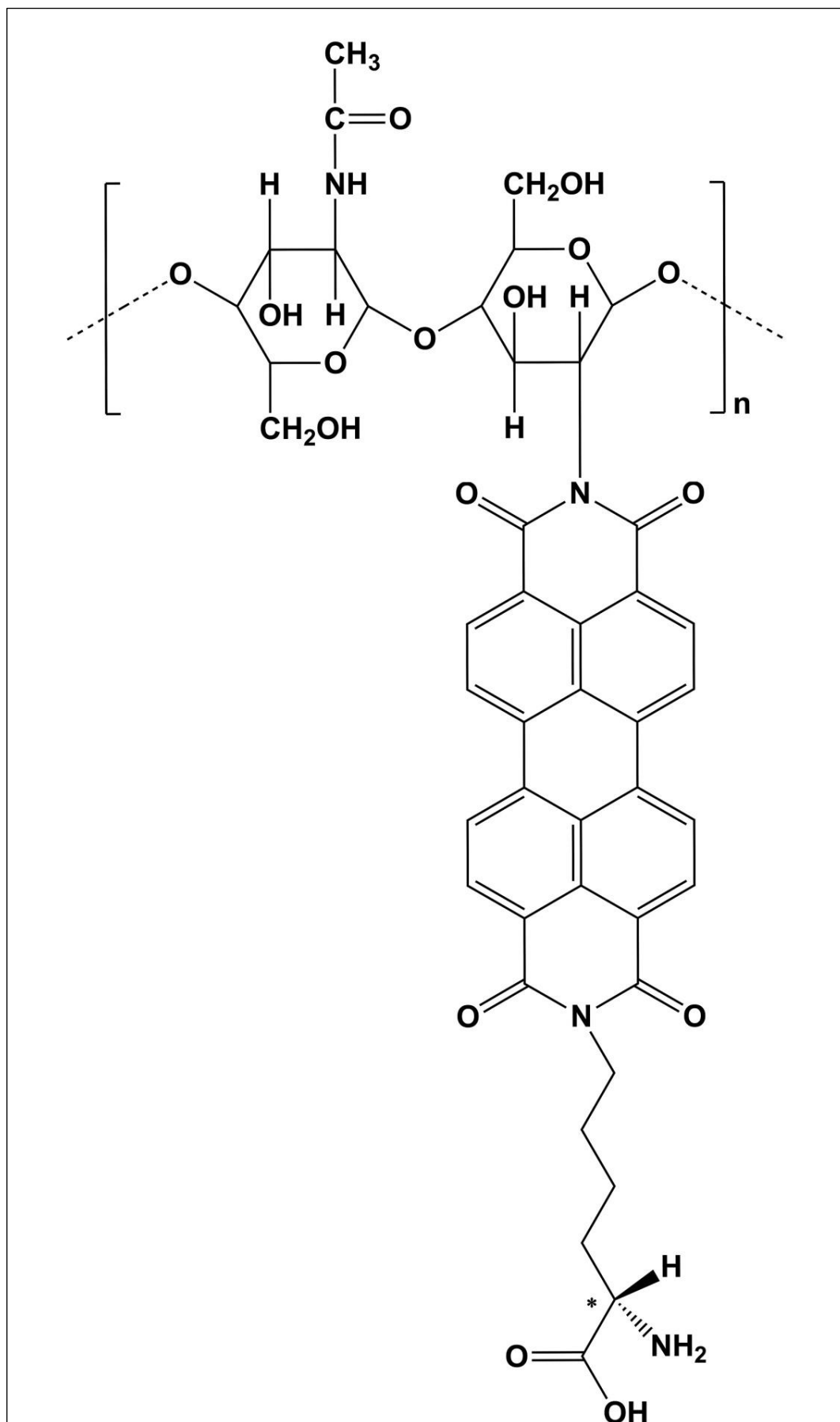


Figure 1.4: the Structure of Lysine Perylene Diimide Conjugated Chitosan (LCP)

## Chapter 2

# THEORETICAL

### 2.1 Synthesis and Application of perylene Diimides and Polymers

#### 2.1.1 Synthesis

Aromatic polyimides had synthesized by Marston Bogert during 1900s. Aromatic polyimides were produced with high molecular weight in 1955 by through two step polycondensation reaction of pyromellitic dianhydride with diamines [23]. During recent years, much attention has been taken to aromatic polyimides. Perylene diimides (PDIs) is one of the most important derivatives of this class which was obtained from perylene-3,4,9,10-tetracarboxylic dianhydride (PTCDA). Figure 2.1 shows the structure of PTCDA and PDIs [24].

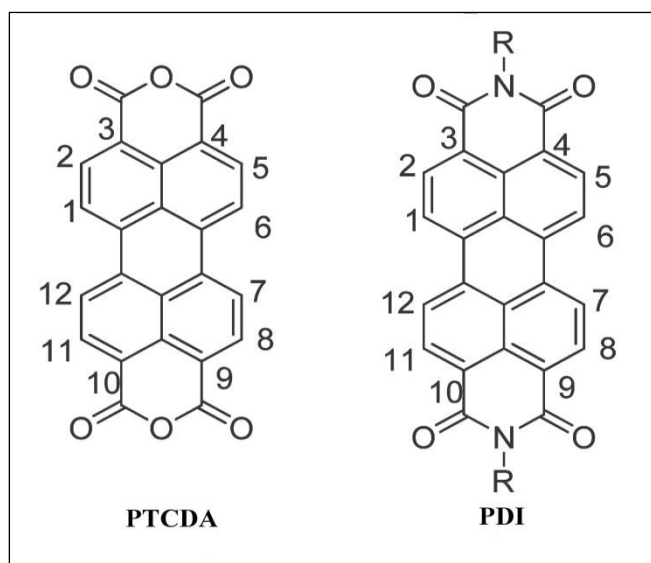
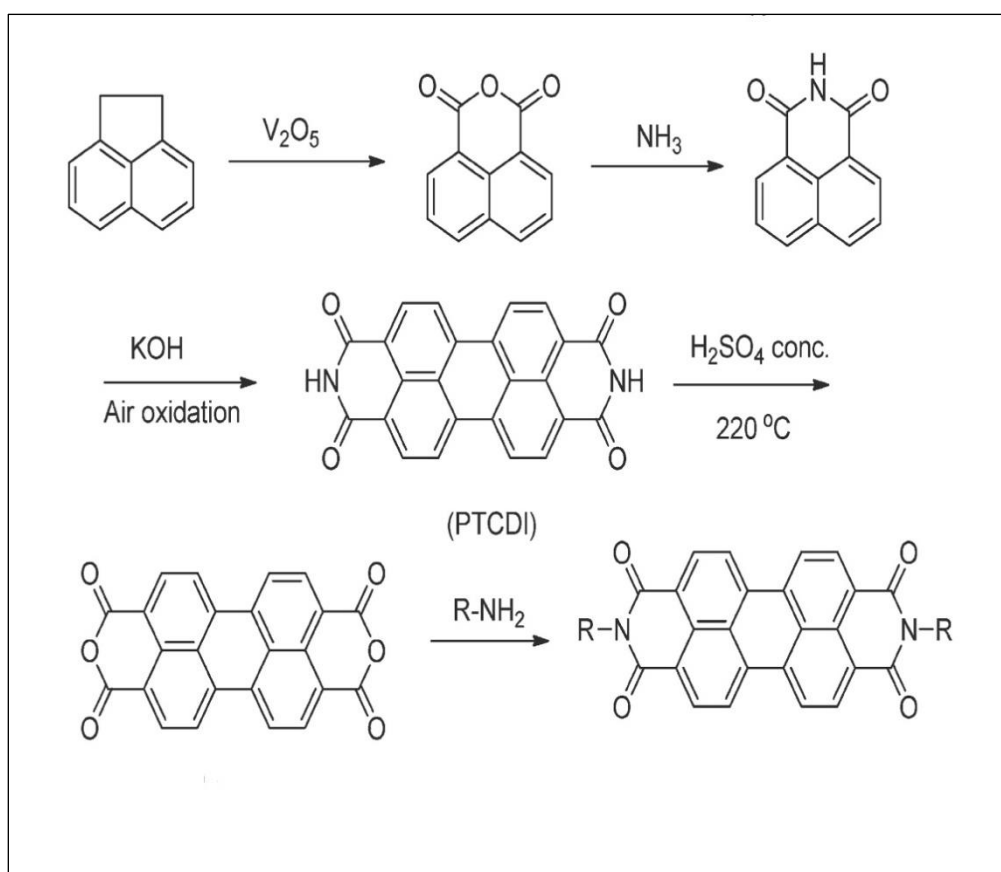


Figure 2.1: Chemical Structure of PTCDA and PDIs



In industrial setting PTCDA is obtained through a series of stages as presented in Scheme 2.1. PTCDA begins with  $V_2O_5$ -catalyzed air oxidation of acenaphthene to form 1,8-naphthalene dicarboxylic acid anhydride and afterward treated with ammonia  $NH_3$  to give naphthalene-1,8-dicarboxylic acid imide. PTCDI is synthesized by mixing 1,8- naphthalene at  $190-220^\circ C$ , that resulted by air oxidation of molten compound. PTCDA is produced out of hydrolyses of perylene-3,4,9,10-tetracarboxylic diimide with conc. sulfuric acid at  $220^\circ C$  [24].



Scheme 2.1: Synthetic Method of Perylene Dyes [24]

### 2.1.2 Applications

PDI's were used as industrial pigments. They are described as a high performance pigments primarily in the red and black shades, based on the chemical structure and molecular packing of the solid state [25]. The derivatives of PDI's were used in several applications due to their excellent properties, including near-unity photoluminescence quantum yield, strong absorption in the visible region, thermal, chemical, electrochemical, photochemical stability and strong electron-accepting capacity [26, 27]. Moreover PDI's are nontoxic and cheap material and are made by low energy technologies [24].

All these particular characteristics indicate the applicability of perylene diimides in the areas of optical and optoelectrical applications including fluorescent solar collectors organic solid state laser dyes, organic light emitting diodes (OLED), liquid-crystal offer color filters, organic field effect transistors (OFETs), optical sensors, photoconducting materials and as probes for biomacromolecules (proteins, DNA, RNA) [5, 9, 28].

Beside the outstanding features, PDI's have some disadvantages involved essentially poor solubility and tendency to aggregate in common organic solvents with themselves owing to  $\pi$ - $\pi$  stacking. Another drawback self quenching leading to low solid-state fluorescence quantum efficiency. Therefore, the photovoltaic conversion is limited [29, 6].

Two different methods have been used to reduce strong intermolecular  $\pi$ - $\pi$  interactions and molecular aggregation in PDI's. First one is introducing bulky substituents at the imide position and second method takes by advantage of using the present core

position by grafting hydrophilic groups [9]. Erika kozma and her co-workers synthesized water-soluble amino acid functionalized perylene diimides and researched the effect of aggregates on the optical properties in organic and aqueous environment of opening the way to the development of PDI-based sensing platform [29].

## **2.2 Synthesis and Application of Chitosan polymers**

### **2.2.1 Synthesis**

Chitin is the most abundant polysaccharide found in the nature after cellulose. Chitin found particularly in the marine animals and in the cells of yeast and fungi. It is synthesized by a large number of living organisms as well [30]. CH is also considered as a natural polymer from renewable sources and obtained by fully or partially deacetylated form of chitin composed of linear 2-Amino-2-deoxy-D-glucose and 2-acetamido-2-deoxy-D-glucose with  $\beta$  (1 $\rightarrow$  4) repeat units [7]. Professor C. Rouget discovered chitosan in 1859 when he treated chitin by alkali at high temperature. After it is cooked glucosamine units made upon the chitosan chain (Figure 2.2.A). All amazing properties of Chitosan back to the free amino groups on the Chitosan backbone. CH thrived during 1930 and 1940s. However, the expansion of synthetic medicines was gained by 1970 and has kept to extend ever since [31].

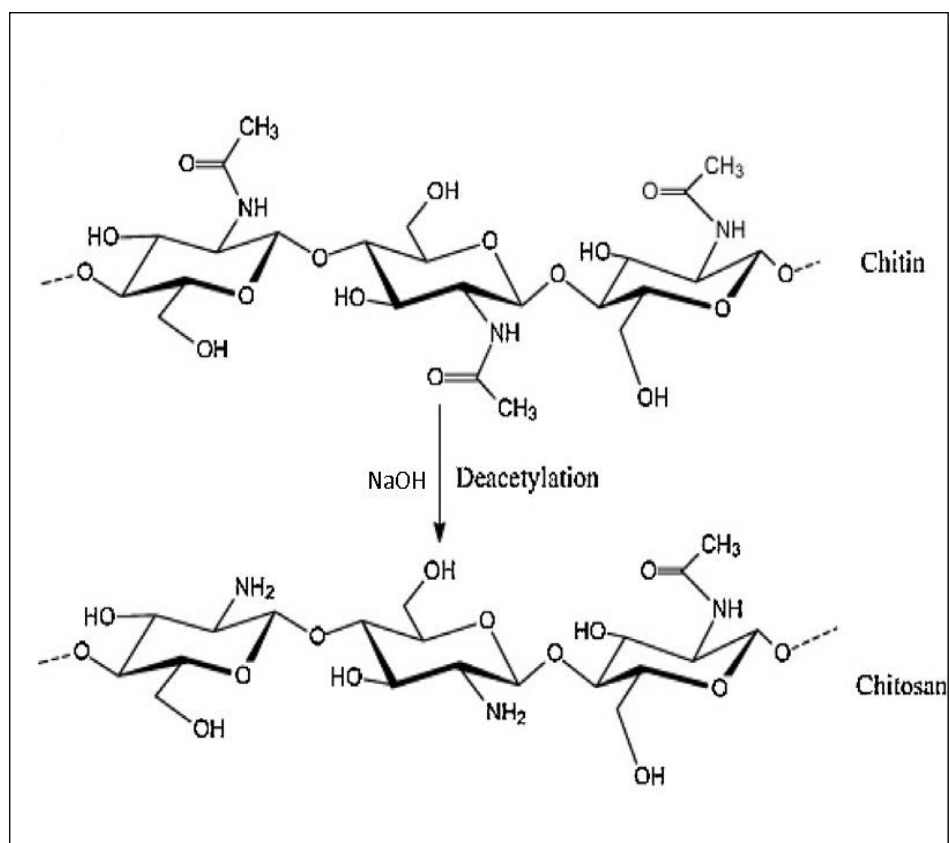


Figure 2.2.A: Conversion of Chitin to Chitosan by Deacetylation

Extraction and purification process of chitosan from shrimp shells which are thinner are widely employed for the production of chitosan by chemical method. Generally, shells of the same species and size are collected, cleaned, then dehydrated and split into small shell segments. Traditionally, three steps were interested in the purification process, (1) demineralization of chitosan. (2) deproteinization, (3) decolorization of chitosan. These steps can be achieved by utilizing chemical or biological (enzymatic) handling. Figure 2.2B explains the steps contributed in chemical and biological treatments of chitosan from crustacean shells. For biomedical or pharmaceutical applications high quality purification is need for the end products of Chitosan to avoid the dangerous side effects of pigments, minerals and residual proteins on the human body [32, 33].

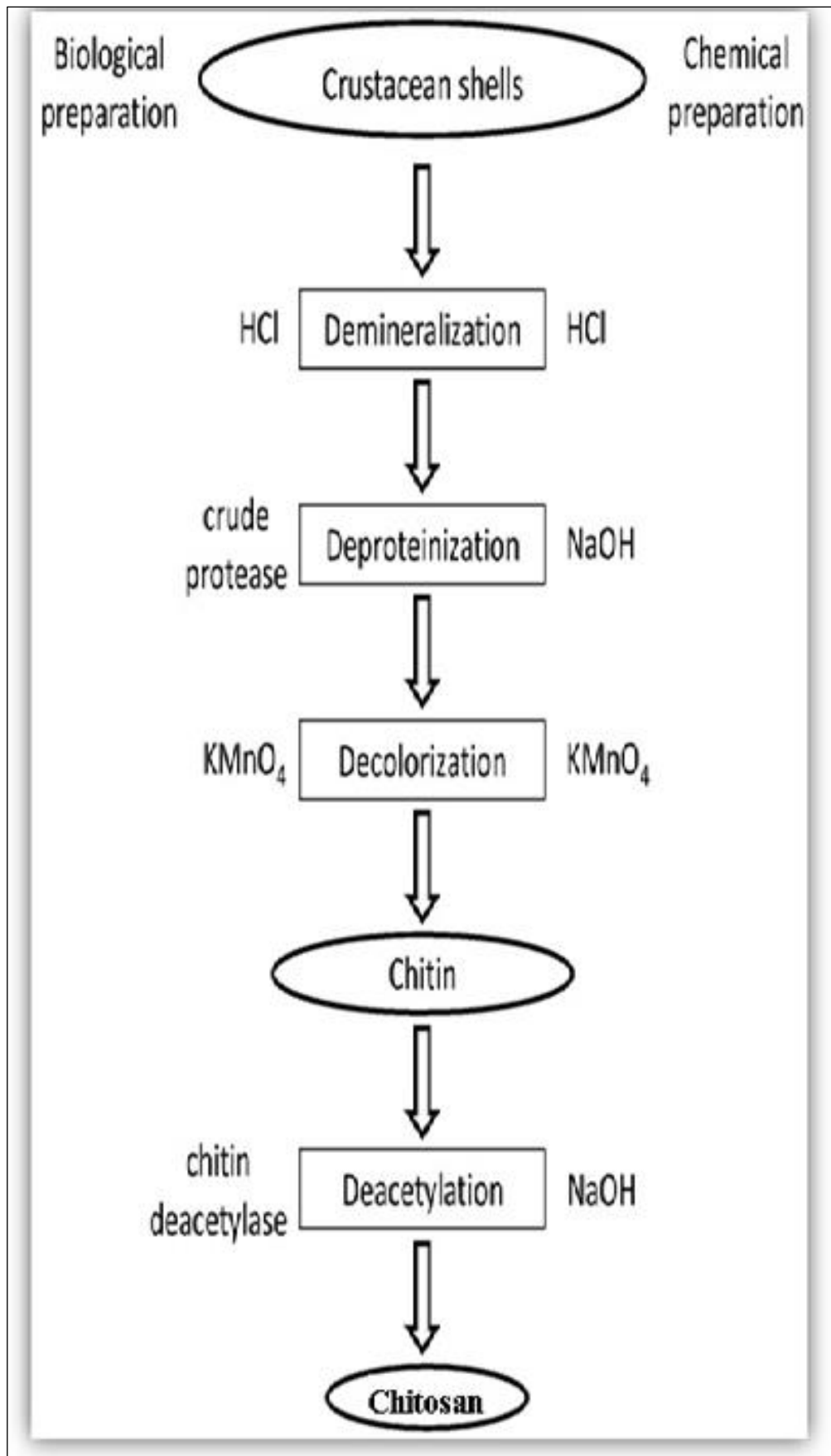


Figure2.2.B: Schematic Representations of Chitosan Preparation From raw Materials.

### **2.2.2 Applications**

Chitosan is one of the most attracted biopolymer due to its beneficial properties, biocompatibility, biodegradability, nontoxicity, hydrophilicity, antimicrobial property and film forming ability. All these intrinsic properties make it more interesting for several fields such as biomedicine, pharmaceuticals, biotechnology, food science, cosmetics, textile, agriculture and water treatment [34, 35].

CH is used as an antimicrobial agent in numerous biomedical areas. For instance, wound dressing materials due to its ability to integrate into fiber, membrane and hydrogel. Also, the particular properties of chitosan, high surface-to-volume ratio, large porosity and diameter in the nanoscales are favorable for preparing wound dressing [36].

Furthermore, CH has been widely desired as a polymer for tissue design engineering because of its novel property which is large porosity, suitable pore space distributions. CH is also used as a carrier system by controlling delivery of anti HIV and cancer drug [37].

Additionally, CH is used to inhibit and delay the growth of bacteria in textile goods. For instance, water-soluble carboxy methyl chitosan is used to treat cotton fabric versus *E.coli* and *S.aureus* at 0.1% concentration. Moreover, wrinkle recovery was well improved. CH has been accepted as an aliment additive and as a compound of packaging substance to delay microorganism development and increase the goodness and expiry of food. In one study, it is observed that chewing gum containing chitosan restrained the expansion of cariogenic bacteria in slaver effectively [38].

In recent years, chitosan film start to use for photovoltaic applications. Due to, the abundant groups such as free amine groups, carboxyl groups and hydroxyl groups on its backbone, CH could be considered as an electron donating bio-poly electrolyte and conductive polymer. In addition, CH might be a useful material for solar cells due to its other unique properties such as compatibility, nontoxicity, easy-handling, cheapness and high mechanical strength [39, 40].

### **2.3 Comb Shaped Amphiphilic Polymers**

Amphiphilic polymers have researched extensively since the beginning of 1990s. These APs consist of hydrophobic and hydrophilic parts within the same macromolecule to form super molecular structures. Comb shaped Amphiphilic polymer is the second most common amphiphilic polymers and their structure came from grafting or conjugating groups onto the polymer backbone. The hydrophobic segments consist of copolymers or homopolymers and the hydrophilic groups are often added to increase water solubility of these polymers, whereas the hydrophobic parts maintain the self assembly of the polymer in the aqueous surroundings due to hydrophobic interaction [21].

Amphiphilic polymer is accepted as one of the most significant polymer for biomedical and pharmaceutical fields because of their supramolecular formation ability in aqueous surroundings. Different supramolecular structures such as polymeric micelles, dense nanoparticles and vesicles have been formed by these comb-shaped amphiphilic polymers. It is reported that carbohydrate polymers such as cellulose, starch and chitosan have been utilized to prepare comb shaped amphiphilic polymers for drugs [41].

Adjusting the structural components of APs has effected directly on the chemical and physical properties of the polymer. Therefore, the aim of this work is to synthesize a chiral amphiphilic chitosan polymer comb-shaped via Lysine-perylene monoimide. The chitosan back bone has a reactive side (amino groups) which can interact with the core active chain end (carbon atom within anhydride group) on the Lysine-perylene mono imide dye by substitution reaction, with a view to obtain an equilibrium between better solubility and the capability to shape stacks by expanded intermolecular  $\pi$  orbital overlap, which is extremely significant for photonics applications [42]. In addition *L*-Lysine is one of components of this comb-shaped polymer has chosen over other amino acids due to its chairlty with various functional side groups and its roles in physiological processes. In this way, A novel comb-shaped and chiral amphiphilic polymer is prepared for pharmaceutical applications including hydrophobic drug solubilization. Schematic representation of comb-shaped polymer is shown in Figure 2.3.



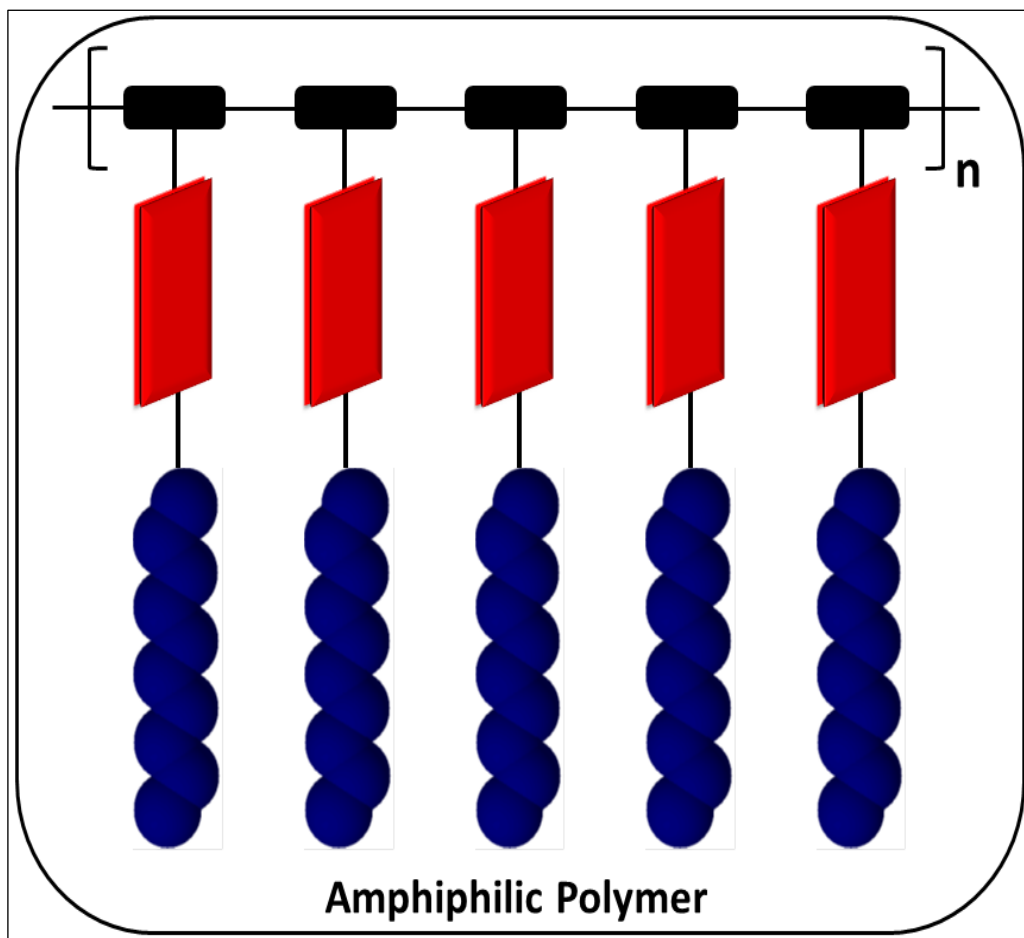


Figure 2.3: The Structure of Comb Shaped Amphiphilic Polymer

## 2.4 Polymer Hydrophobicity and Aggregation

The arrangement of the polar regions of molecules in a polar solvent such as water could be oriented outwards towards the solvent, whereas the nonpolar regions directed inward apart from the polar solvent by the hydrophobic effect. This can spontaneously attributed to the self-assemblies of molecules by non-covalent interaction, such as Van der Waals attractive forces between the molecules, which is called molecular aggregates [43].

In the past years, the interest was increased on amphiphilic polymers for applications envisaged in biological and pharmaceutical areas due to their particular property to self-assembles and aggregate behavior in aqueous environments. The self-assembling

process involves amphiphilic polymer chains; hydrophobic segments, at most orient inside, and hydrophilic units are oriented in outer surfaces. Hydrogen bonding interaction and Van der Waals attractive forces play a role to increase the stability of folded structure [44].

The self-assembly of amphiphilic polymers into highly systematic aggregates that would produce required structures such as spherical micelles or spherical bilayer vesicles or rod like micelles [45]. The formation of these desired aggregate morphologies depends on molecular structures, shapes, sizes and the proportional fraction of hydrophilic and hydrophobic parts, as well as the solvent environments. It is reported that the nano aggregates of perylene diimides with specific morphology were obtained by self-assembly of variously shaped amphiphilic PDIs in liquid solutions [46].

The critical aggregation concentration (CAC) is the minimal concentration desired for polymeric aggregates to obtain in hydrous medium. Generally, block copolymers have a lower CAC value than comb-shaped amphiphilic polymers. This could be imputed to the formation of looser and larger aggregates in comb-shaped amphiphilic polymers [21].

## **2.5 Drug Delivery**

Drug delivery systems extend their biological effectiveness of their target sites and non-target sites, which generally give a rise to undesired side effects. A lack of selectivity and poor bio-distribution hampers their treatment of many diseases. This asserts the importance of existing selective active compounds within drug delivery systems to increase their efficiency of the disease treatments. So, one of the prime diffi-

culties in drug delivery system is the evolution of drug carriers enhancing selective and delivery of therapeutics to tissue targets. For this aim, drug carriers must possess intrinsic properties such as, high stability in the blood, enough drug loading capacity, high selectivity at the target sites, suitable drug release protocols and biocompatibility [47, 48].

The importance of chitosan is increasing daily in drug delivery systems because of its outstanding properties. CH has been extensively used in different forms such as micelles, microspheres, tablets vaccines, hydrogels, nucleic acids, conjugates and nanoparticles. However, CH surface does not contain any hydrophobic segments therefore, several chemical modifications are carried out at its amino groups or glucosidic groups with hydrophobic substituents to increase its activity. CH micelles were formed with an internal hydrophobic center and an external hydrophilic shield. In aqueous solution, self-assembled core-shell nanostructures were formed by chitosan micelles. These nanoparticles present excellent biocompatible and biodegradable properties that have been examined widely as drug carriers [48, 49].

Recently, photoresponsive nanoparticles are increasingly being explored for their use in drug delivery systems due to their capability to dominate the release of bioactive molecules. It is reported that, perylene-3-ylmethanol nanoparticles which a single-component photoresponsive nano carrier and was used as an anticancer drug [50]. The cardinal aim of this study is to combine chitosan polymer with one of perylene derivatives. The synthesis of an amphiphilic Chitosan polymer having a comb shaped fluorescent peryleneimide chromophores could be a useful compound for delivery of bioactive agents such as anticancer drug.

## Chapter 3

# EXPERIMENTAL

### 3.1 Materials

*N*-((2*S*)-amino hexanoic acid)-3,4,9,10- perylene tetracarboxylic-3,4-anhydride-9,10-imide (LPMI) [10]. Low molecular weight chitosan (CH), Zinc acetate, m-cresol and isoquinoline were obtained from Aldrich company. For spectroscopic measurements, spectroscopic solvents were used. Additionally, all the solvents were purified by distillation.

### 3.2 Instruments

#### Fourier Transform Infrared Spectra

The synthesized compounds were recorded with KBr disk by employing a JASCO FT-IR spectrophotometer.

#### Ultraviolet Absorption spectra

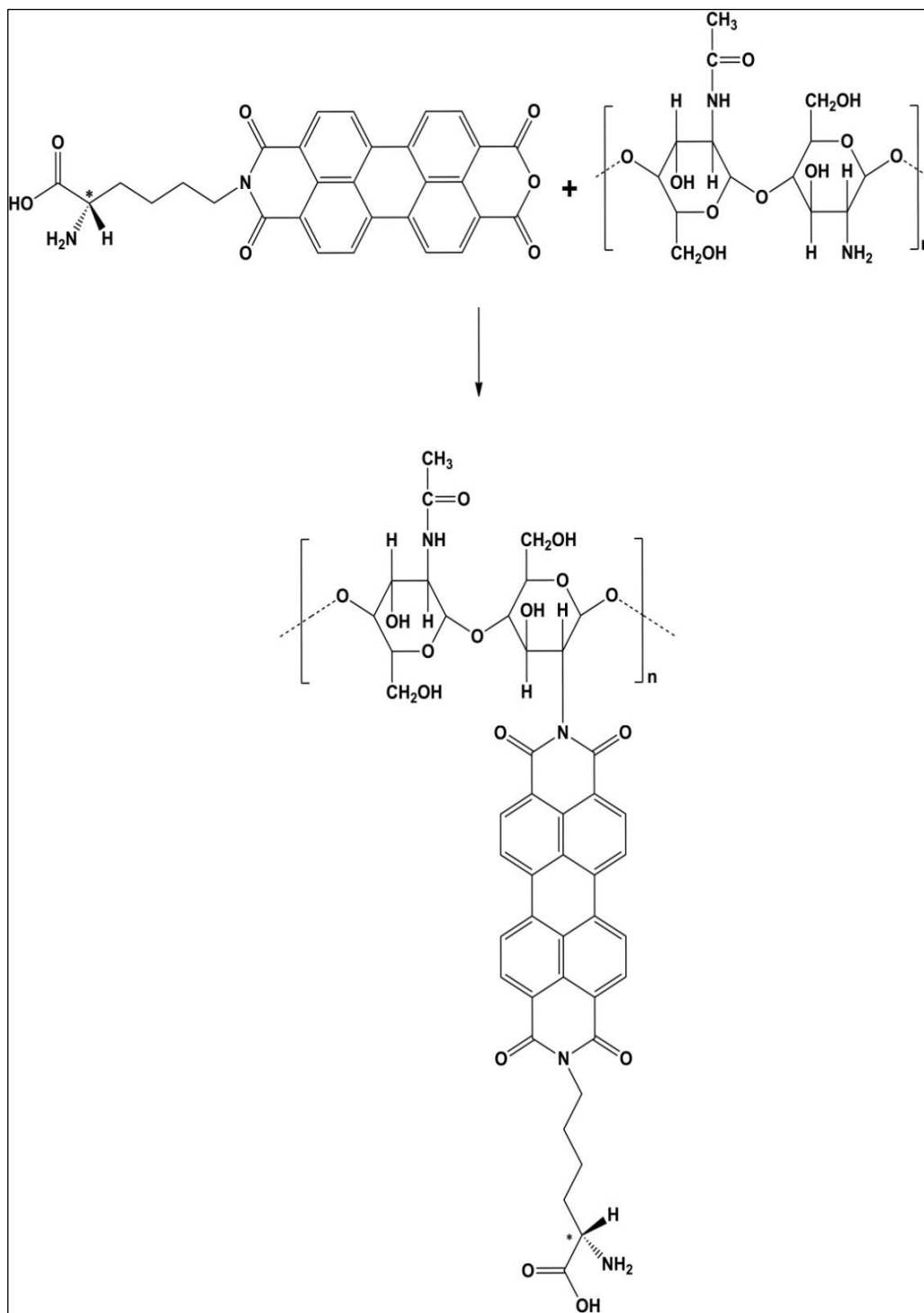
All the synthesized compounds were investigated in different solvents by using Varian Cary-100 Spectrophotometer.

#### Emission Spectra

The synthesized compounds were investigated in various solvents by Varian Cary Eclipse Spectrophotometer.

### 3.3 Methods of Synthesis

*N*-((2*S*)-amino hexanoic acid)-3,4,9,10-perylene tetracarboxylic-3,4-anhydride-9,10-imide conjugated chitosan (LCP) derivatives were successfully synthesized via substitution reaction of *N*-((2*S*)-amino hexanoic acid)-3,4,9,10-perylene tetracarboxylic-3,4-anhydride-9,10-imide (LPMI) and low molecular weight chitosan (CH) in *m*-cresol and isoquinoline solvent mixture . Scheme 3.1 illustrates the general synthesis of LCP.



Scheme 3.1: General Synthesis of LCP

### **3.4 Synthesis of *N*-((2*S*)-amino hexanoic acid)-3,4,9,10-perylene tetracarboxylic-3,4-anhydride-9,10-imide conjugated chitosan(LCP1)**

*N*-((2*S*)-amino hexanoic acid)-3,4,9,10-perylene tetracarboxylic-3,4-anhydride-9,10-imide (LPMI) (0.034 g, 0.0653 mmol), low molecular weight chitosan (CH) (0.782 g, 4.852 mmol) and zinc acetate (0.014 g, 0.0638 mmol) were stirred in an accurately dried solvent mixture of isoquinoline (8 mL) and *m*-cresol (40 mL) under argon atmosphere at 80 °C for 4 h, at 120 °C for 6 h, at 140 °C for 2 h, at 180 °C for 2 h and finally at 200 °C for 2 h. The reaction solution was transferred into 300 mL of cold methanol. The solution was filtered by suction filtration. The synthesized crude product first washed with water and acetic acid (1 %), then the synthesized compound was purified by chloroform Soxhlet extraction for 24 h. After that, a vacuum at 100 °C was used to dry the pure product.

**Yield:** 0.296 g

**Color:** Black

**FT-IR (KBr, cm<sup>-1</sup>):**  $\nu$  = 3384, 3049, 2922, 1687, 1656, 1597, 1444, 1336, 1269, 1069, 811, 739.

**UV-vis (DMF) ( $\lambda_{\max}$ /nm):** 487, 522

**Fluorescence (DMF) ( $\lambda_{\max}$ /nm):** 534, 574, 625

**$\Phi_f$  (Fluorescence Quantum Yield, DMF):** 0.5.

### **3.5 Synthesis of *N*-((2*S*)-amino hexanoic acid)-3,4,10-perylene tetracarboxylic-3,4-anhydride-9,10-imide conjugated chitosan (LCP2).**

LPMI (0.066 g, 0.127 mmol), low molecular weight chitosan (CH) (0.8 g, 4.9640 mmol) and zinc acetate (0.028 g, 0.127 mmol) were stirred in an accurately dried solvent mixture of isoquinoline (8 mL) and *m*-cresol (40 mL) under argon atmosphere at 80 °C for 4 h, at 120 °C for 6 h, at 140 °C for 2 h, at 180 °C for 2 h and finally at 200 °C for 2 h. The reaction solution was transferred into 300 mL of cold methanol. The solution was filtered by suction filtration. The synthesized crude product first washed with water and acetic acid (1 %), then the synthesized compound was purified by chloroform Soxhlet extraction for 24 h. After that, a vacuum at 100 °C was used to dry the pure product.

**Yield:** 0.339 g

**Color:** Black

**FT-IR (KBr, cm<sup>-1</sup>):**  $\nu = 3391, 3063, 2920, 2894, 1689, 1654, 1597, 1436, 1342, 1277, 1041, 811, 747.$

**UV-vis (DMF) ( $\lambda_{\max}/\text{nm}$ ):** 456, 487, 522

**Fluorescence (DMF) ( $\lambda_{\max}/\text{nm}$ ):** 534, 574, 624

**$\Phi_f$  (Fluorescence Quantum Yield, DMF):** 0.7.



### **3.6 Synthesis of *N*-((2*S*)-amino hexanoic acid)-3,4,10-perylene tetracarboxylic-3,4-anhydride-9,10-imide conjugated chitosan (LCP3).**

LPMI (0.133 g, 0.255 mmol), low molecular weight chitosan (CH) (0.8 g, 4.9640 mmol) and zinc acetate (0.057 g, 0.26 mmol) were stirred in an accurately dried solvent mixture of isoquinoline (8 mL) and *m*-cresol (40 mL) under argon atmosphere at 80 °C for 4 h, at 120 °C for 6 h, at 140 °C for 2 h, at 180 °C for 2 h and finally at 200 °C for 2 h. The reaction solution was transferred into 300 mL of cold methanol. The solution was filtered by suction filtration. The synthesized crude product first washed with water and acetic acid (1 %), then synthesized compound was purified by chloroform Soxhlet extraction for 24 h. After that, a vacuum at 100 °C was used to dry the pure product.

**Yield:** 0.394 g

**Color:** Black

**FT-IR (KBr, cm<sup>-1</sup>):**  $\nu = 3386, 3061, 2920, 2851, 1691, 1655, 1593, 1438, 1342, 1252, 1064, 809, 746.$

**UV-vis (DMF) ( $\lambda_{\max}/\text{nm}$ ):** 460, 488, 522

**Fluorescence (DMF) ( $\lambda_{\max}/\text{nm}$ ):** 533, 573, 623

**$\Phi_f$  (Fluorescence Quantum Yield, DMF):** 0.73.

### **3.7 Synthesis of *N*-((2*S*)-amino hexanoic acid)-3,4,10-perylene tetracarboxylic-3,4-anhydride-9,10-imide conjugated chitosan (LCP4).**

LPMI (0.2 g, 0.384 mmol), low molecular weight chitosan (CH) (0.8 g, 4.9640 mmol) and zinc acetate (0.085 g, 0.387 mmol) were stirred in an accurately dried solvent mixture of isoquinoline (8 mL) and *m*-cresol (40 mL) under argon atmosphere at 80 °C for 4 h, at 120 °C for 6 h, at 140 °C for 2 h, at 180 °C for 2 h and finally at 200 °C for 2 h. The reaction solution was transferred into 300 mL of cold methanol. The solution was filtered by suction filtration. The synthesized crude product first washed with water and acetic acid (1 %), then the synthesized compound was purified by chloroform Soxhlet extraction for 24 h. After that, a vacuum at 100 °C was used to dry the pure product.

**Yield:** 0.416 g

**Color:** Black

**FT-IR (KBr, cm<sup>-1</sup>):**  $\nu = 3386, 3061, 2922, 2852, 1692, 1655, 1593, 1438, 1342, 1252, 1066, 810, 746.$

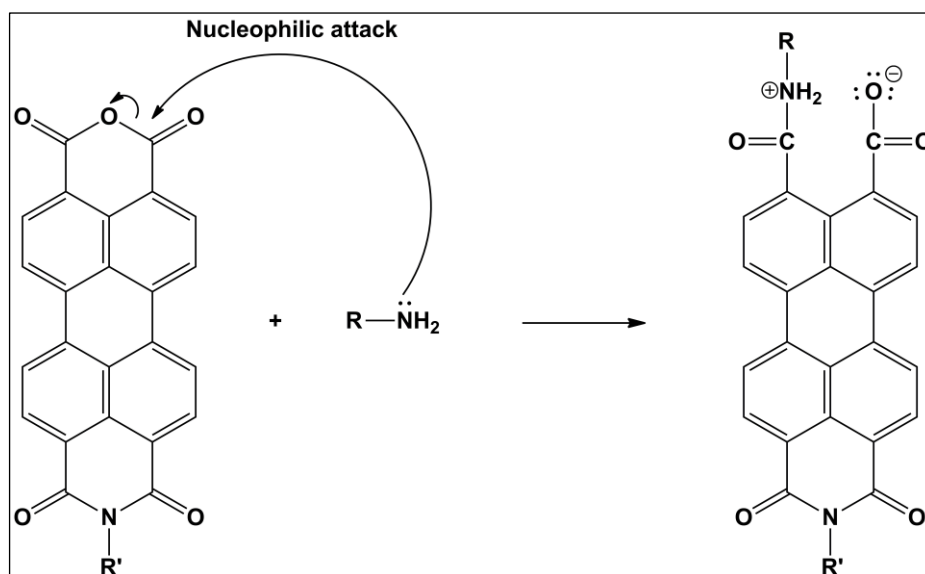
**UV-vis (DMF) ( $\lambda_{\max}/\text{nm}$ ):** 487, 523.

**Fluorescence (DMF) ( $\lambda_{\max}/\text{nm}$ ):** 534, 574, 625.

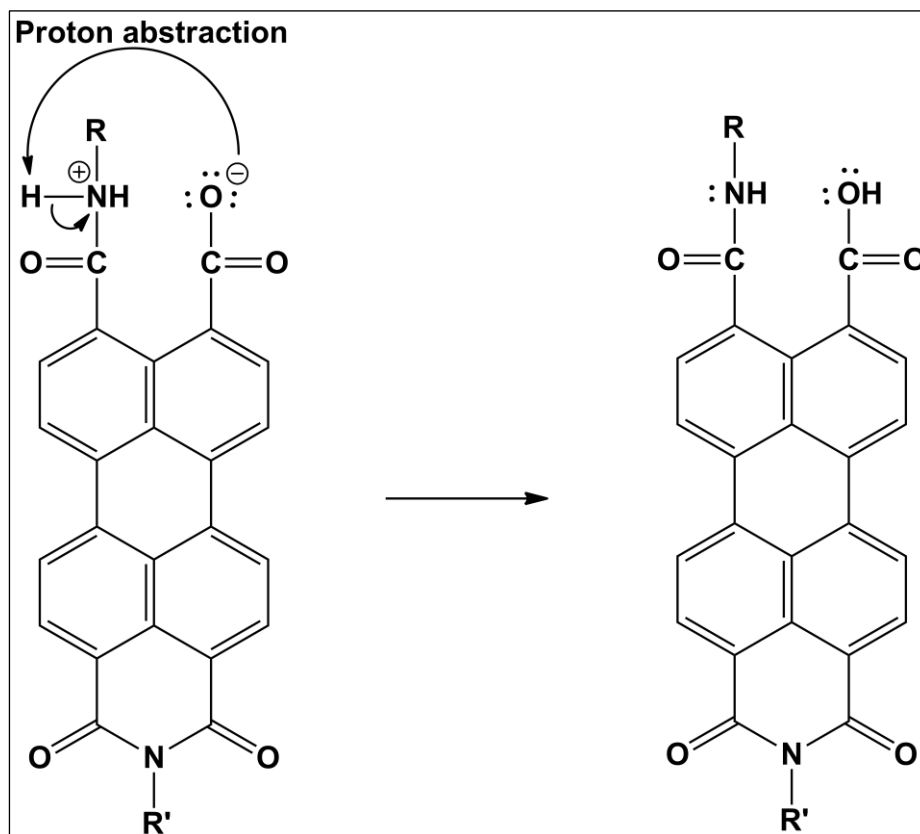
**$\Phi_f$  (Fluorescence Quantum Yield, DMF):** 0.87.

### 3.8 General Reaction Mechanism of PDI

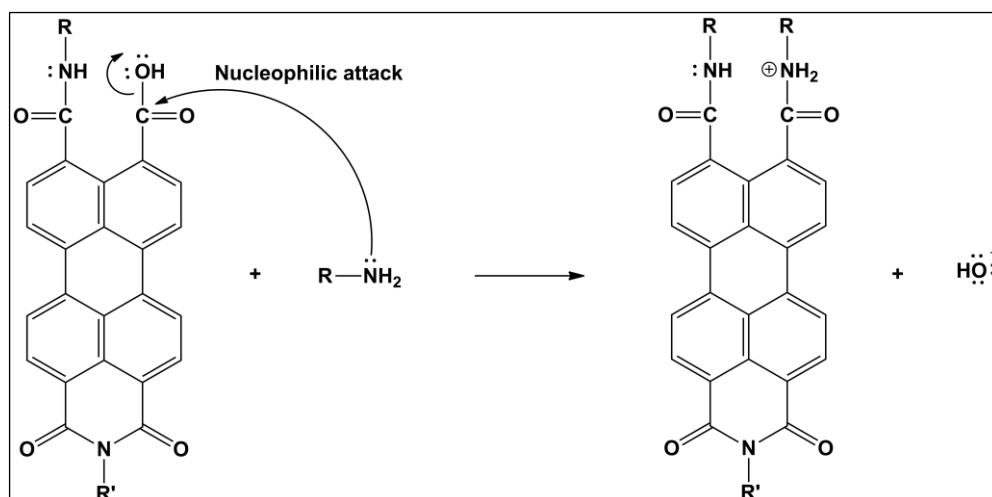
#### Step 1



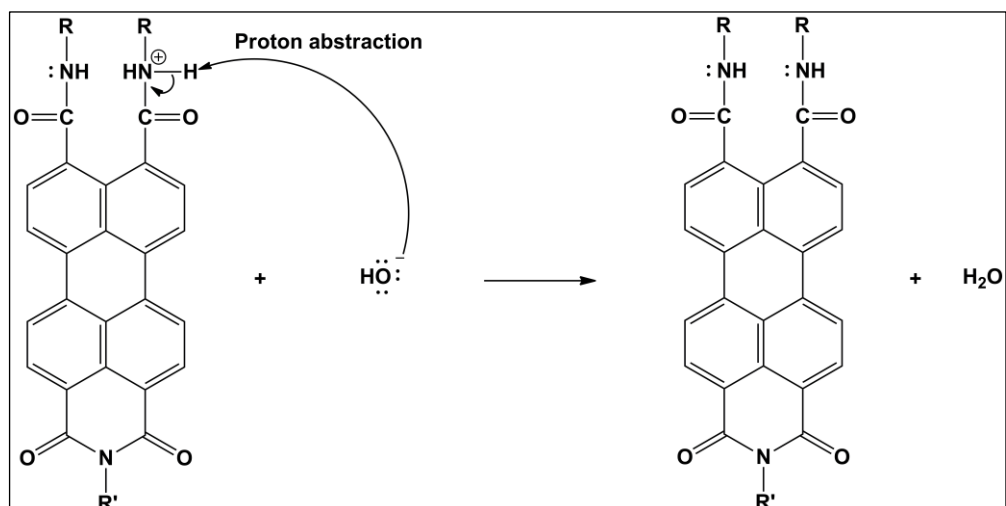
#### Step 2



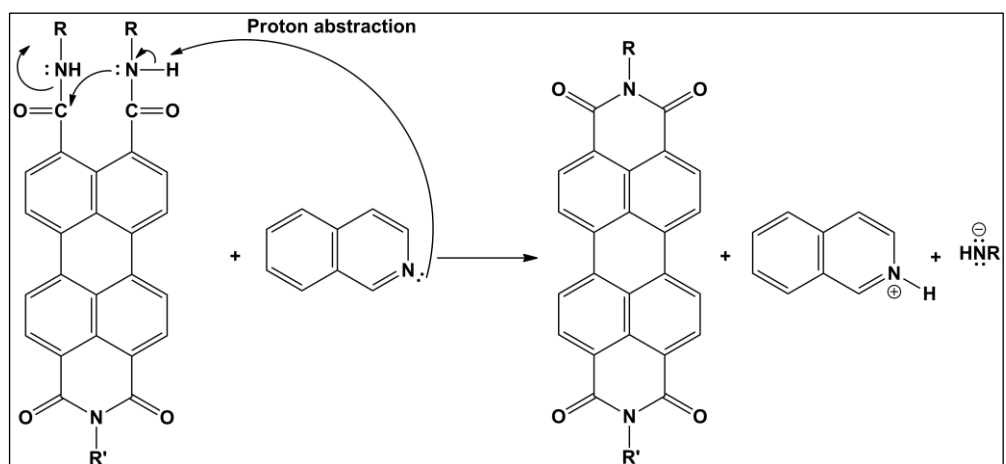
### Step 3



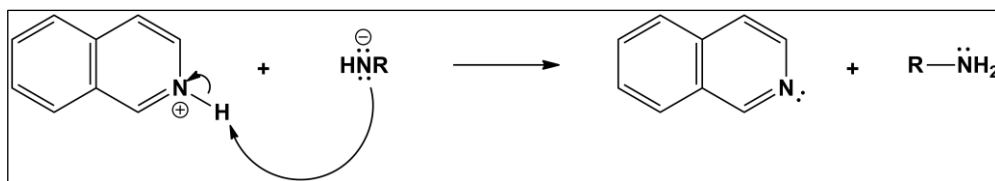
### Step 4



### Step 5



## Step 6



## Chapter 4

# DATA AND CALCULATION

### 4.1 Optical and Photochemical Properties

#### 4.1.1 Fluorescence Quantum Yield ( $\Phi_f$ )

If a chromophore absorbs a light, substantially excited state will formed. At the end process, this chromophore return to the ground state via deactivation processes (loss of energy). Different deactivation processes could occur, such as fluorescence emission, phosphorescence, internal conversion, energy transfer, etc (Figure 4.1).

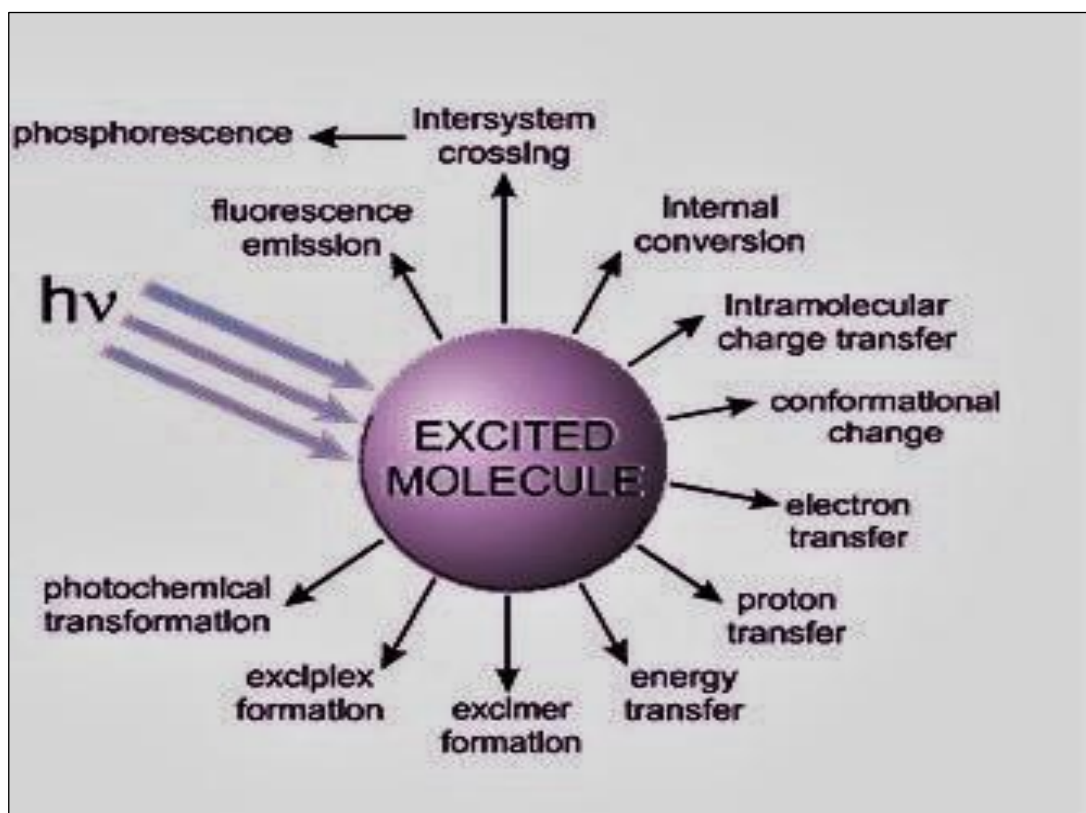


Figure 4.1: Possible Deactivation Pathways of Excited Molecules

Among these processes, fluorescence emission is the most important radiative process. ( $\Phi_f$ ) is the ratio of photons absorbed and emitted through the fluorescence emission process.

The comparative methodology is the most accurate process for recording  $\Phi_f$  which involved the application of completely characterized standard samples with recognized  $\Phi_f$  numeric values. Basically, standard solutions of knowing samples and unknown compound with similar absorbance at equal excitation wavelengths could be supposed to be absorbing the similar amount of light. Thus, the ratio of the integrated emission intensity of standard and unknown solutions would yield fluorescence quantum yield ratio [51].

$$\Phi_f(\text{U}) = \Phi_r \times \frac{A_r}{A_u} \times \frac{S_u}{S_r} \times \left[ \frac{n_u}{n_r} \right]^2 \quad (\text{Eqn. 4.1})$$

Where,

$\Phi_f(\text{U})$ : Fluorescence quantum yield of unknown

$\Phi_r$ : Fluorescence quantum yield of reference

$A_r$ : Absorbance of the reference at the excitation wavelength

$A_u$ : Absorbance of the unknown excitation wavelength

$S_r$ : Intergrated emission area across the band of reference

$S_u$ : Intergrated emission area across the band of unknown

$n_r$ : Refractive index of reference solvent

$n_u$ : Refractive index of unknown solvent

In this thesis,  $\Phi_f$  of synthesized compounds were measured in various solvents by using *N,N'*-di(dodecyl)-3,4,9,10-perylenebis(dicaroximide) ( $\Phi_f = 1$ ) as reference in

chloroform. ( $\lambda_{\max} = 485 \text{ nm}$ ). Both, the reference and unknown compounds were excited at 485 nm wavelength.

$\Phi_f$  calculation of LCP4 in DMF

$$\Phi_f = 1$$

$$A_r = 0.1003$$

$$A_u = 0.1065$$

$$S_u = 816.211$$

$$S_r = 851.81$$

$$n_r = 1.4458$$

$$n_u = 1.4305$$

$$\Phi_f (U) = 1 \times \frac{0.1003}{0.1065} \times \frac{816.211}{851.81} \times \left[ \frac{1.4305}{1.4458} \right]^2$$

$$\Phi_f (U) = 0.87$$

The fluorescence quantum yield of all the synthesized LCPs at various solvents were calculated by using the similar method. Table 4.1 shows the obtained  $\Phi_f$  values.



Table 4.1: Fluorescence quantum yield values of LCPs

Solvent	LCP1	LCP2	LCP3	LCP4
	$\Phi_f$	$\Phi_f$	$\Phi_f$	$\Phi_f$
NMP	0.21	0.38	0.25	0.22
DMF	0.50	0.70	0.73	0.87
DMAc	0.12	0.23	0.12	0.26
DMSO	0.10	0.2	0.09	0.18

#### 4.1.2 Half-Width of Selected Absorption Band ( $\Delta\bar{\nu}_{1/2}$ )

The half-width of absorption band is described by the curve at half maximum intensity. The Equation 4.2 was used to determine the half-width of the selected maximum absorption of the synthesized compounds.

$$\Delta\bar{\nu}_{1/2} = \bar{\nu}_1 - \bar{\nu}_2 \quad (\text{Eqn. 4.2})$$

Where,

$\bar{\nu}_1, \bar{\nu}_2$ : The wavenumber from absorption spectrum

$\Delta\bar{\nu}_{1/2}$ : Half-width of the selected maximum absorption

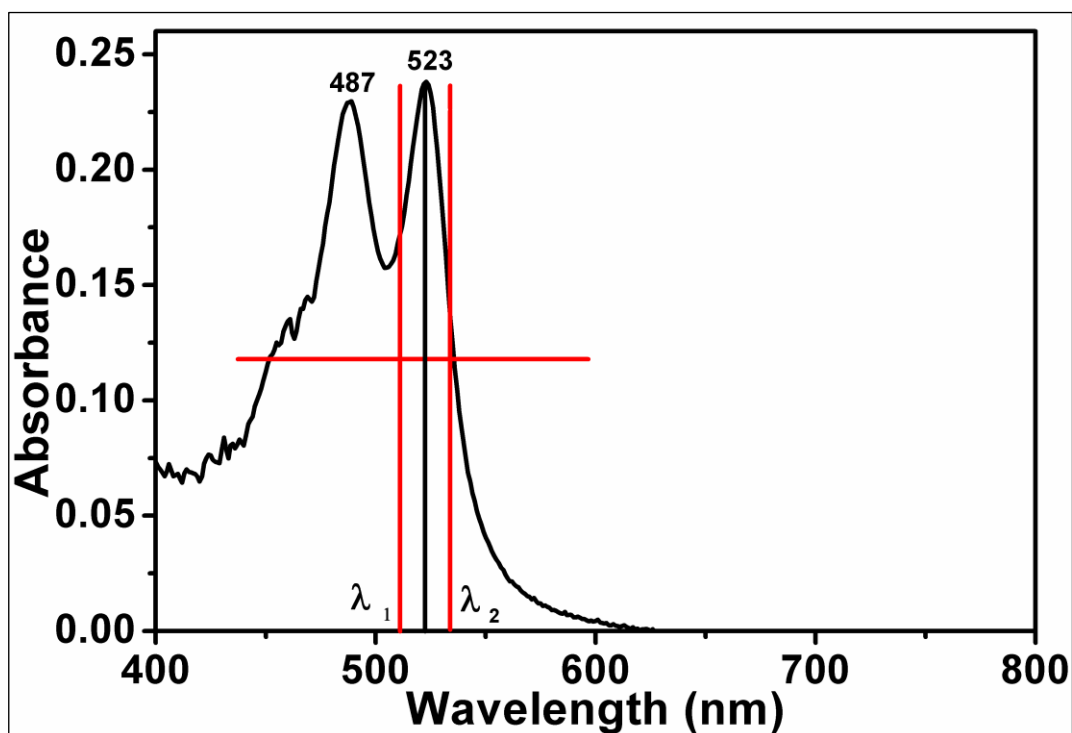


Figure 4.2: LCP4, Plot to deduce the Half-width (DMF)

From the Figure 4.2,

$$\lambda_{\max} = 523 \text{ nm}$$

$$\text{Absorption of half-width} = 0.122$$

$$\lambda_1 = 508 \text{ nm}$$

$$\lambda_2 = 530 \text{ nm} \quad \lambda_1 = 508 \times \frac{10^{-9} \text{ m}}{1 \text{ nm}} \times \frac{1 \text{ cm}}{10^{-9} \text{ m}} = 5.08 \times 10^{-5} \text{ cm}$$

$$\bar{\nu}_1 = \frac{1}{\lambda_1} = \frac{1}{5.08 \times 10^{-5}} = 19685.04 \text{ cm}^{-1}$$

$$\lambda_2 = 530 \text{ nm} \times \frac{10^{-9} \text{ m}}{1 \text{ nm}} \times \frac{1 \text{ cm}}{10^{-2} \text{ m}} = 5.3 \times 10^{-5} \text{ cm}$$

$$\bar{\nu}_2 = \frac{1}{\lambda_2} = \frac{1}{5.30 \times 10^{-5}} = 18867.92 \text{ cm}^{-1}$$

$$\Delta\bar{\nu}_{1/2} = \bar{\nu}_1 - \bar{\nu}_2 = 19685.04 - 18867.92 = 817.12 \text{ cm}^{-1}$$

Similar steps were done to calculate the half-widths of LCPs in various solvents the results were represented in the following tab

Table 4.2: The half-widths of LCPs in various solvents

Solvents	LCP1				LCP2				LCP3				LCP4			
	$\lambda_{\max}$ (nm)	$\lambda_1$ (nm)	$\lambda_2$ (nm)	$\Delta\bar{\nu}_{1/2}$ ( $\text{cm}^{-1}$ )	$\lambda_{\max}$ (nm)	$\lambda_1$ (nm)	$\lambda_2$ (nm)	$\Delta\bar{\nu}_{1/2}$ ( $\text{cm}^{-1}$ )	$\lambda_{\max}$ (nm)	$\lambda_1$ (nm)	$\lambda_2$ (nm)	$\Delta\bar{\nu}_{1/2}$ ( $\text{cm}^{-1}$ )	$\lambda_{\max}$ (nm)	$\lambda_1$ (nm)	$\lambda_2$ (nm)	$\Delta\bar{\nu}_{1/2}$ ( $\text{cm}^{-1}$ )
<b>NMP</b>	524	512	554	1480.7	522	504	548	1593.1	524	506	550	1581	524	508	544	1302.7
<b>DMF</b>	522	504	542	1391.1	522	504	538	1253.9	522	504	540	1322.7	523	508	530	817.12
<b>DMAc</b>	523	502	562	2126.7	522	504	546	1526.2	524	508	550	1503.2	522	506	546	1447.8
<b>DMSO</b>	526	508	550	1503.2	526	508	524	601.07	526	512	550	1349.4	526	510	546	1292.8

### 4.1.3 Singlet Energies ( $E_S$ )

For a fluorophore, singlet energy is the least amount of energy required to form excited state. Equation 4.3 was used to calculate the singlet energies of LCPs polymer in different solvents.

$$E_S = \frac{2.86 \times 10^5}{\lambda_{max}} \quad (\text{Eqn. 4.3})$$

Where,

$E_S$ : Singlet energy in kcal.mol<sup>-1</sup>

$\lambda_{max}$ : The maximum absorption wavelength in Å

$E_S$  calculation of LCP4 in DMF

At  $\lambda_{max} = 524 \text{ nm}$

$$\lambda_{max} = 524 \text{ nm} \times \frac{10^{-9} \text{ m}}{1 \text{ nm}} \times \frac{1 \text{ \AA}}{10^{-10} \text{ m}} = 5240 \text{ \AA}$$

$$E_S = \frac{2.86 \times 10^5}{5240}$$

$$E_S = 54.58 \text{ kcal.mol}^{-1}$$

The calculated values of singlet energies of LCPs in different solvents were represented in the following table.

Table 4.3: The singlet energies of LCPs in various solvents

Solvent	LCP1		LCP2		LCP3		LCP4	
	$\lambda_{\max}$ (Å)	$E_s$ (kcal.mol <sup>-1</sup> )	$\lambda_{\max}$ (Å)	$E_s$ (kcal.mol <sup>-1</sup> )	$\lambda_{\max}$ (Å)	$E_s$ (kcal.mol <sup>-1</sup> )	$\lambda_{\max}$ (Å)	$E_s$ (kcal. mol <sup>-1</sup> )
<b>NMP</b>	5240	54.58	5220	54.79	5240	54.58	5240	54.58
<b>DMF</b>	5220	54.79	5220	54.79	5220	54.79	5230	54.68
<b>DMAc</b>	5230	54.68	5220	54.79	5240	54.58	5220	54.79
<b>DMSO</b>	5260	54.37	5260	54.37	5260	54.37	5260	54.37

#### 4.1.4 Optical Band Gap Energies ( $E_g$ )

The optical band gap energy was deduced from the absorption spectrum of the substance by extrapolating the maximum absorption ( $0 \rightarrow 0$  absorption band) to zero absorbance. It was determined by using Equation 4.4 [52].

$$E_g = \frac{1240 \text{ eV nm}}{\lambda} \quad (\text{Eqn. 4.4})$$

Where,

$E_g$ : Band gap energy (eV)

$\lambda$ : Cut-off wave length of the absorption band (nm)

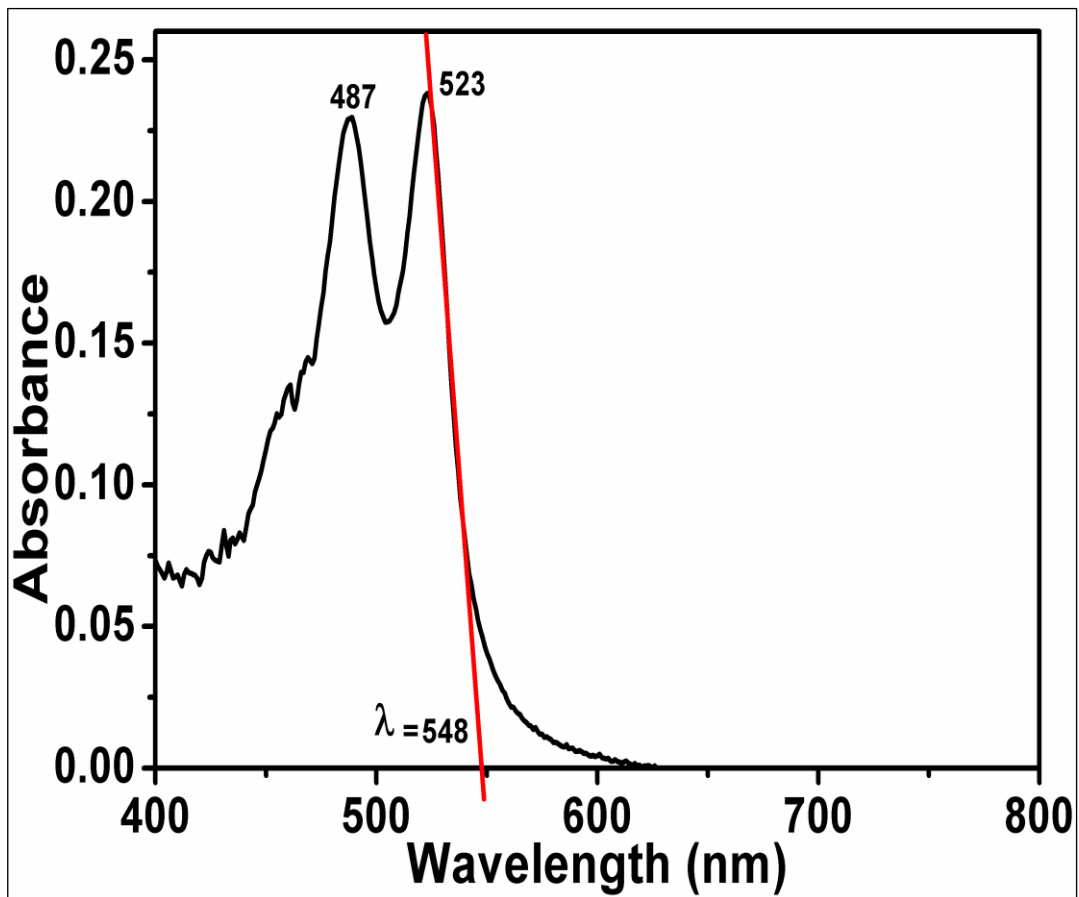


Figure 4.3: LCP4, Plot to deduce the band gap energy (DMF)

As shown in Figure 4.3

At  $\lambda = 548$  nm

$$E_g = \frac{1240 \text{ eV nm}}{548 \text{ nm}} = 2.263 \text{ eV}$$

$$E_g = 2.263 \text{ eV}$$

The calculated values of singlet energies of LCPs in different solvents were summarized below in the Table 4.4.





Table 4.4: Optical band gap energies of LCPs in different solvent

<b>Solvent</b>	<b>LCP1</b>		<b>LCP2</b>		<b>LCP3</b>		<b>LCP4</b>	
	$\lambda$ (nm)	$E_g$ (eV)	$\lambda$ (nm)	$E_g$ (eV)	$\lambda$ (nm)	$E_g$ (eV)	$\lambda$ (nm)	$E_g$ (eV)
<b>NMP</b>	592	2.094	568	2.183	574	2.160	570	2.175
<b>DMF</b>	560	2.214	554	2.238	556	2.230	548	2.263
<b>DMAc</b>	600	2.067	580	2.138	580	2.138	572	2.168
<b>DMSO</b>	578	2.145	558	2.222	538	2.305	562	2.206



### 4.1.5 Absorption Intensity Ratios

Absorption intensity ratio is described as the ratio of the absorption between  $0 \rightarrow 0$  and  $0 \rightarrow 1$  where  $0 \rightarrow 0$  and  $0 \rightarrow 1$  are vibronic transition. Aggregation of molecules can be indicated from intensity ratio values. When  $A^{0 \rightarrow 0}/A^{0 \rightarrow 1} \approx 1.6$ , the monomeric molecules display normal Franck-Condon progression. But, if  $A^{0 \rightarrow 0}/A^{0 \rightarrow 1} \leq 0.7$ , chromophores show strongly aggregation in solvents [10]. The intensity ratios of the LCPs polymers were calculated by using Equation 4.5.

$$\text{Intensity ratio} = R_{\text{abs}} = \frac{A^{0 \rightarrow 0}}{A^{0 \rightarrow 1}} \quad (\text{Eqn 4.5})$$

Where,

$A^{0 \rightarrow 0}$ : Absorption intensity of  $0 \rightarrow 0$  vibronic transition

$A^{0 \rightarrow 1}$ : Absorption intensity of  $0 \rightarrow 1$  vibronic transition

Table 4.5: Intensity ratios of LCPs in different solvent

Solvent	LCP1 $\frac{A^{0 \rightarrow 0}}{A^{0 \rightarrow 1}}$	LCP2 $\frac{A^{0 \rightarrow 0}}{A^{0 \rightarrow 1}}$	LCP3 $\frac{A^{0 \rightarrow 0}}{A^{0 \rightarrow 1}}$	LCP4 $\frac{A^{0 \rightarrow 0}}{A^{0 \rightarrow 1}}$
<b>NMP</b>	0.84	0.97	0.93	0.858
<b>DMF</b>	1.02	1.08	1.08	1.04
<b>DMAc</b>	0.97	0.94	0.91	0.86
<b>DMSO</b>	1.0	1.076	0.88	0.89

### 4.1.6 Stokes Shifts

The difference between excitation and emission maximum called Stokes's shift which relatively indicate the amount of nonradiative energy that was lost. Stokes shifts of LCPs compounds was calculated and represented in the Table 4.6.

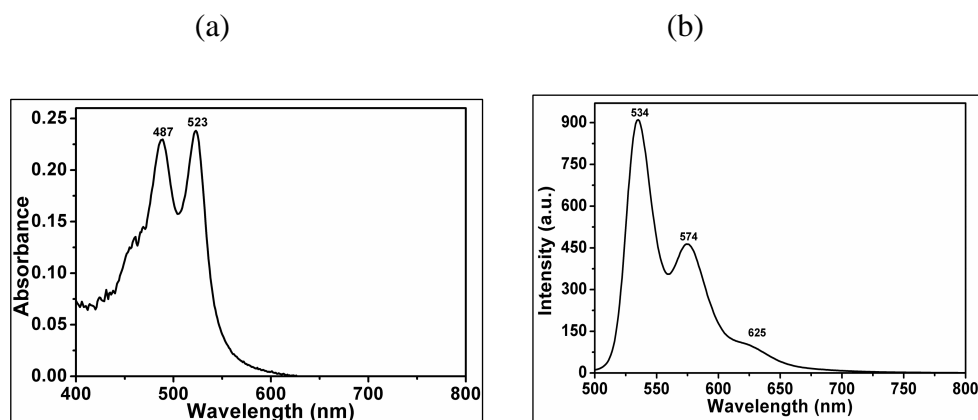


Figure 4.4: (a) Absorption and

(b) emission of LCP4 in DMF

Table 4.6: Stokes shifts of LCPs in different solvents

Solvent	LCP1		LCP2		LCP3		LCP4	
	Stokes Shift (nm)	Stokes Shift (cm <sup>-1</sup> )	Stokes Shift (nm)	Stokes Shift (cm <sup>-1</sup> )	Stokes Shift (nm)	Stokes Shift (cm <sup>-1</sup> )	Stokes Shift (nm)	Stokes Shift (cm <sup>-1</sup> )
NMP	11	909,090	14	714,285	11	909,090	12	833,333
DMF	12	833,333	12	833,333	12	833,333	11	909,090
DMAc	10	1,000,000	11	909,090	9	1,111,111	11	909,090
DMSO	12	833,333	12	833,333	13	769,230	14	714.285

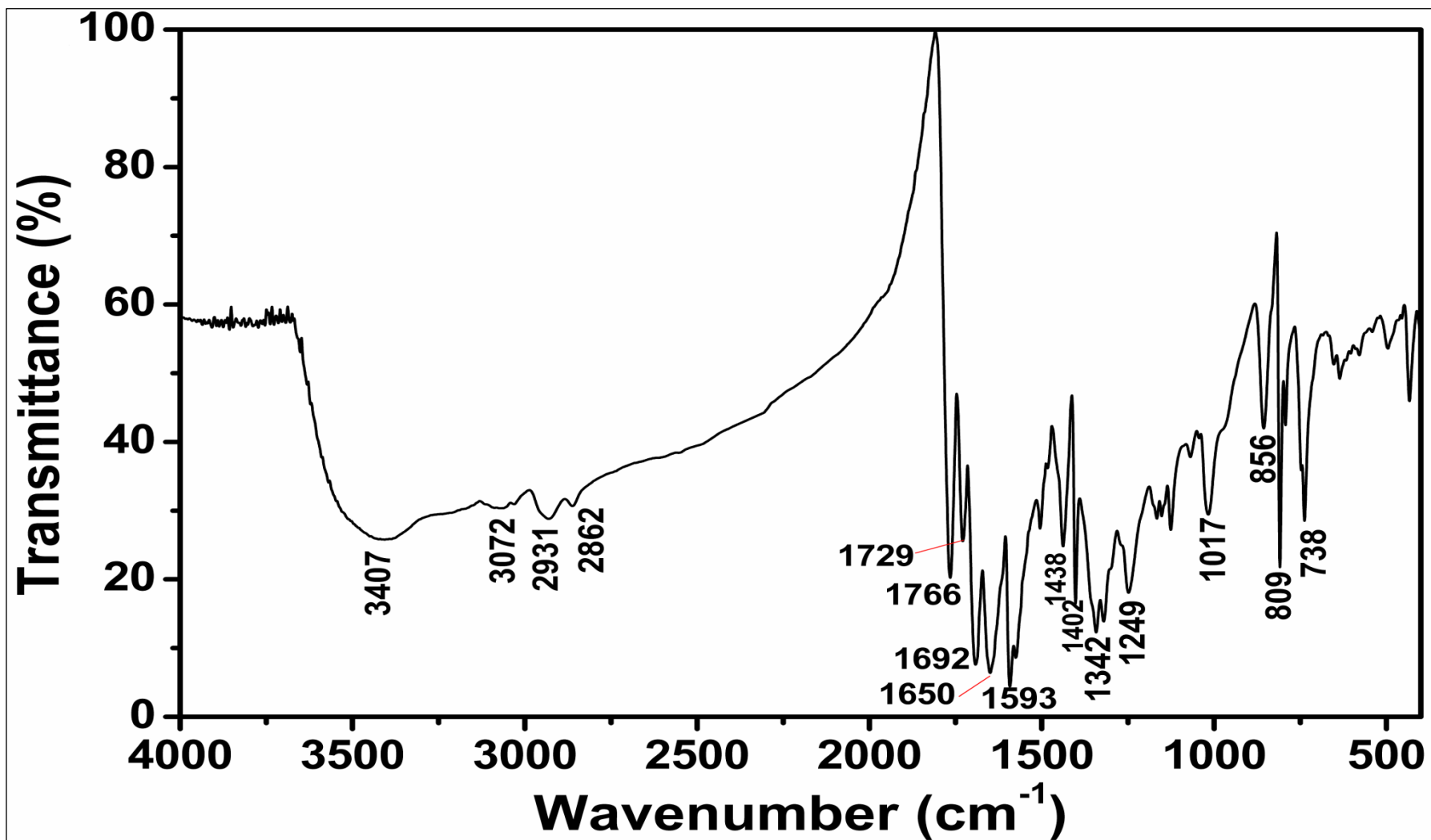


Figure 4.5: LPMI, FTIR Spectrum

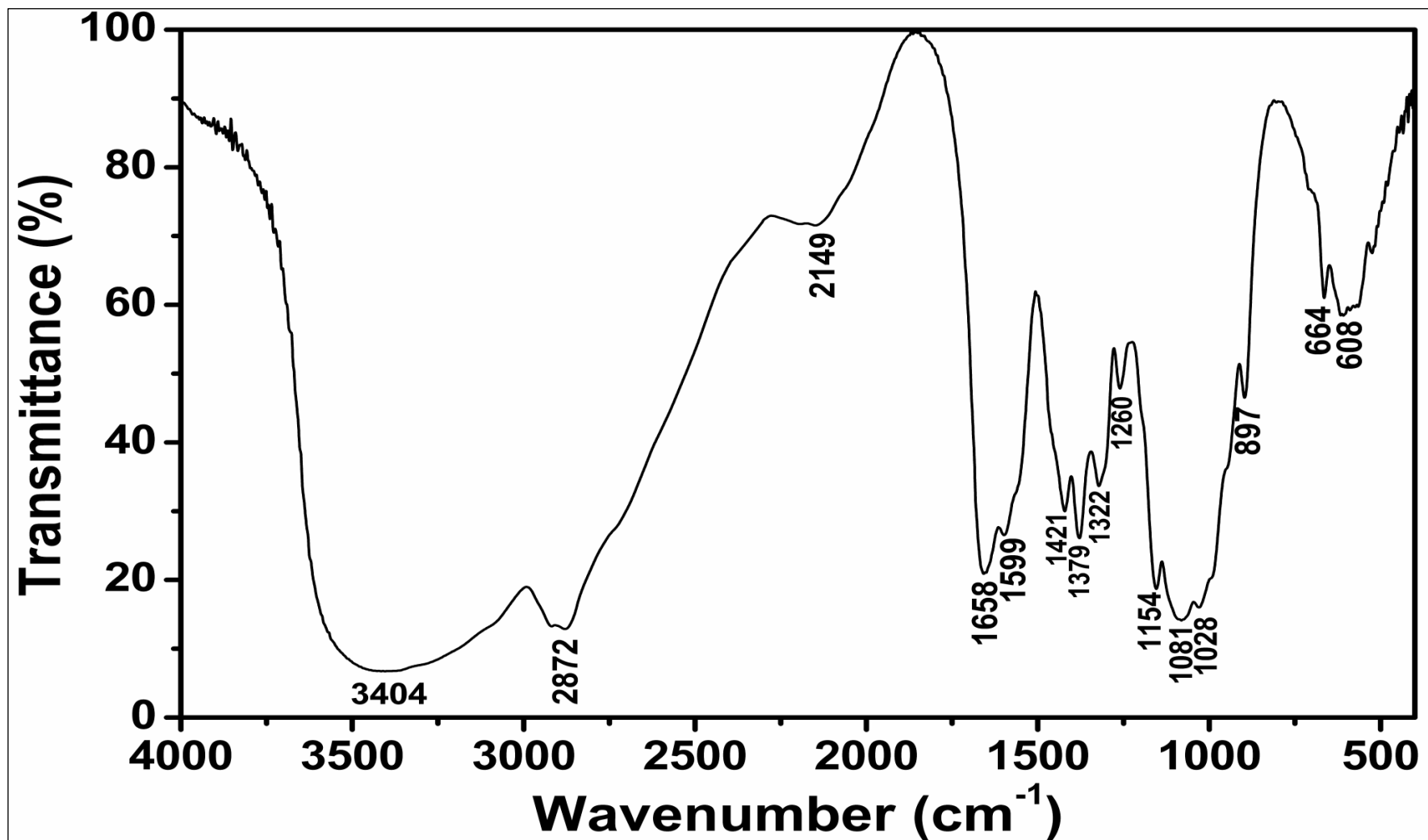


Figure 4.6: CH, FTIR Spectrum

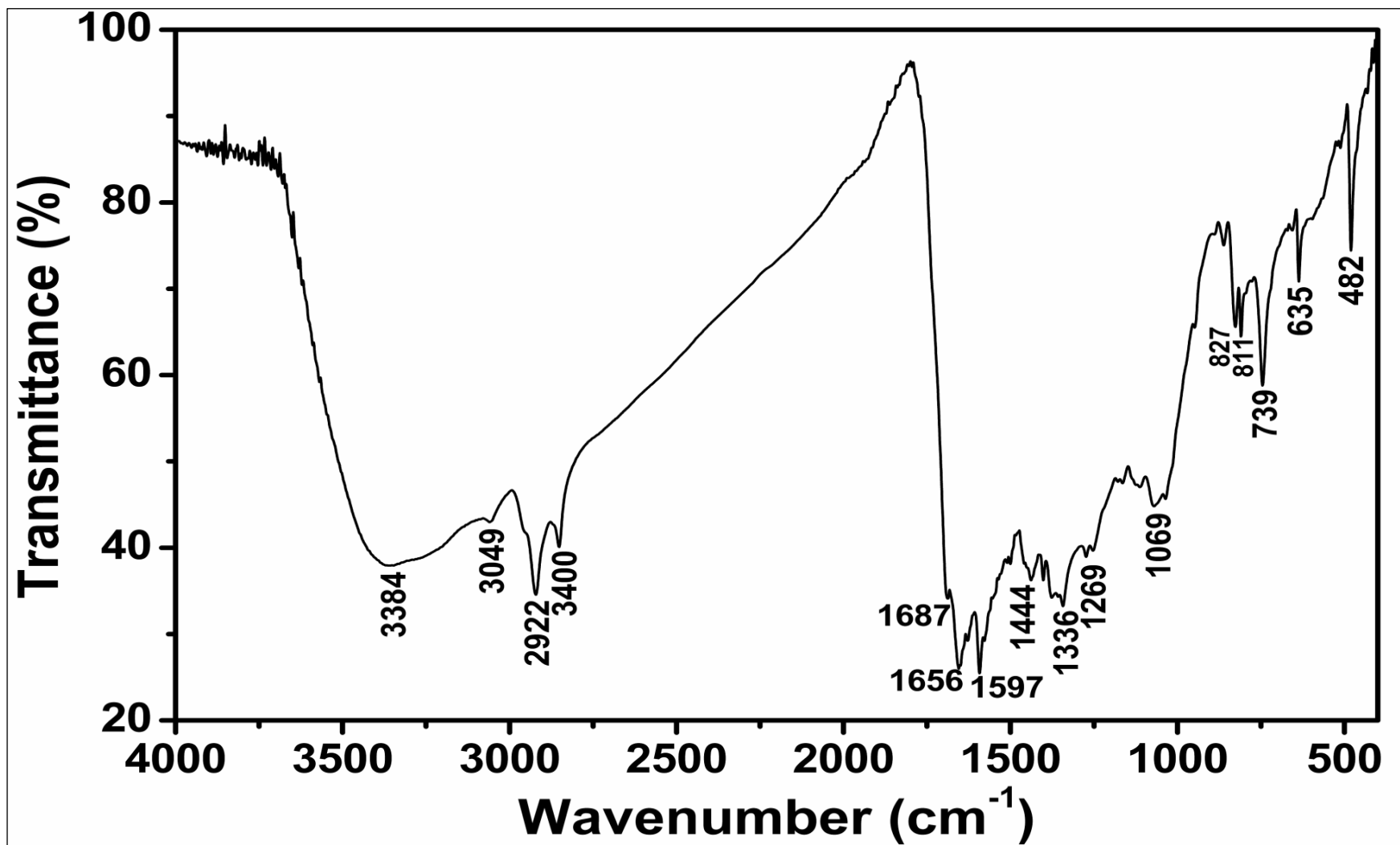


Figure 4.7: LCPI, FTIR Spectrum

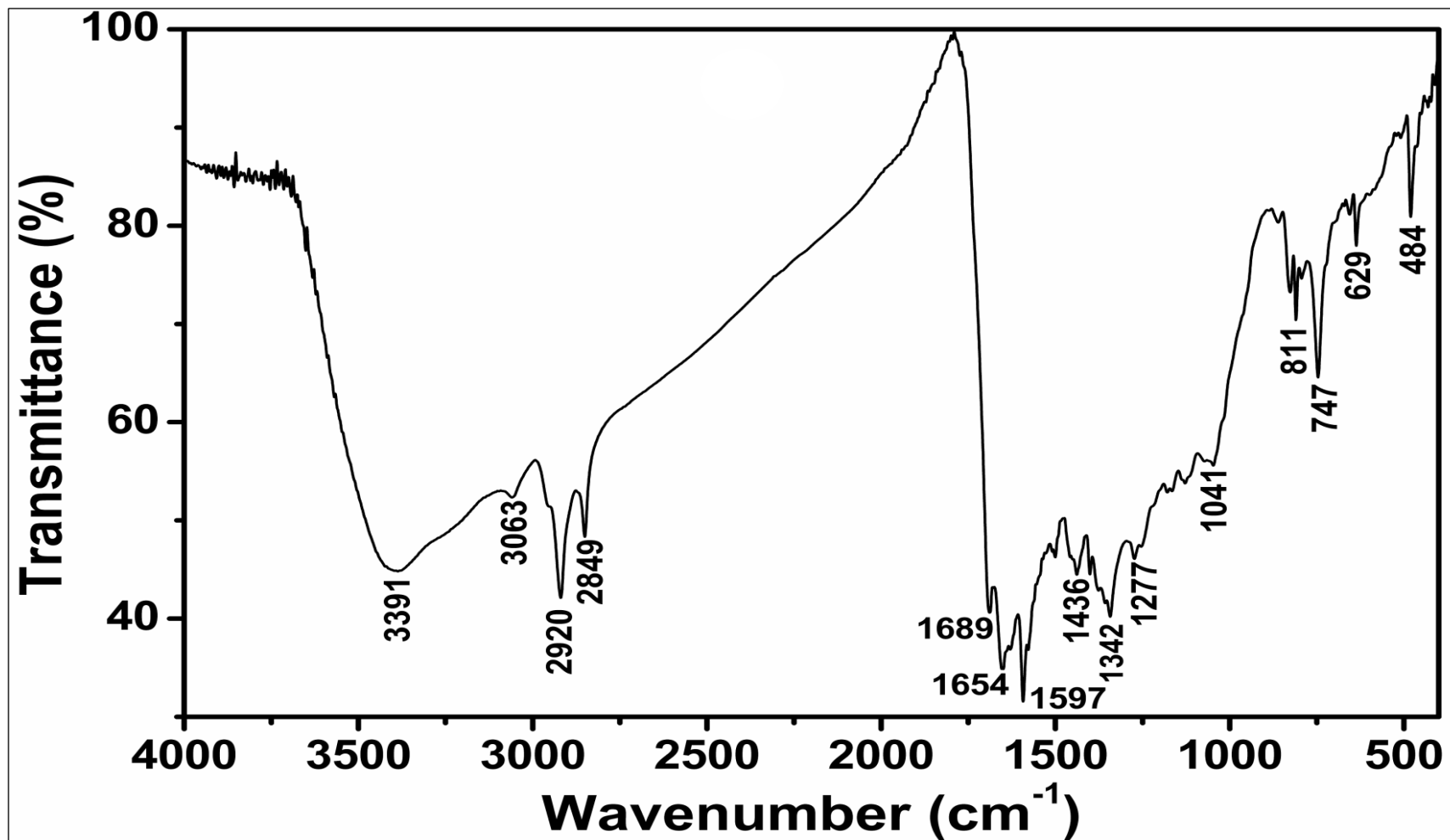


Figure 4.8: LCP2, FTIR Spectrum



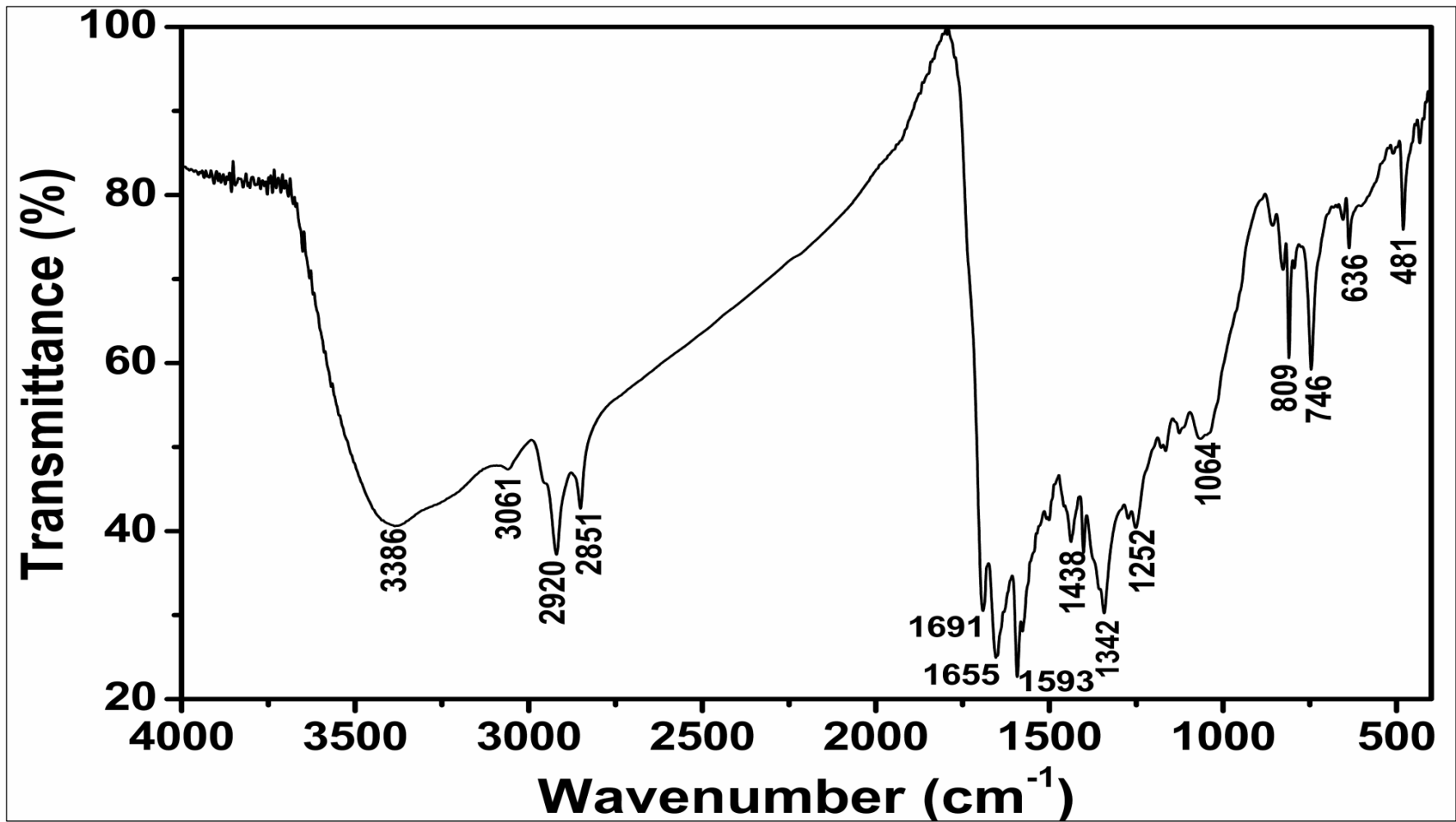


Figure 4.9: LCP3, FTIR Spectrum

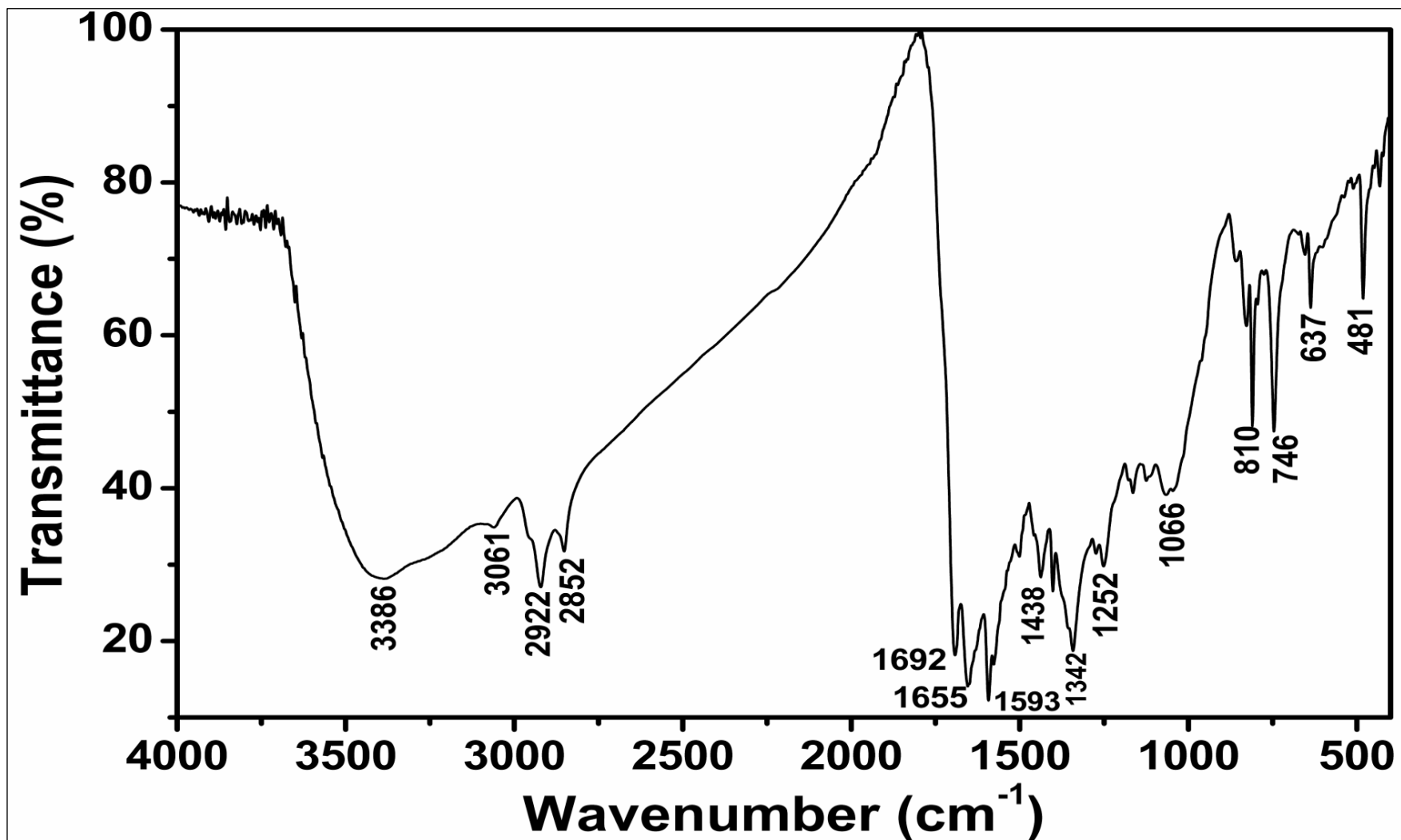


Figure 4.10: LCP4, FTIR Spectrum

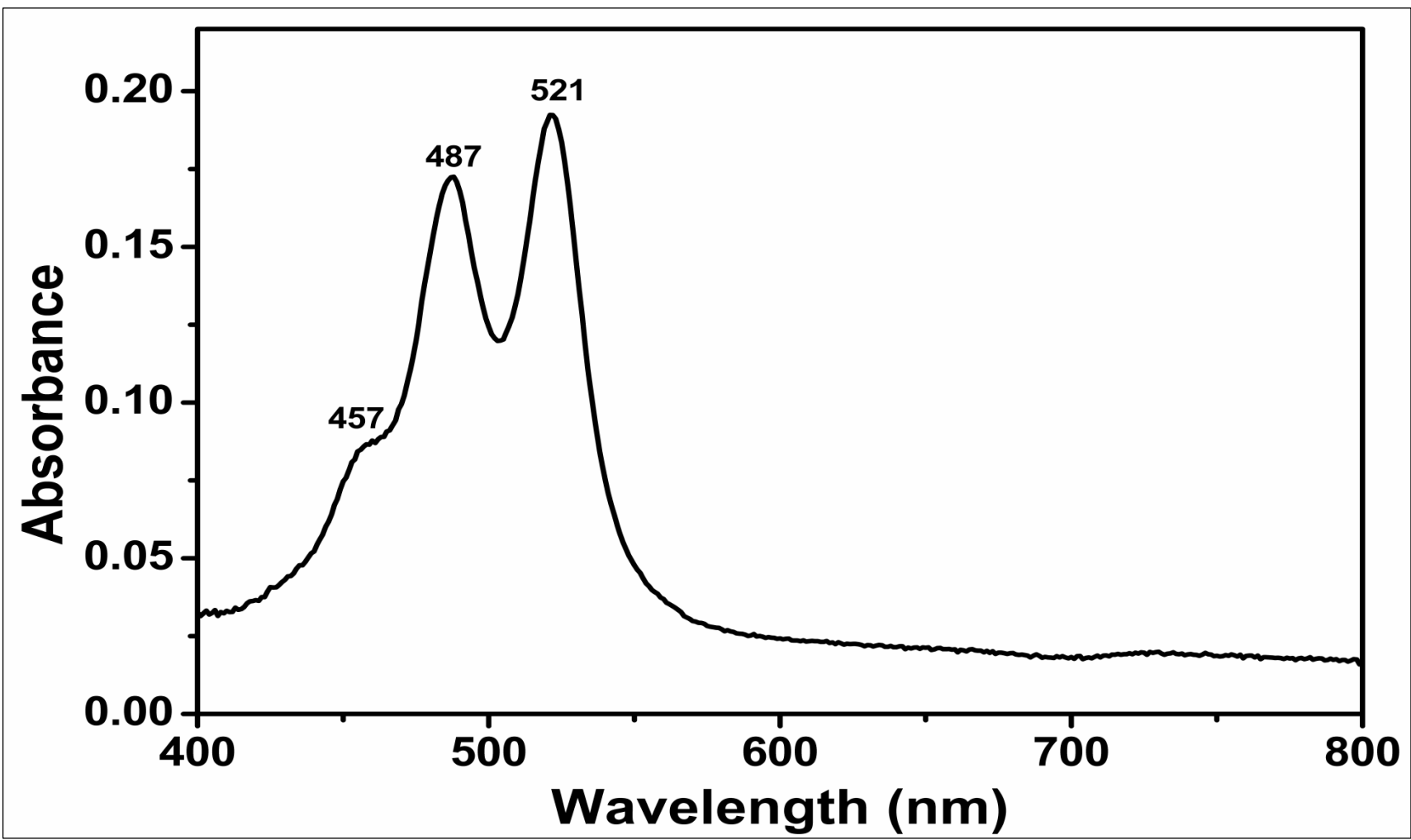


Figure 4.11: LPMI, Absorption Spectrum (DMSO)

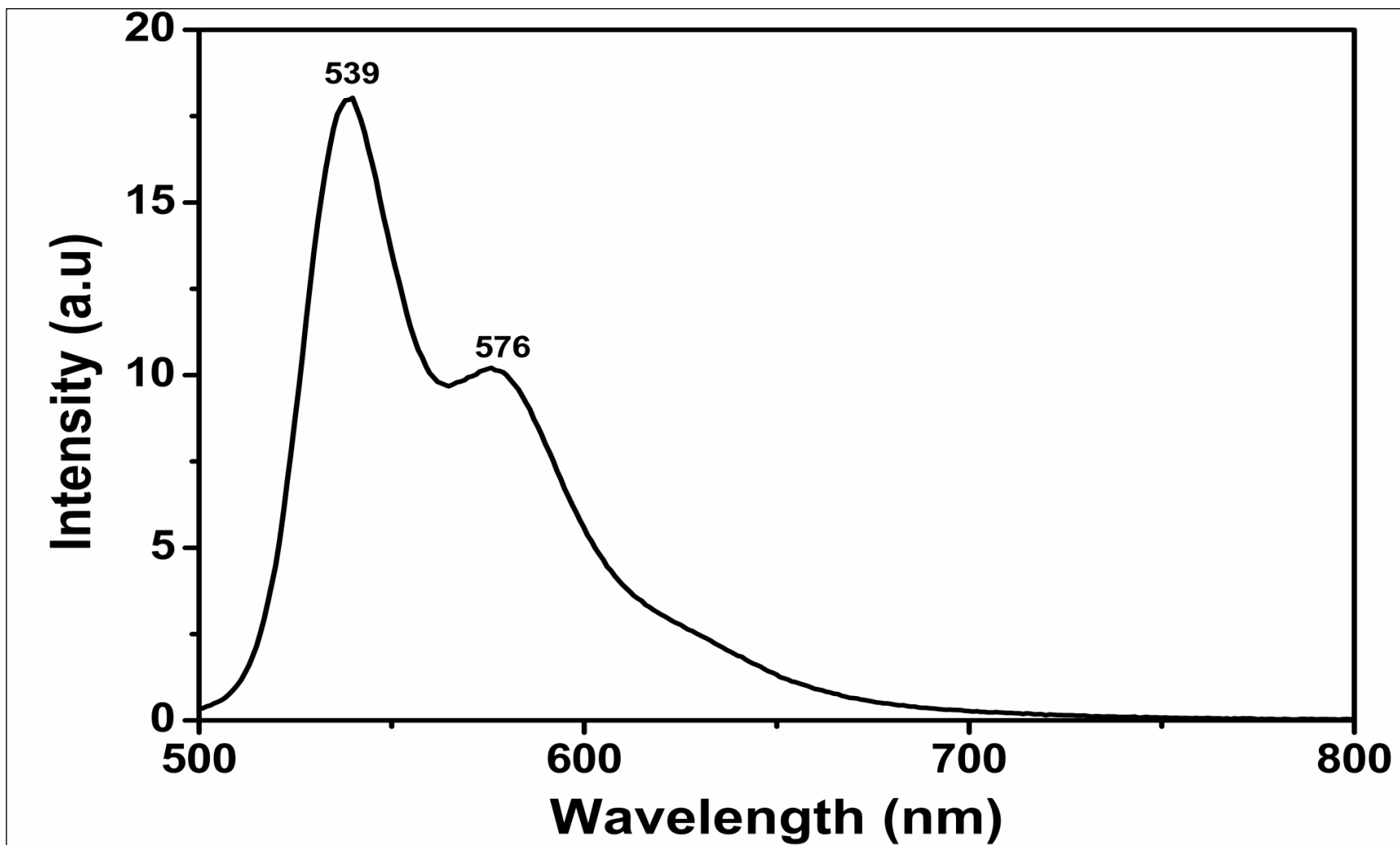


Figure 4.12: LPMI, Emission Spectrum (DMSO)

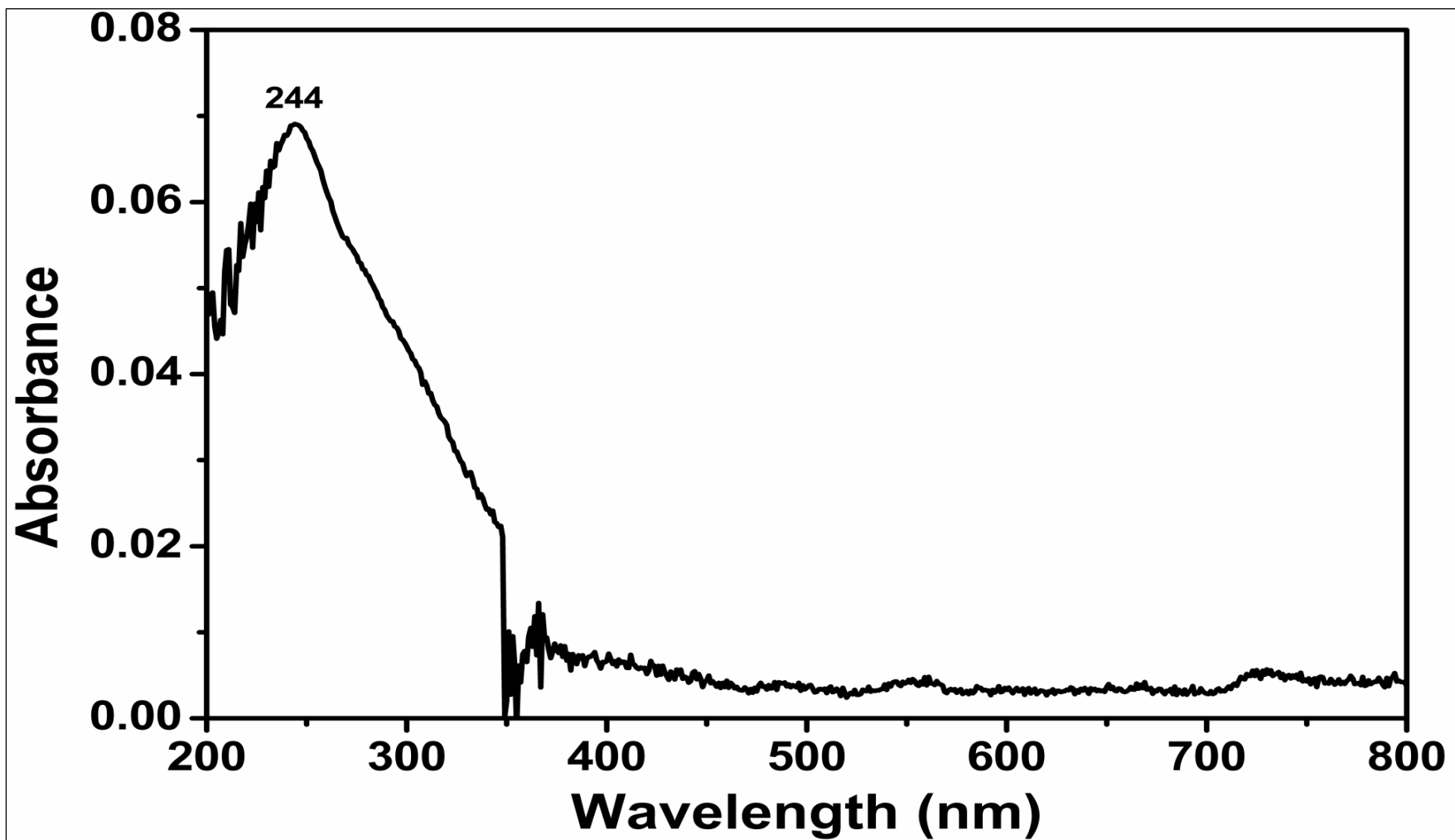


Figure 4.13: CH, Absorption Spectrum (1 %  $\text{CH}_3\text{COOH}$ )

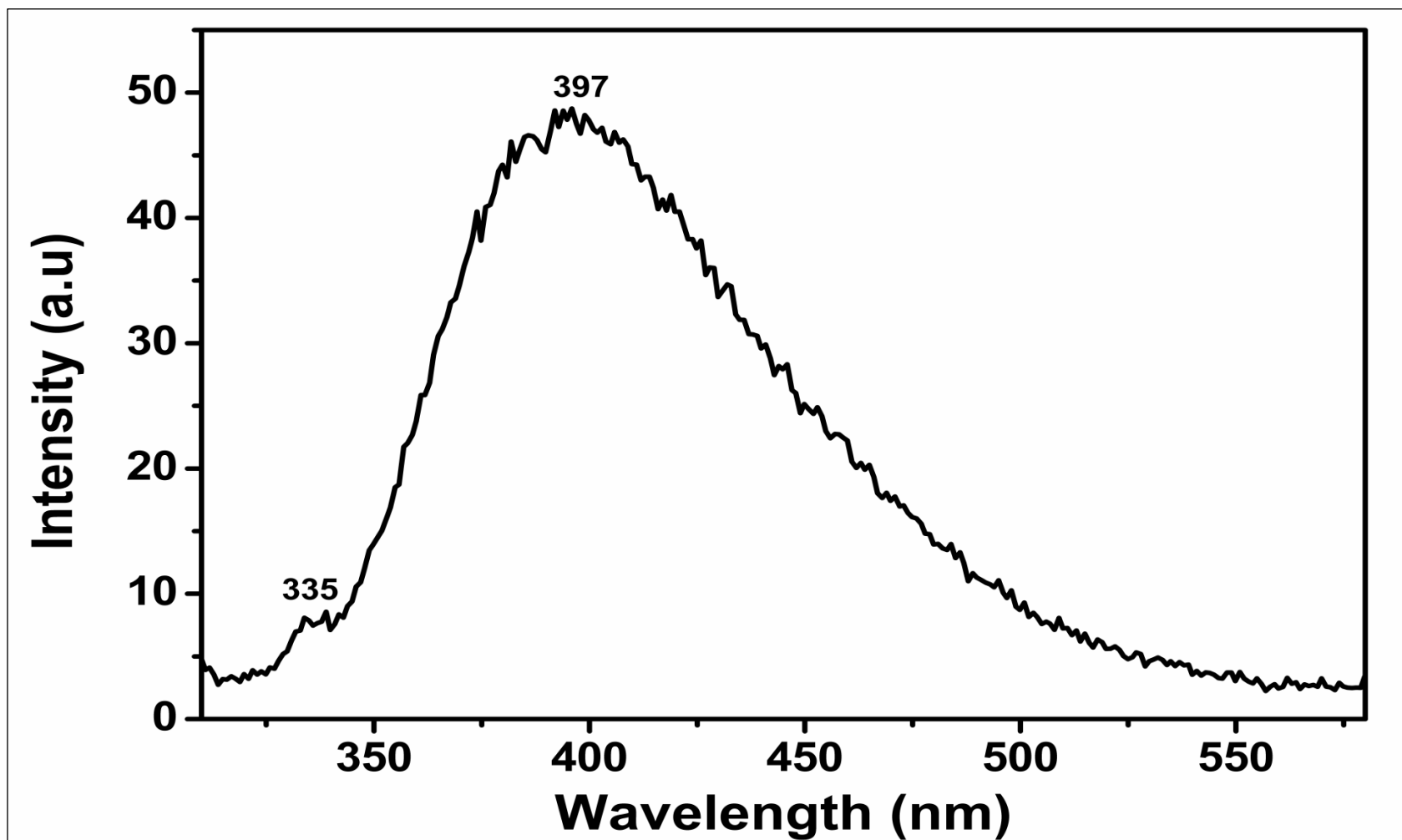


Figure 4.14: CH, Emission Spectrum (1 % CH<sub>3</sub>COOH)

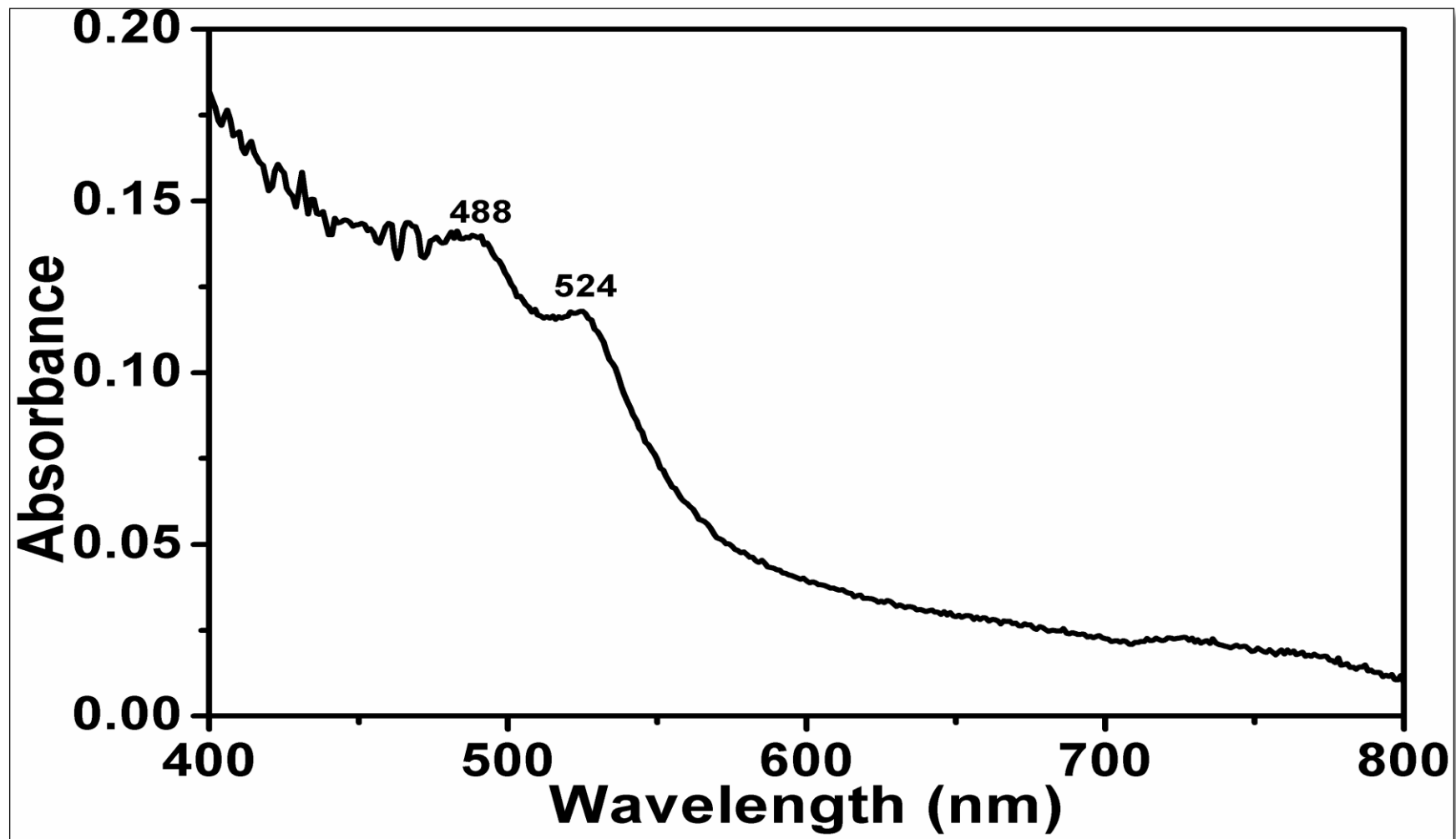


Figure 4.15: LCP1, Absorption Spectrum (NMP)

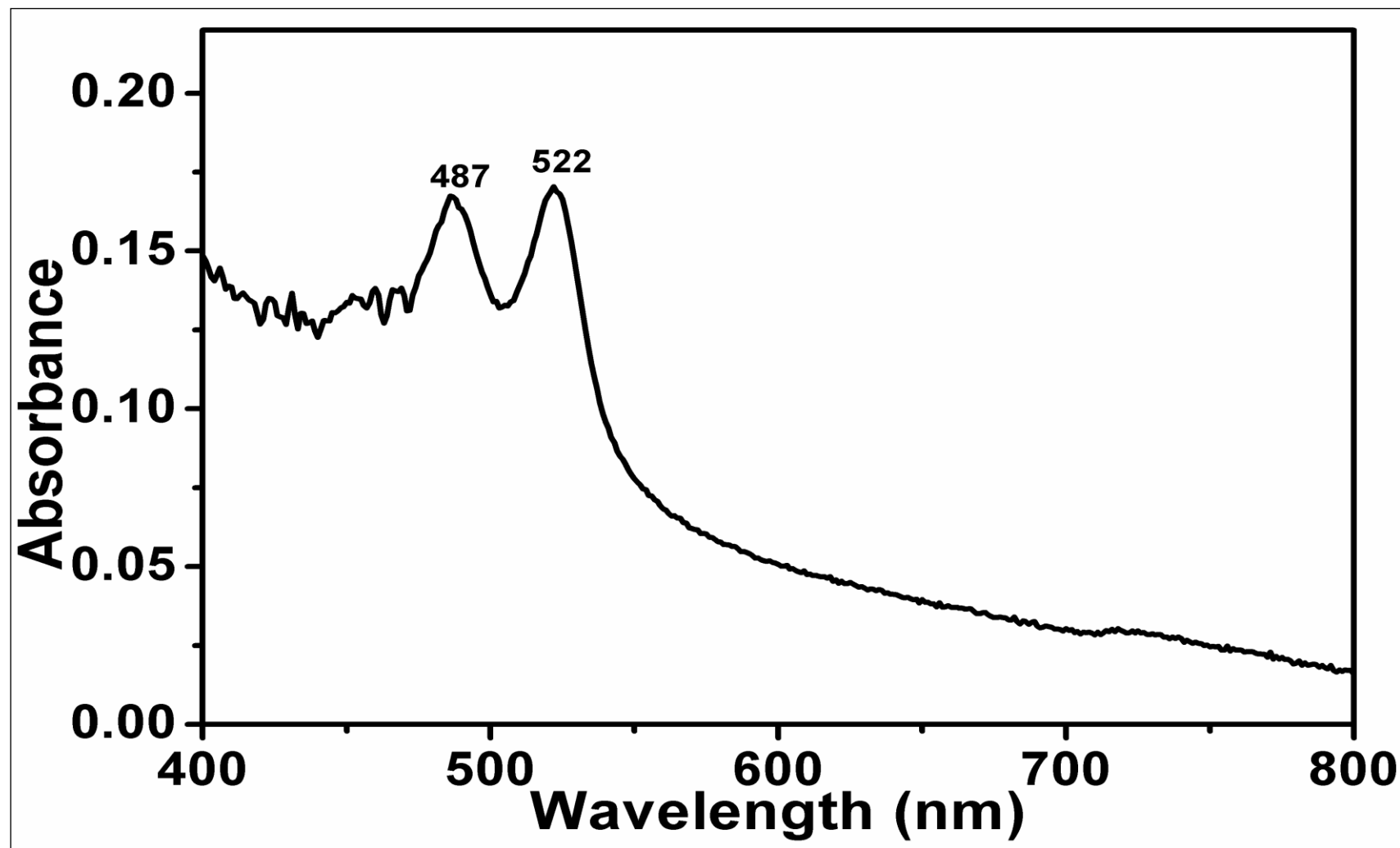


Figure 4.16: LCPI, Absorption Spectrum (DMF)



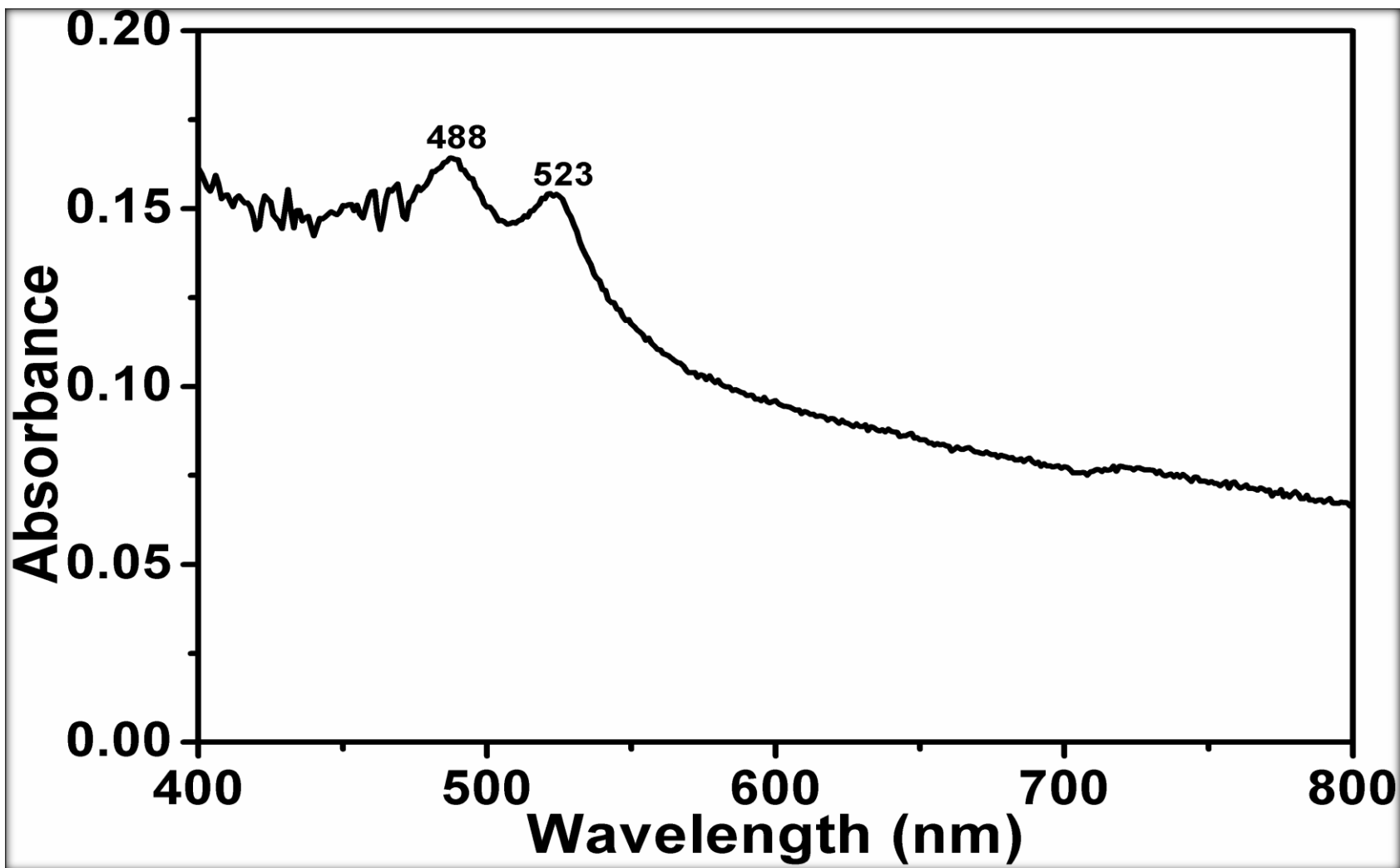


Figure 4.17: LCP1, Absorption Spectrum (DMAc)

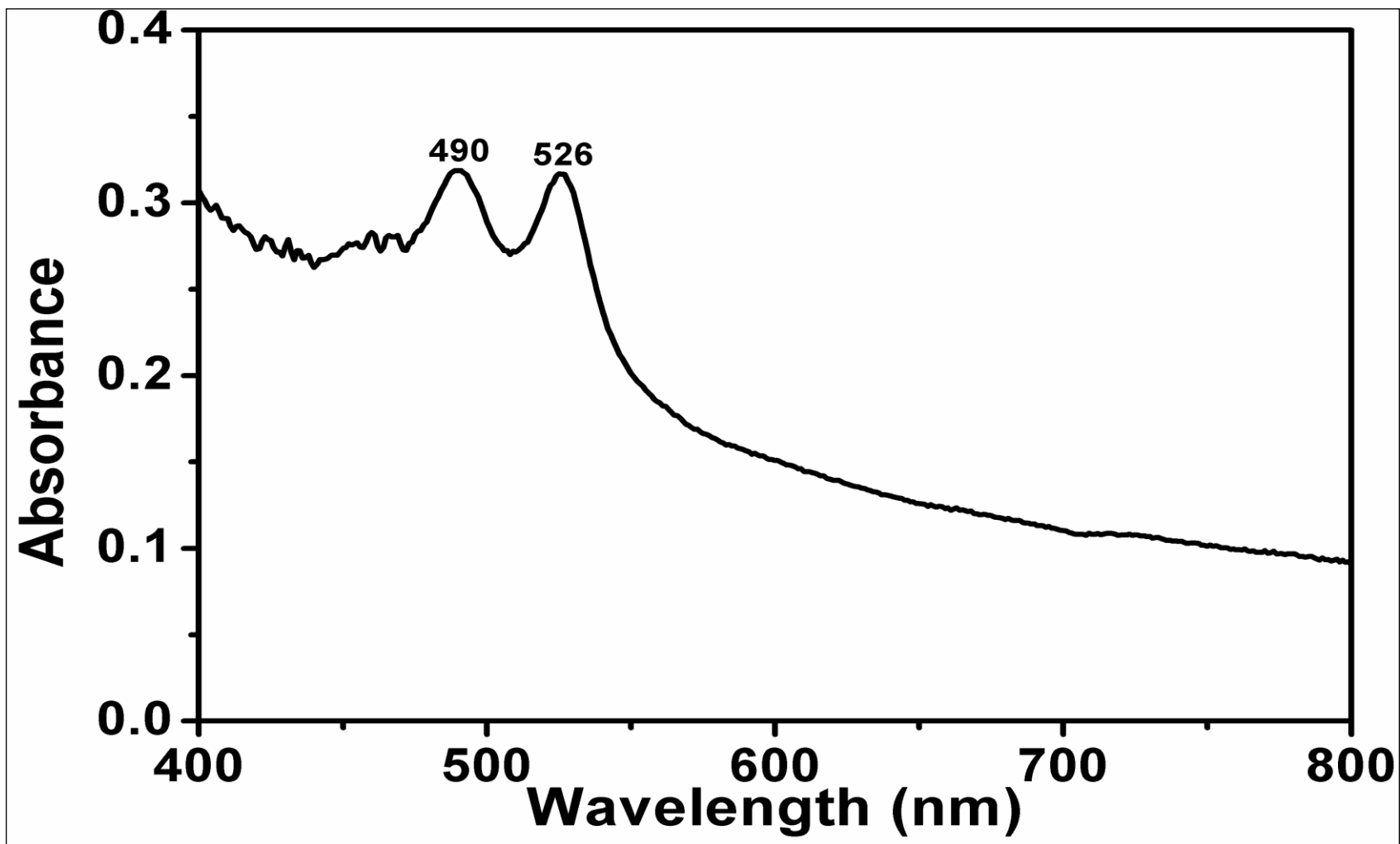


Figure 4.18: LCPI, Absorption Spectrum (DMSO)

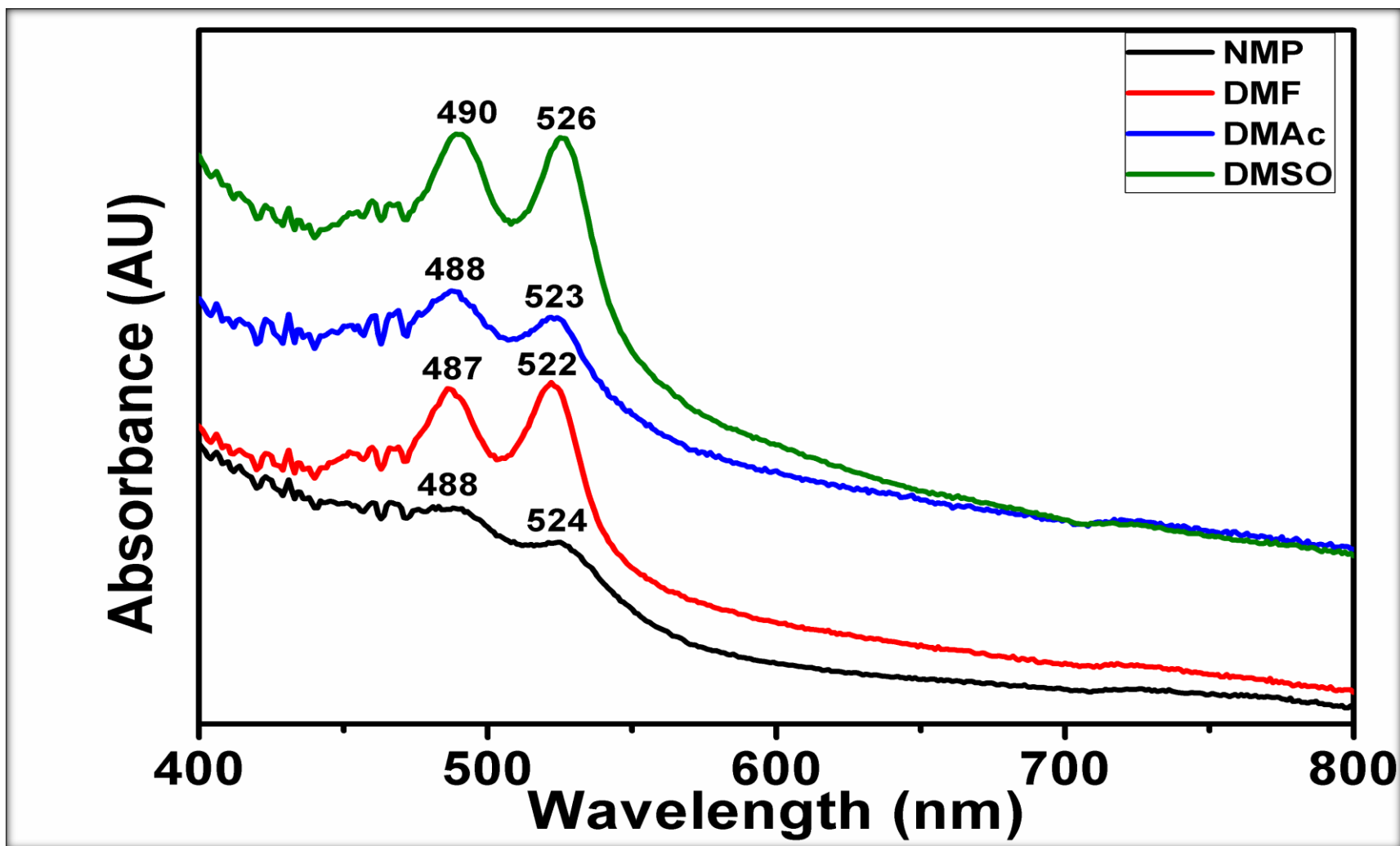


Figure 4.19: LCP1, Absorption Spectra (NMP, DMF, DMAc and DMSO)

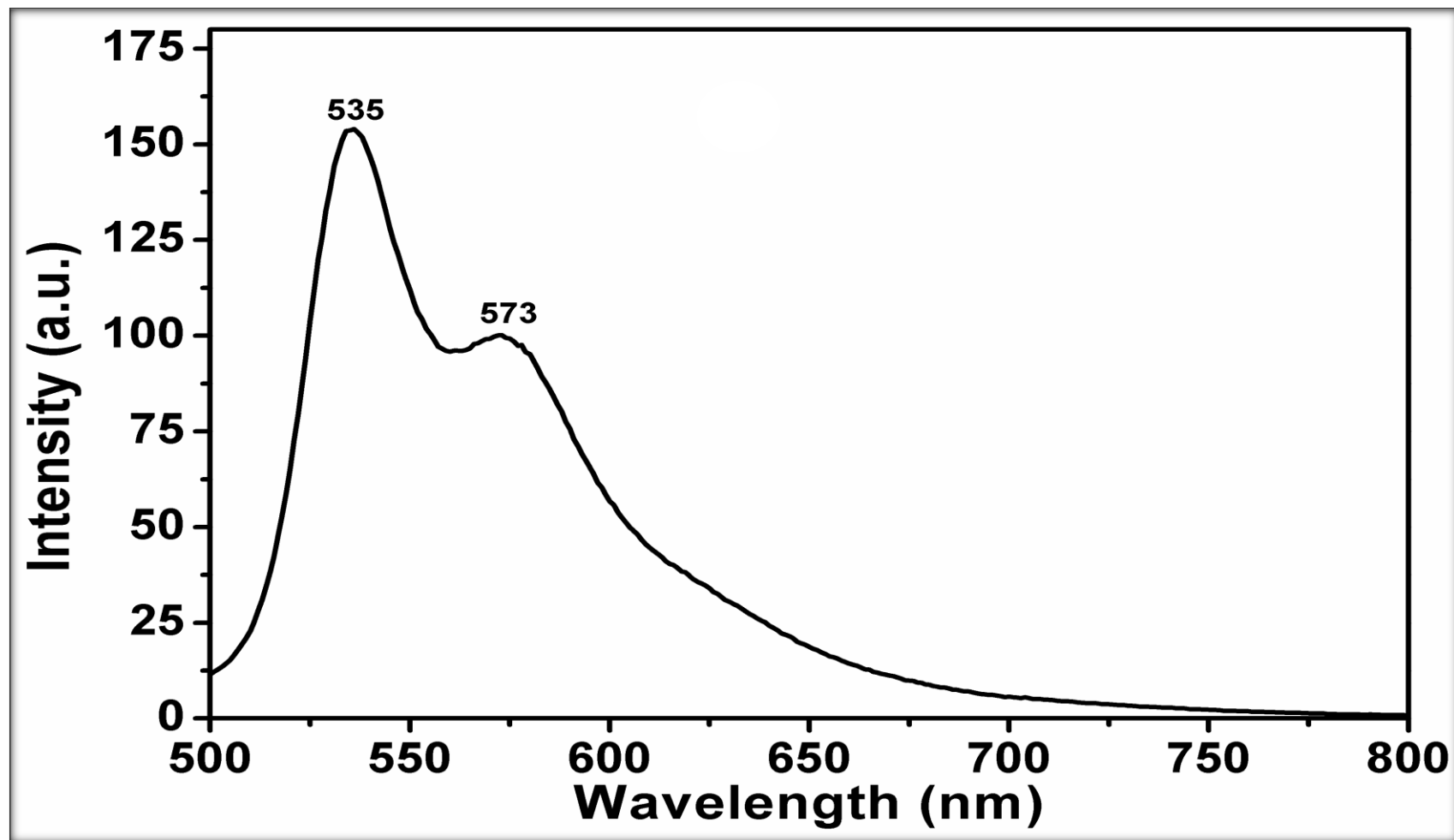


Figure 4.20: LCPI, Emission Spectrum (NMP)

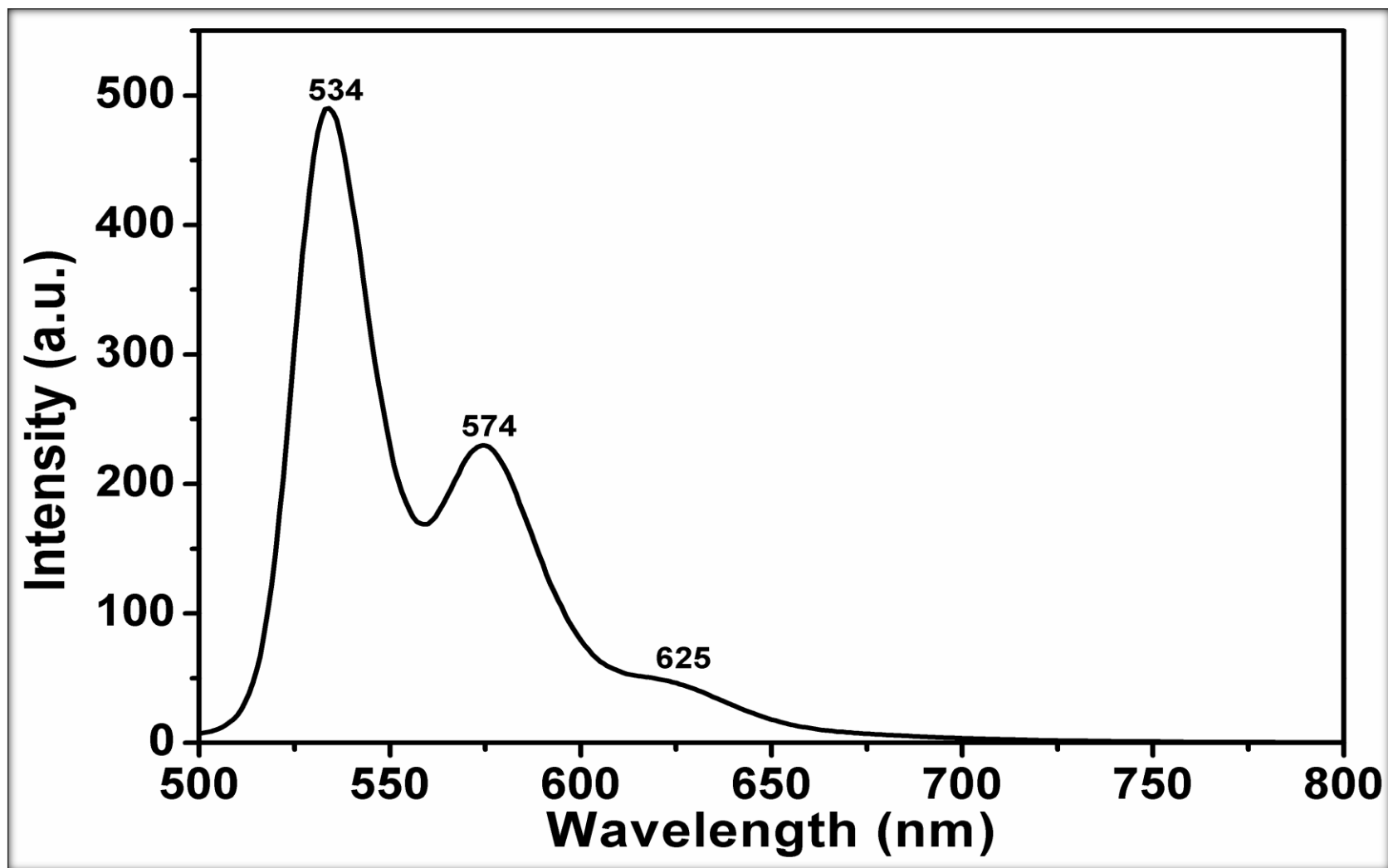


Figure 4.21: LCP1, Emission Spectrum (DMF)

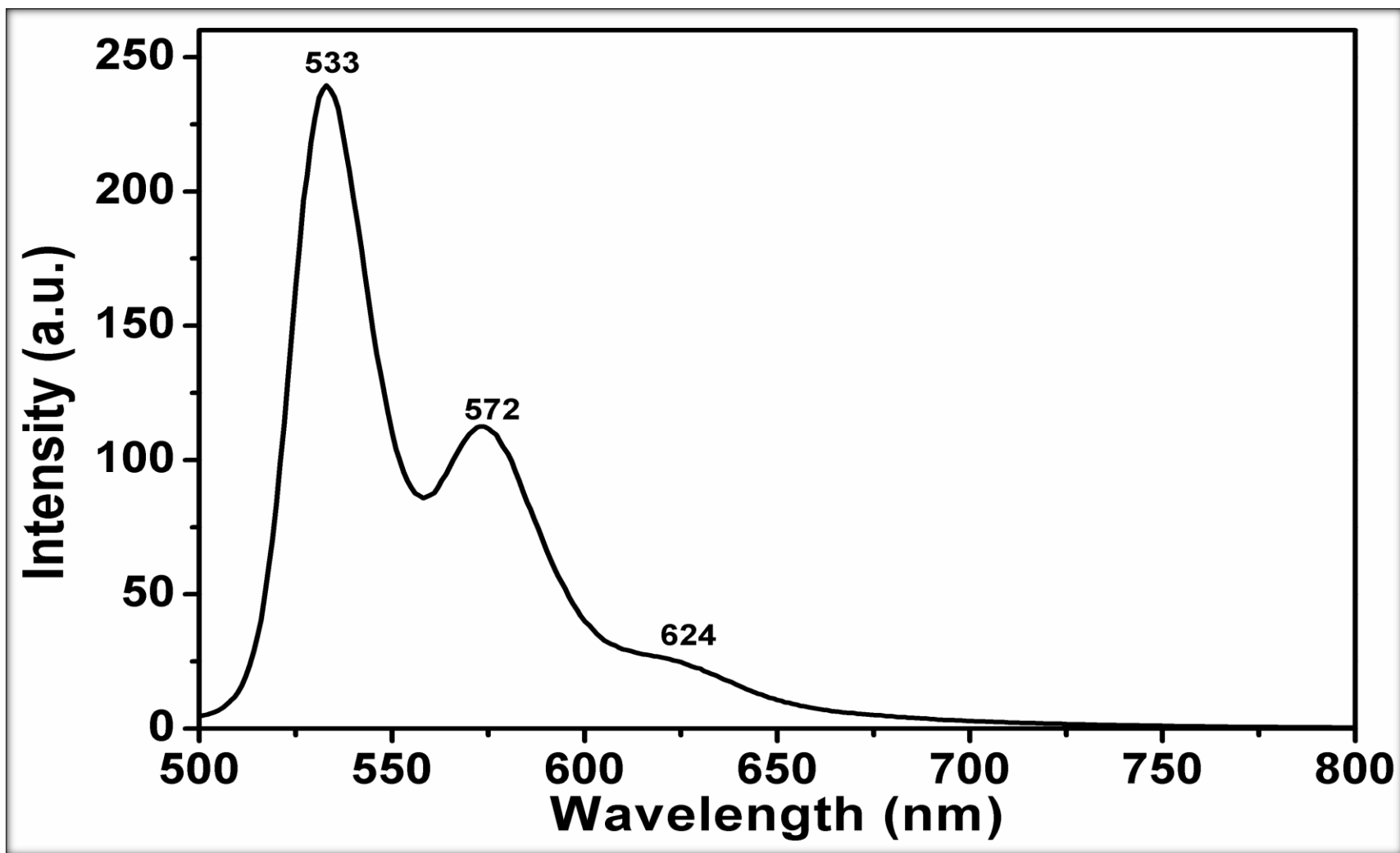


Figure 4.22: LCP1, Emission Spectrum (DMAc)

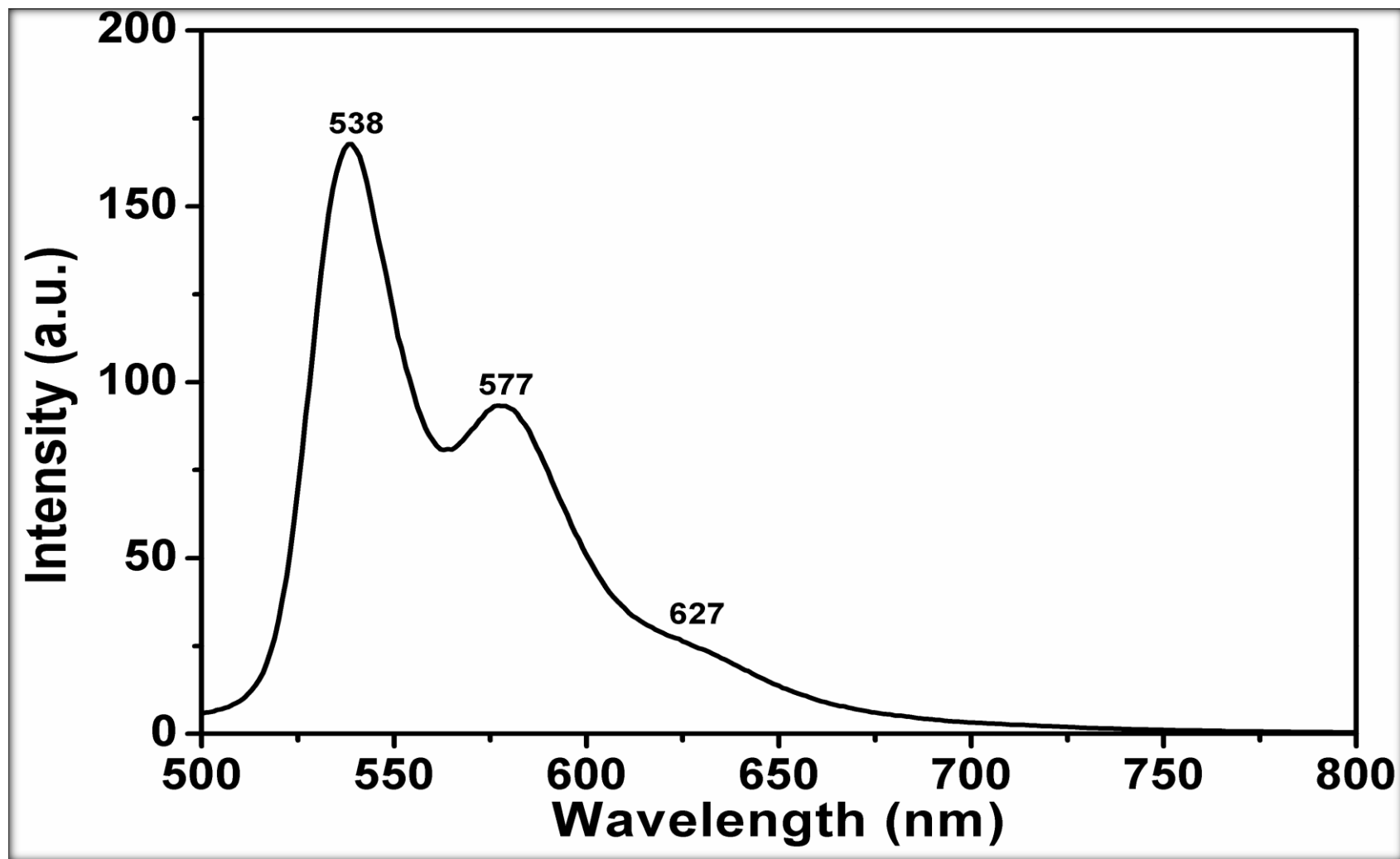


Figure 4.23: LCP1, Emission Spectrum (DMSO)

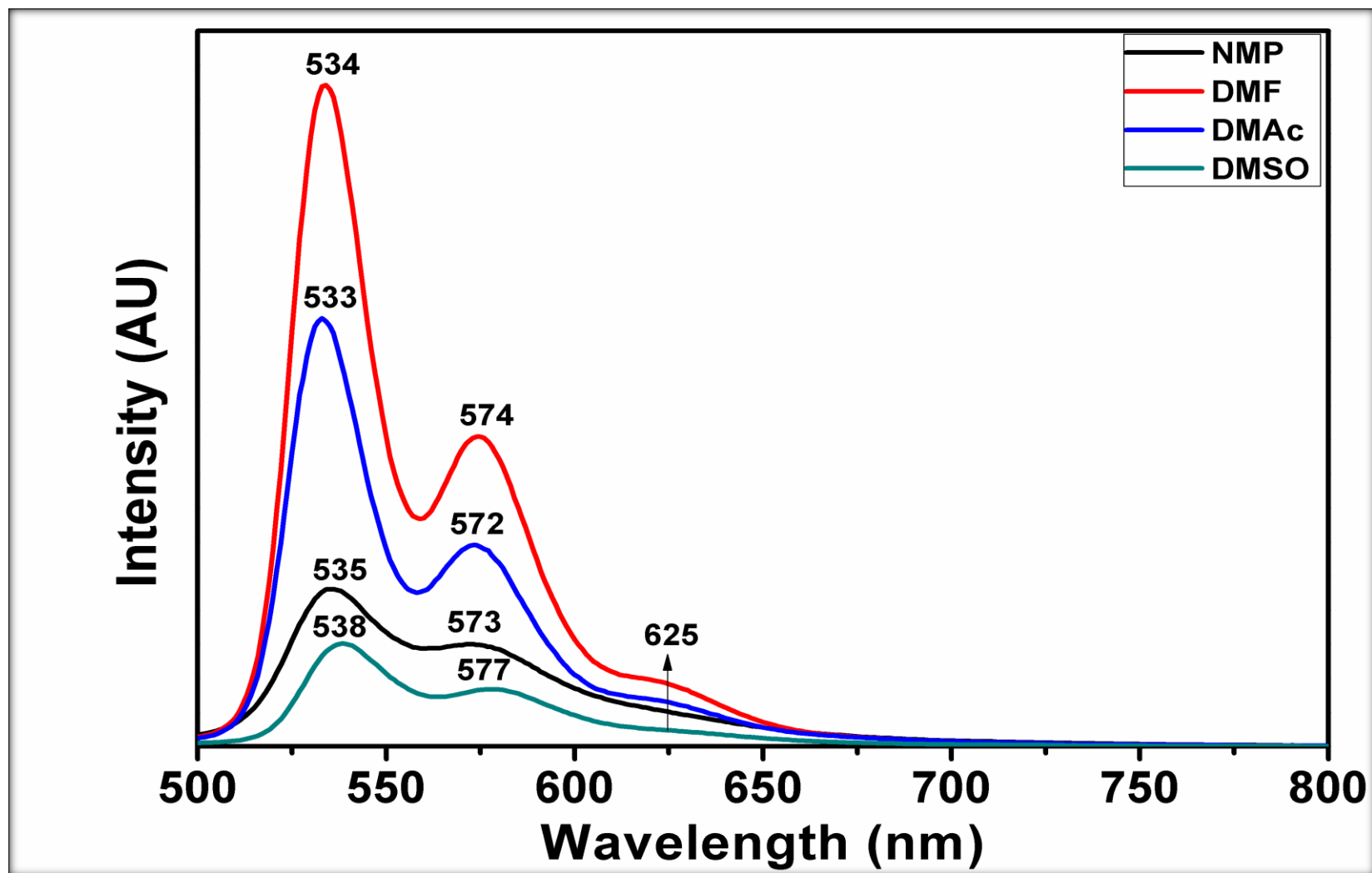


Figure 4.24: LCPI, Emission Spectra (NMP, DMF, DMAc and DMSO)



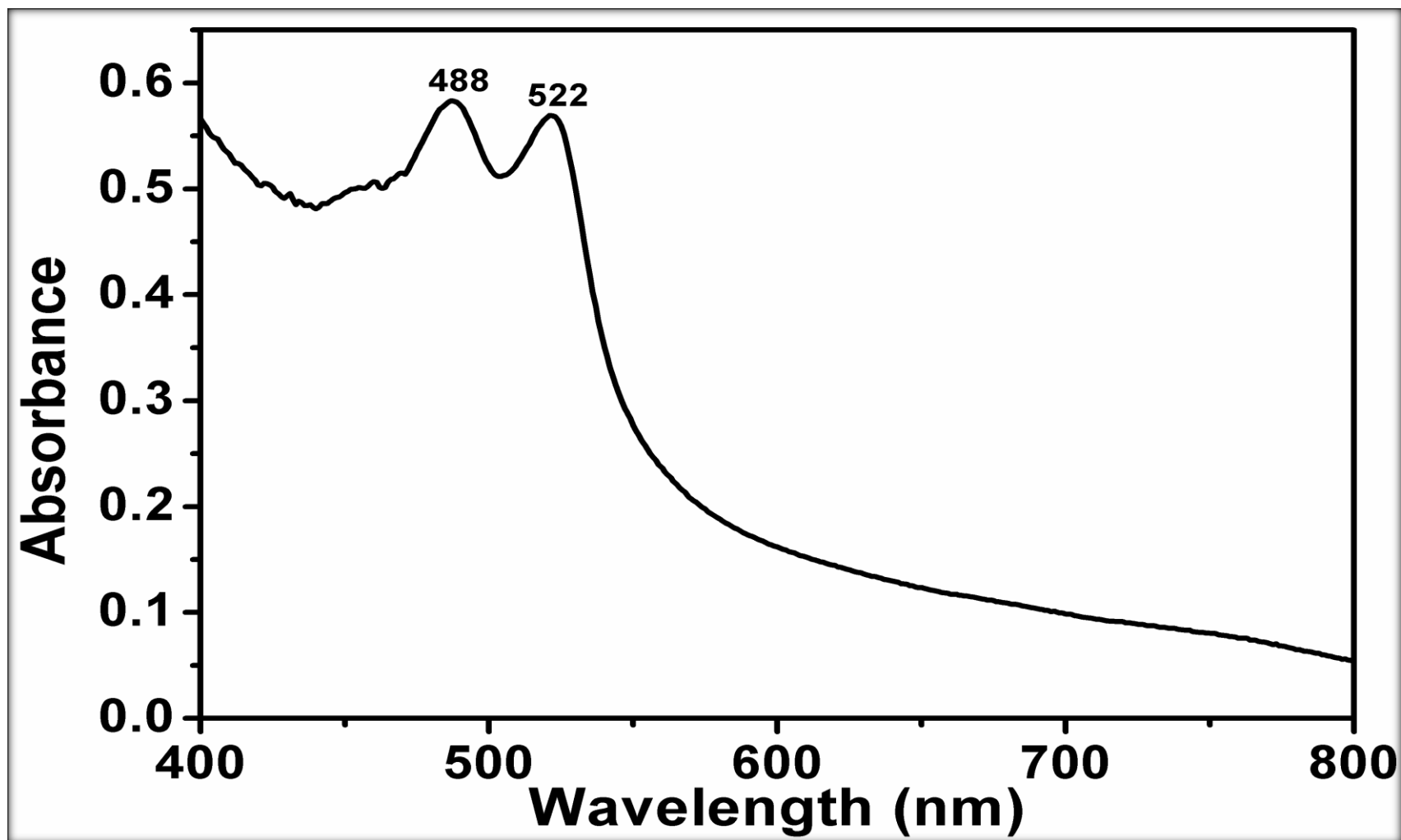


Figure 4.25: LCP2, Absorption Spectrum (NMP)

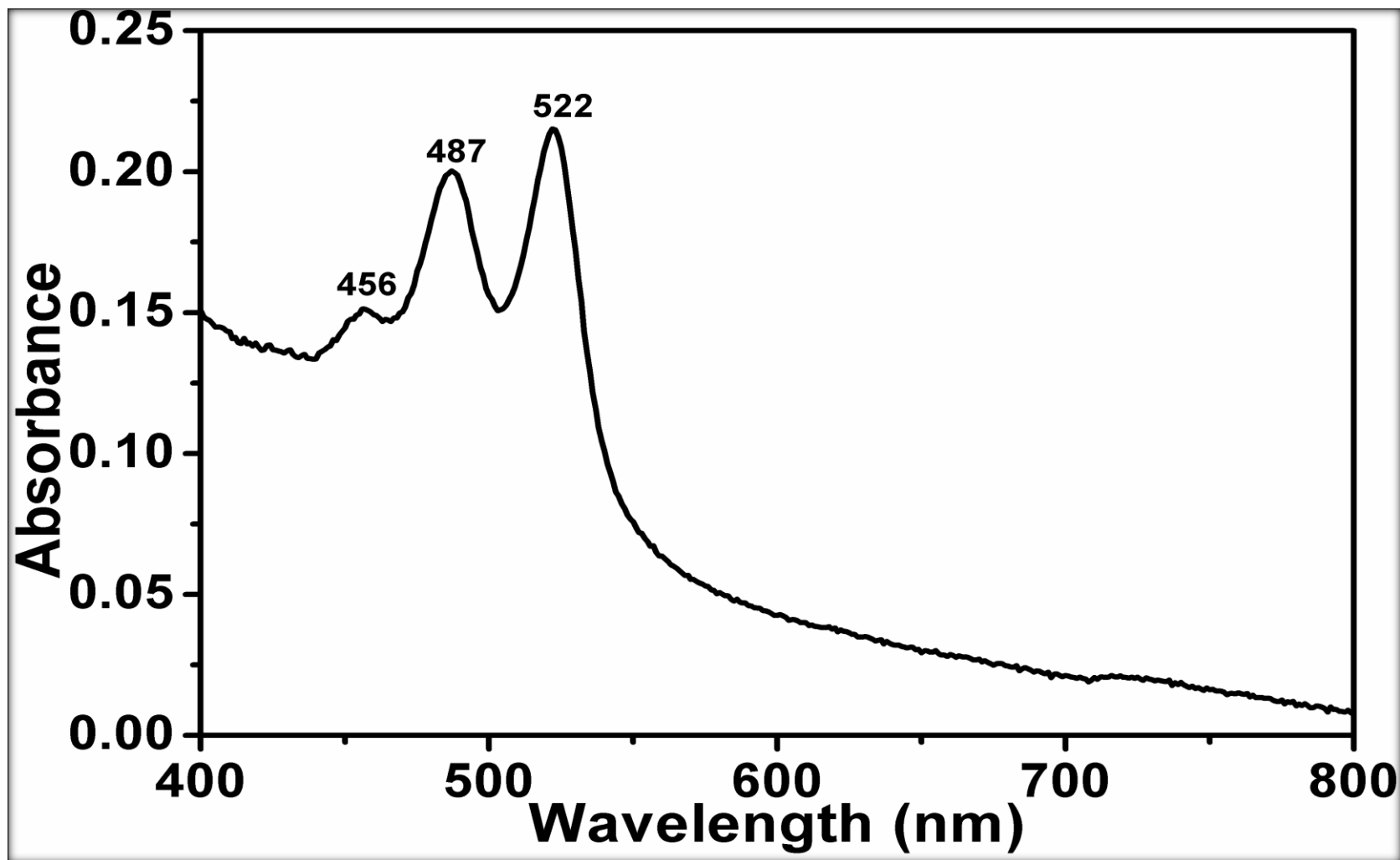


Figure 4.26: LCP2, Absorption Spectrum (DMF)

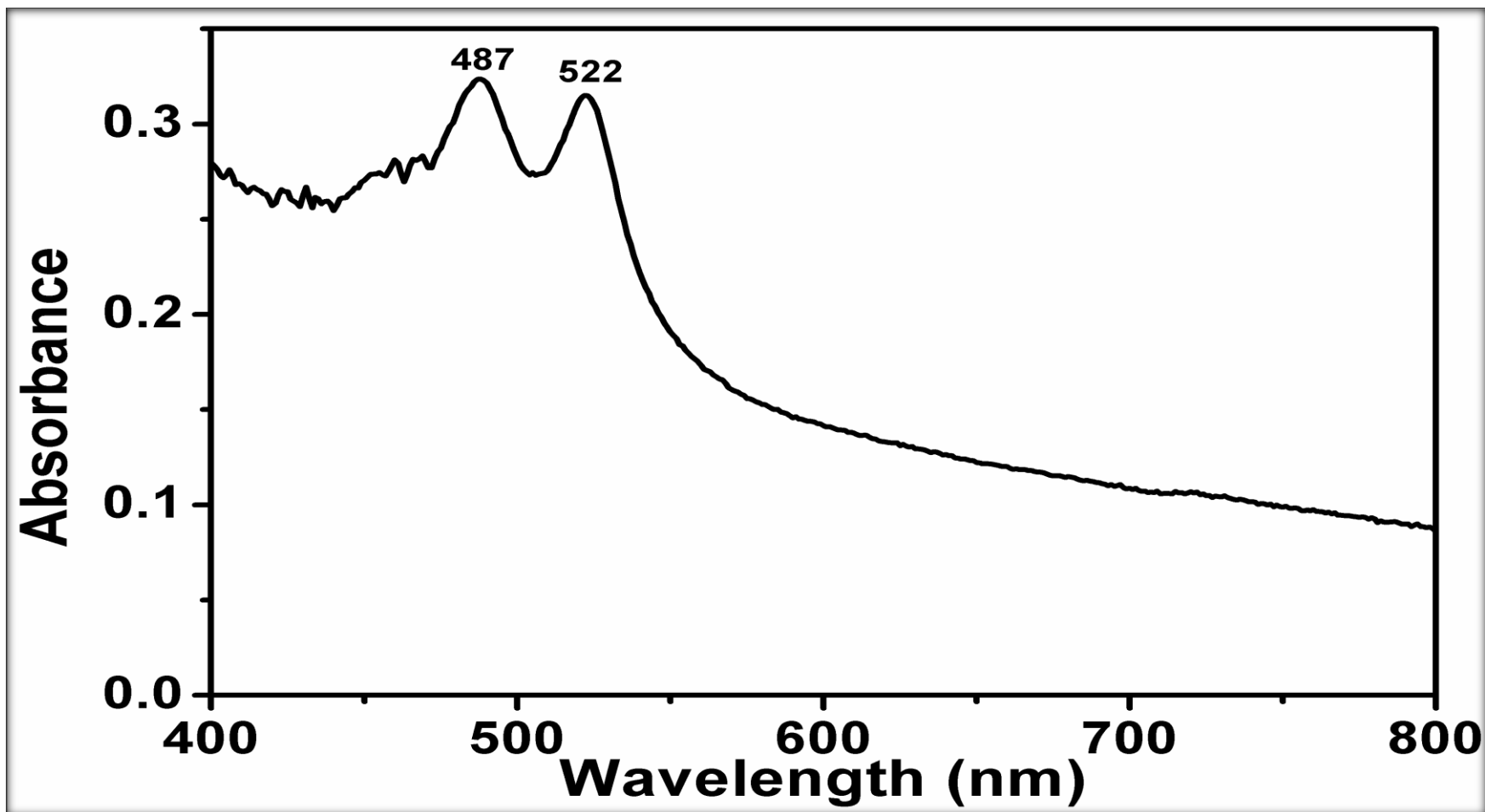


Figure 4.27: LCP2, Absorption Spectrum (DMAc)

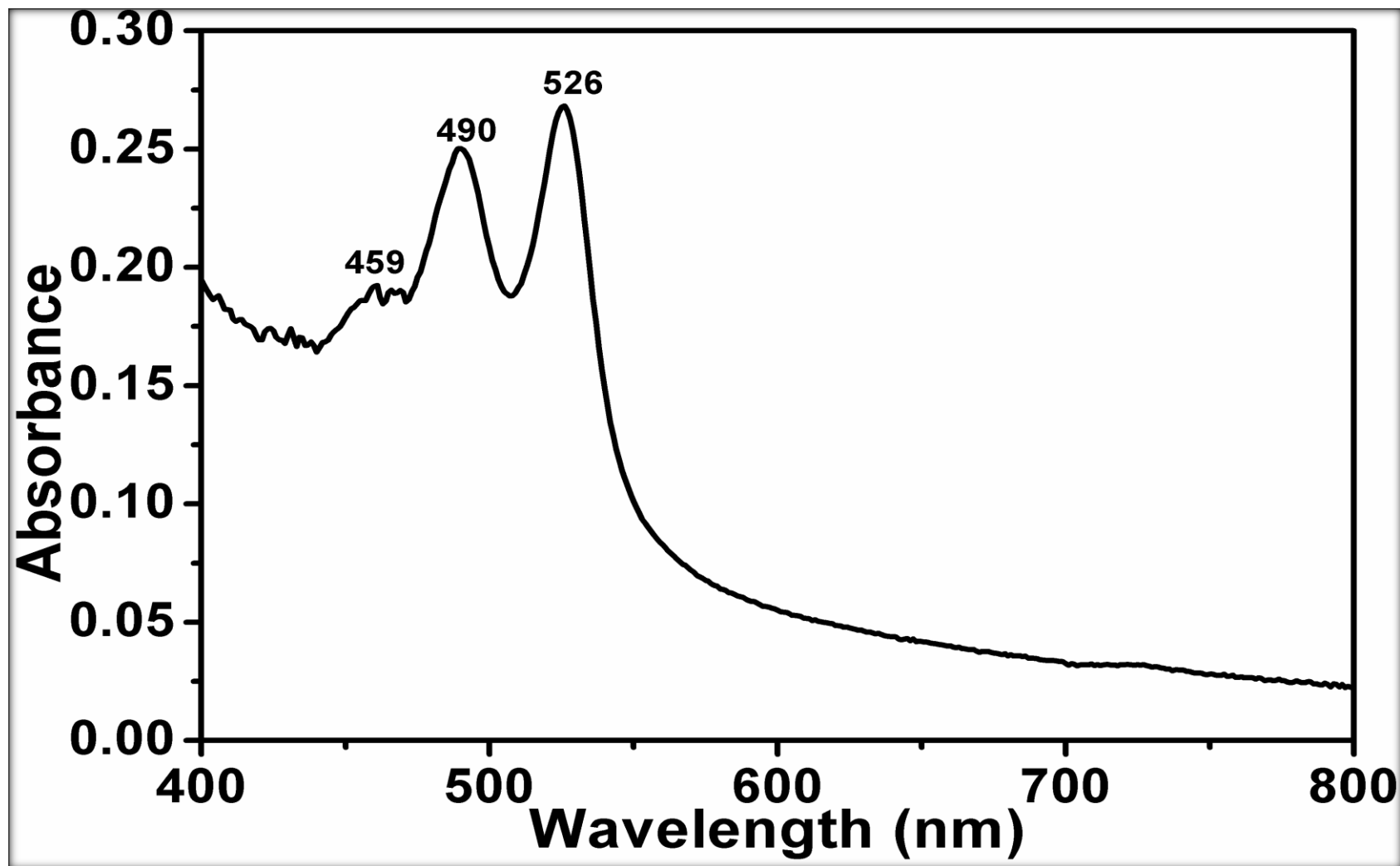


Figure 4.28: LCP2, Absorption Spectrum (DMSO)

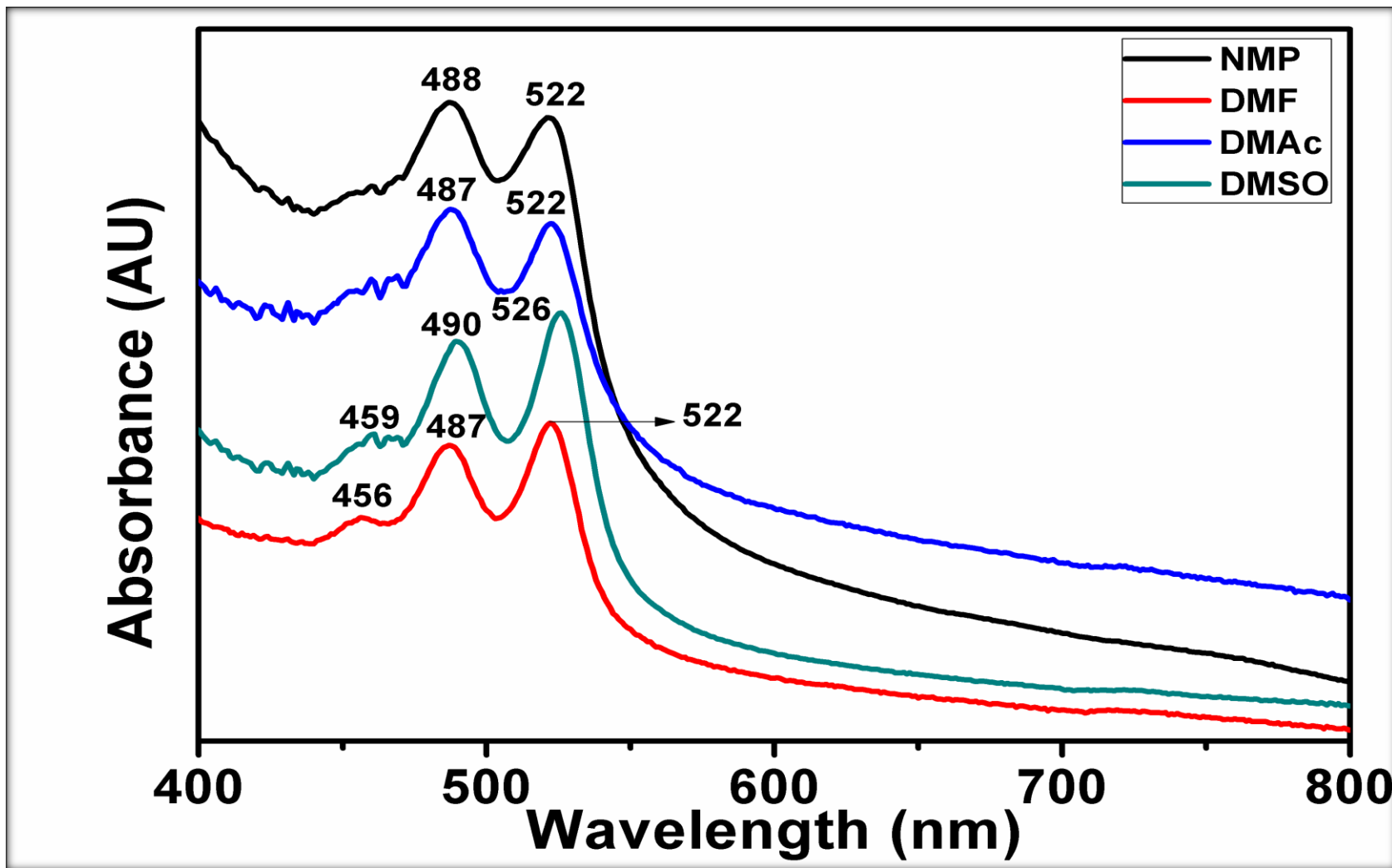


Figure 4.29: LCP2, Absorption Spectra (NMP, DMF, DMAc and DMSO)

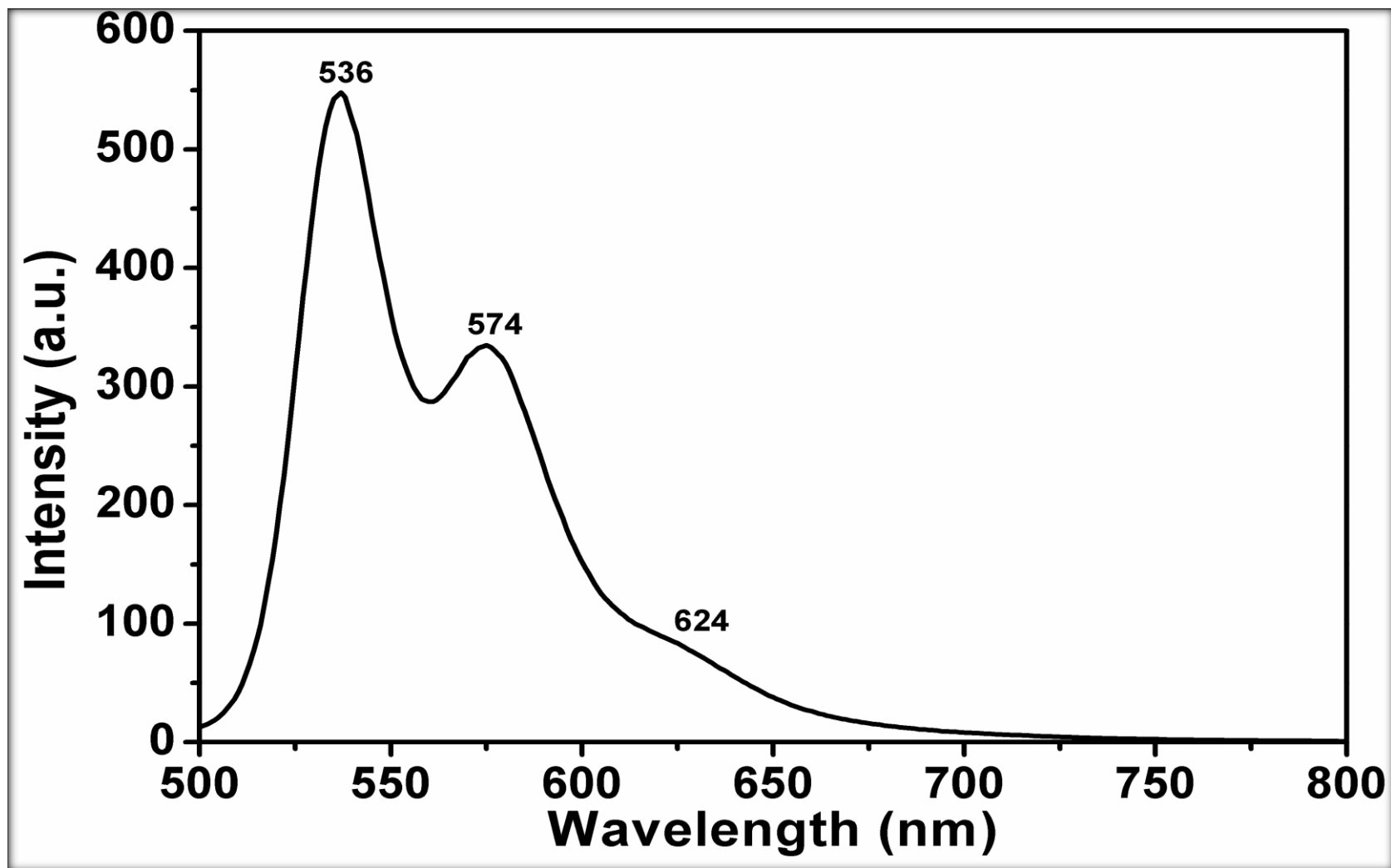


Figure 4.30: LCP2, Emission Spectrum (NMP)

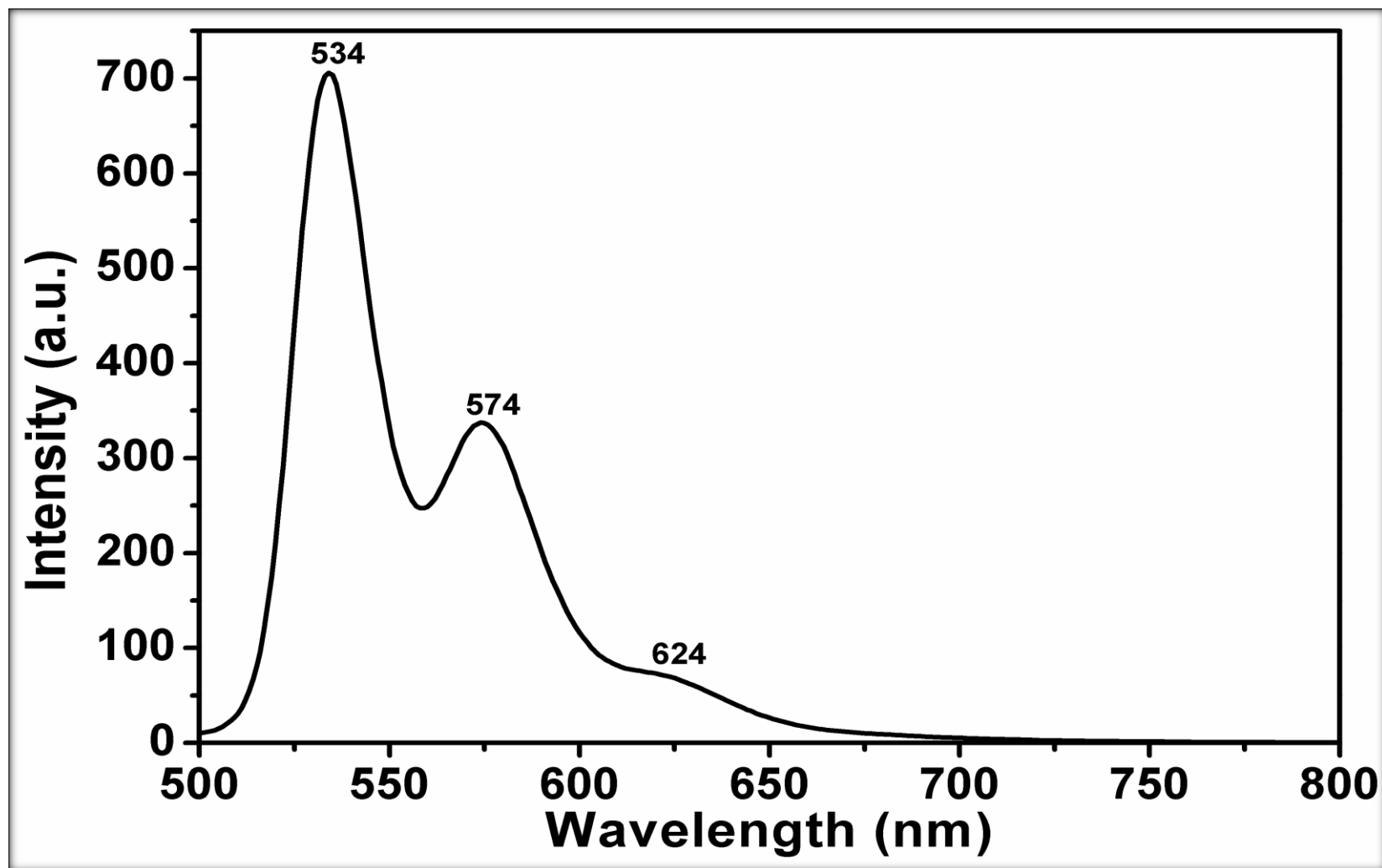


Figure 4.31: LCP2, Emission Spectrum (DMF)

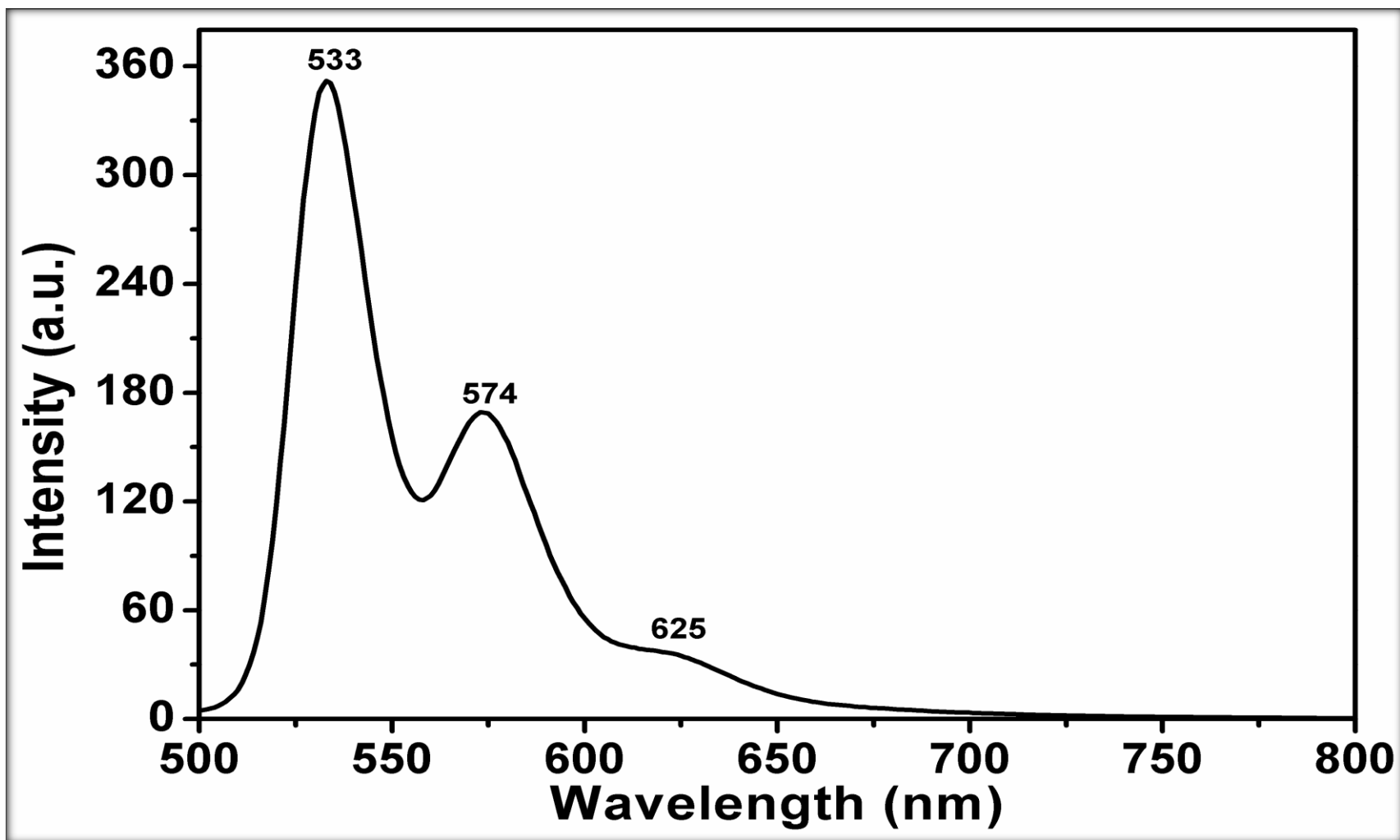


Figure 4.32: LCP2, Emission Spectrum (DMAc)



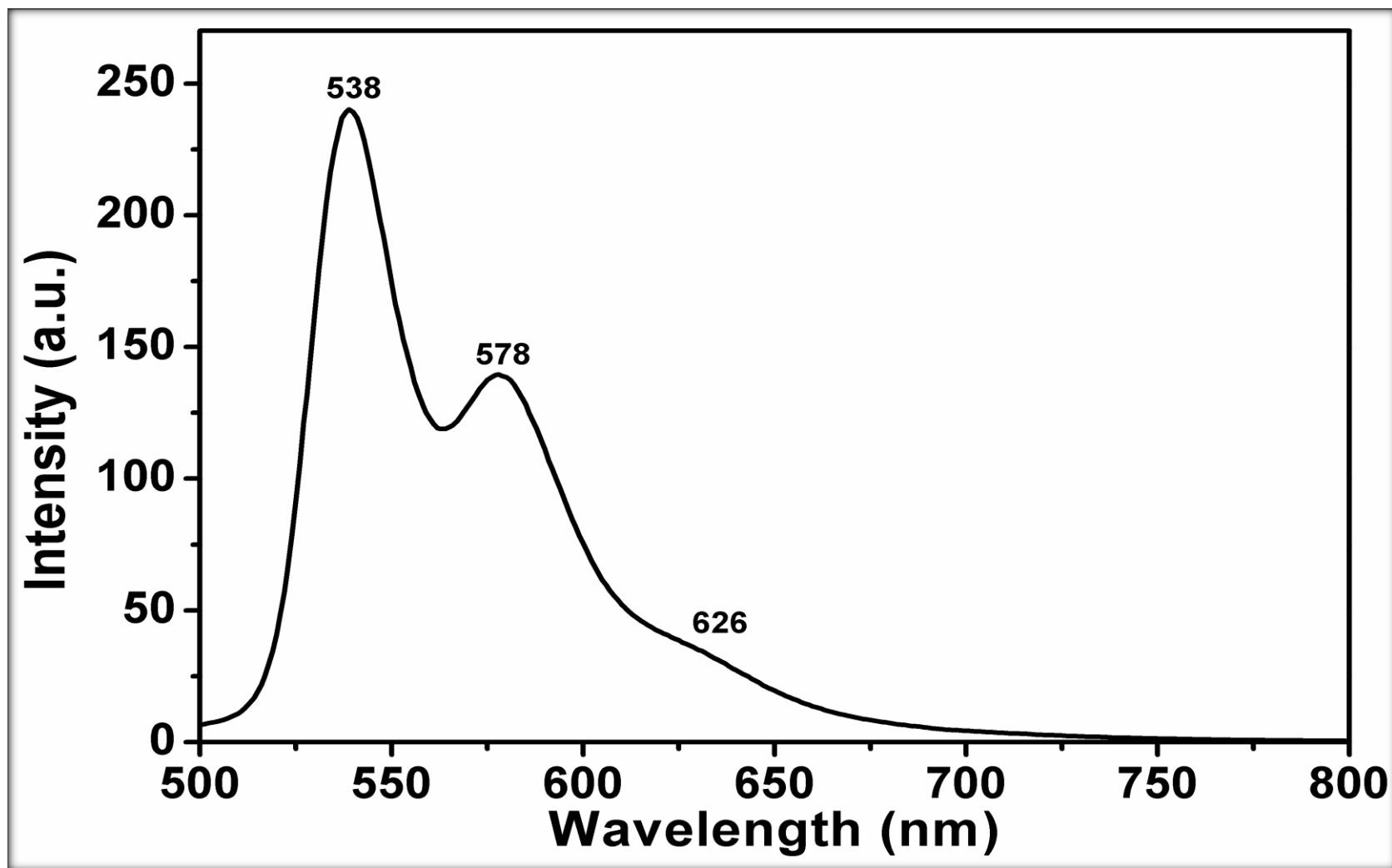


Figure 4.33: LCP2, Emission Spectrum (DMSO)

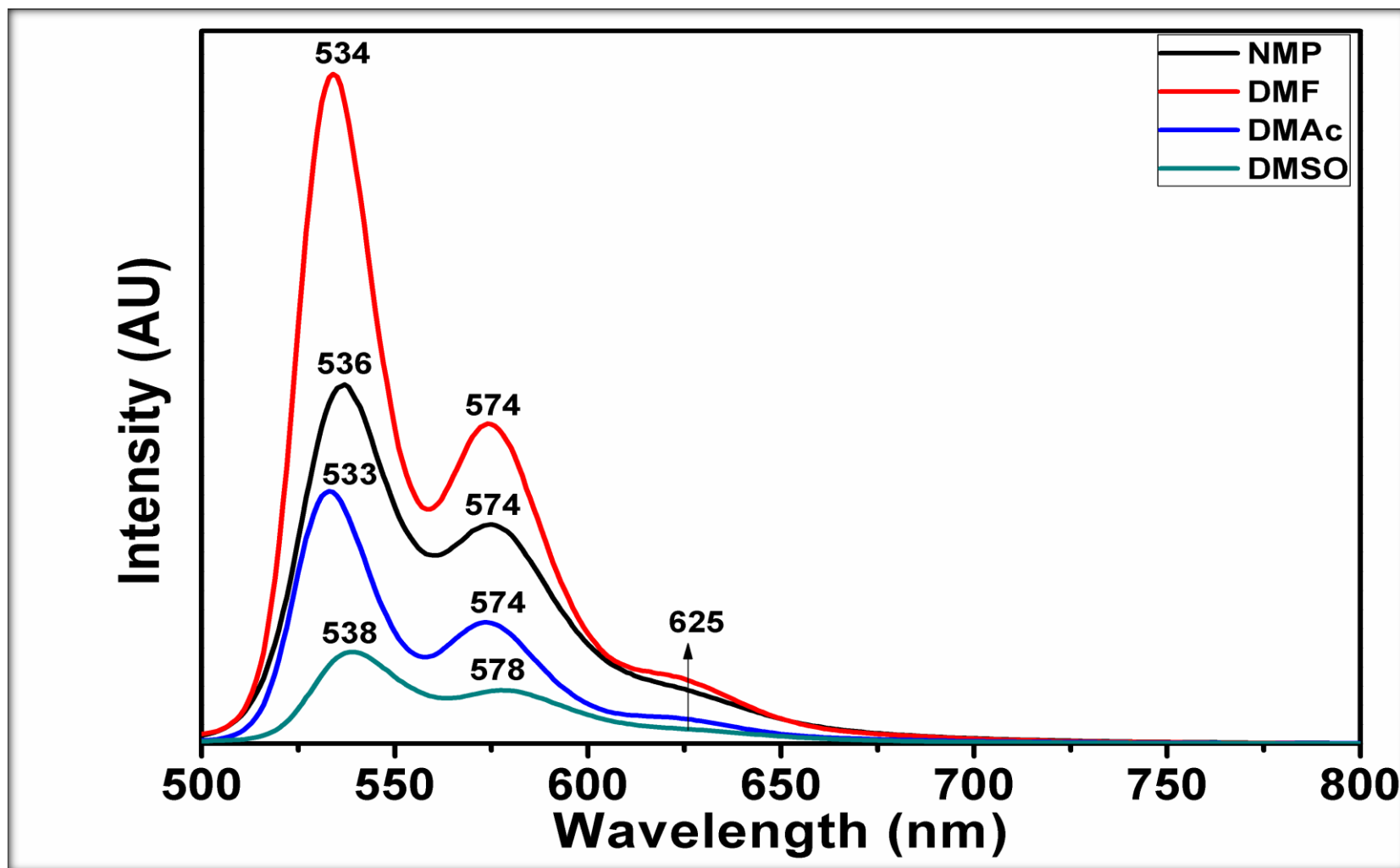


Figure 4.34: LCP2, Emission Spectra (NMP, DMF, DMAc and DMSO)

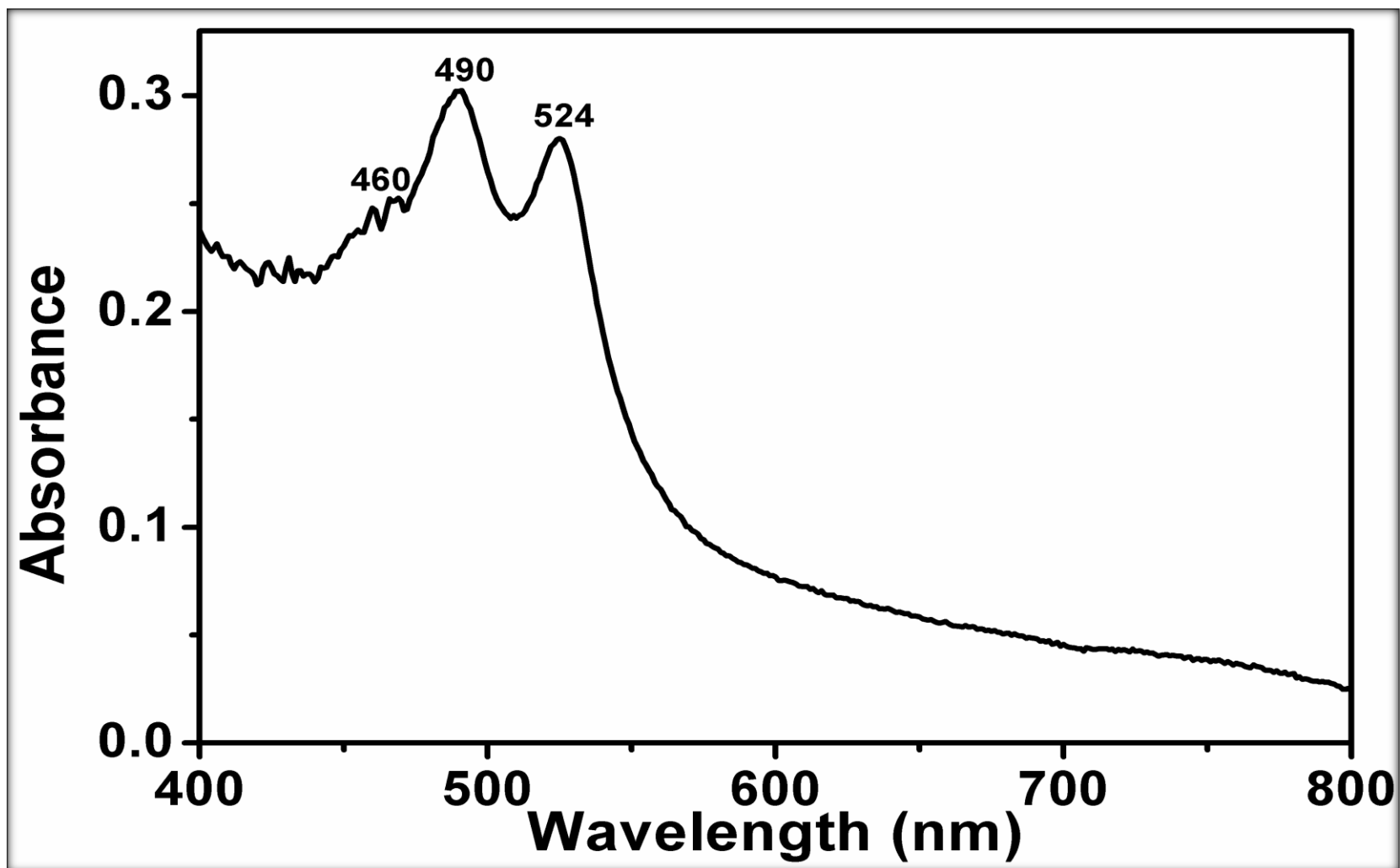


Figure 4.35: LCP3, Absorption Spectrum (NMP)

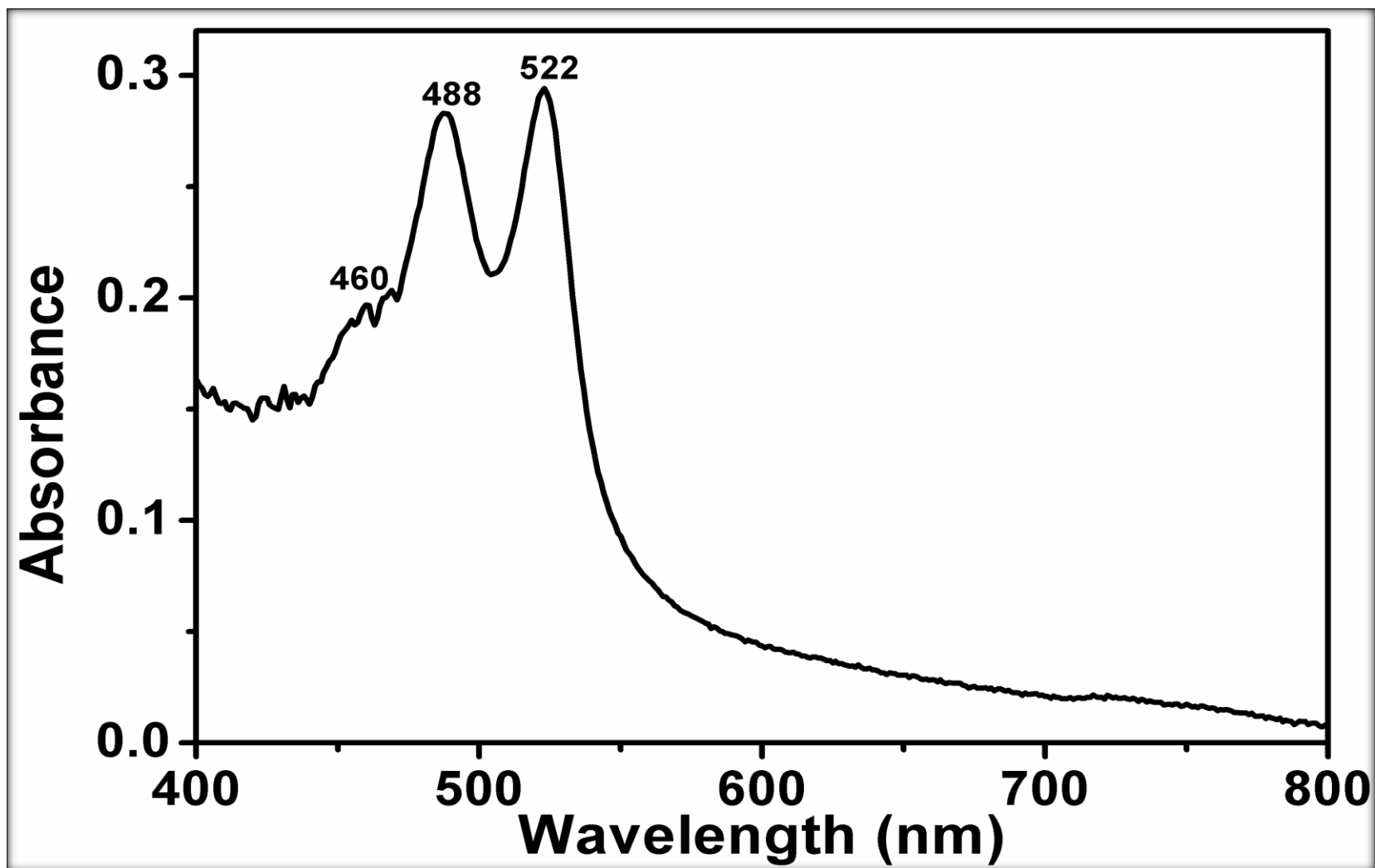


Figure 4.36: LCP3, Absorption Spectrum (DMF)

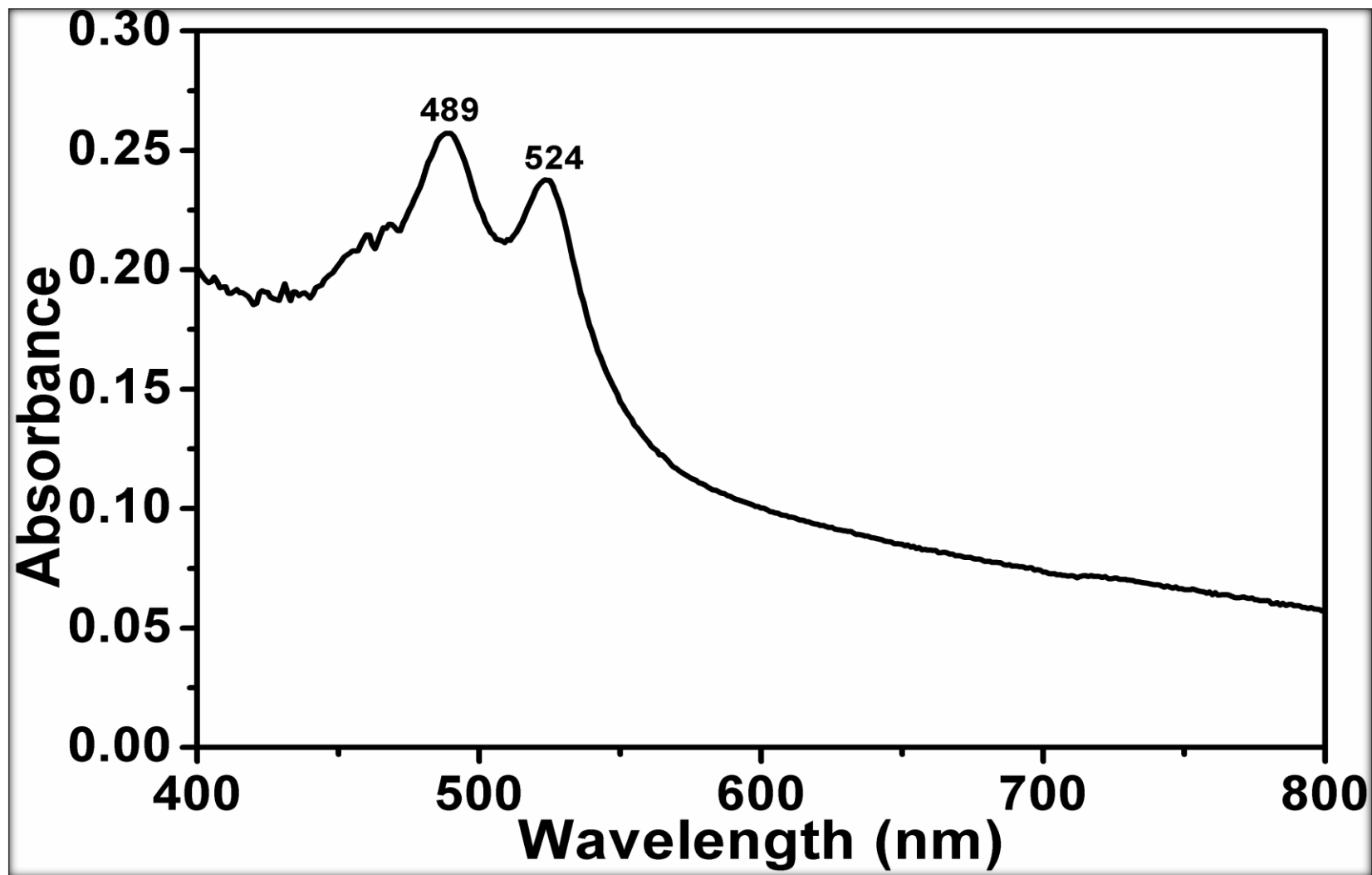


Figure 4.37: LCP3, Absorption Spectrum (DMAc)

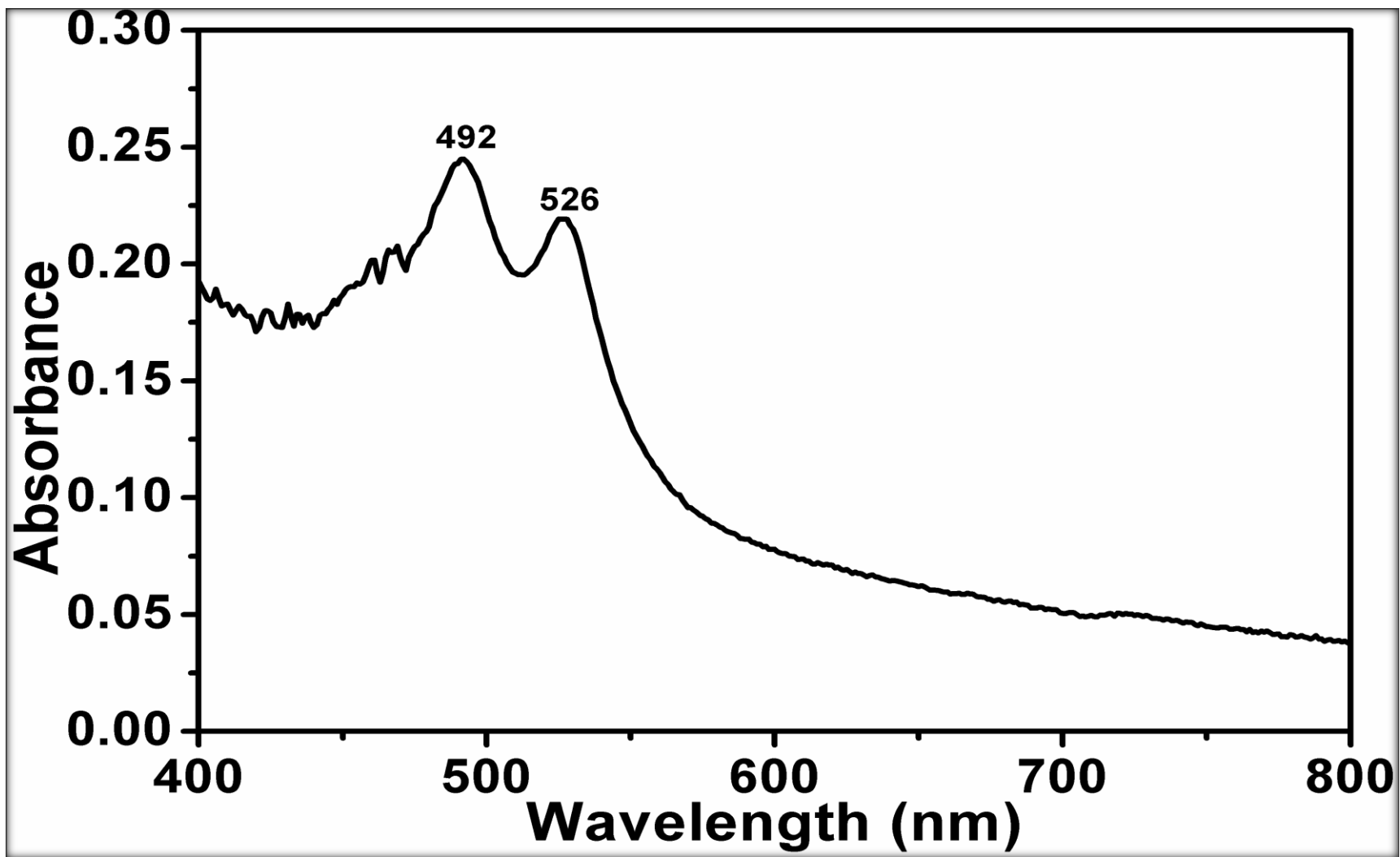


Figure 4.38: LCP3, Absorption Spectrum (DMSO)

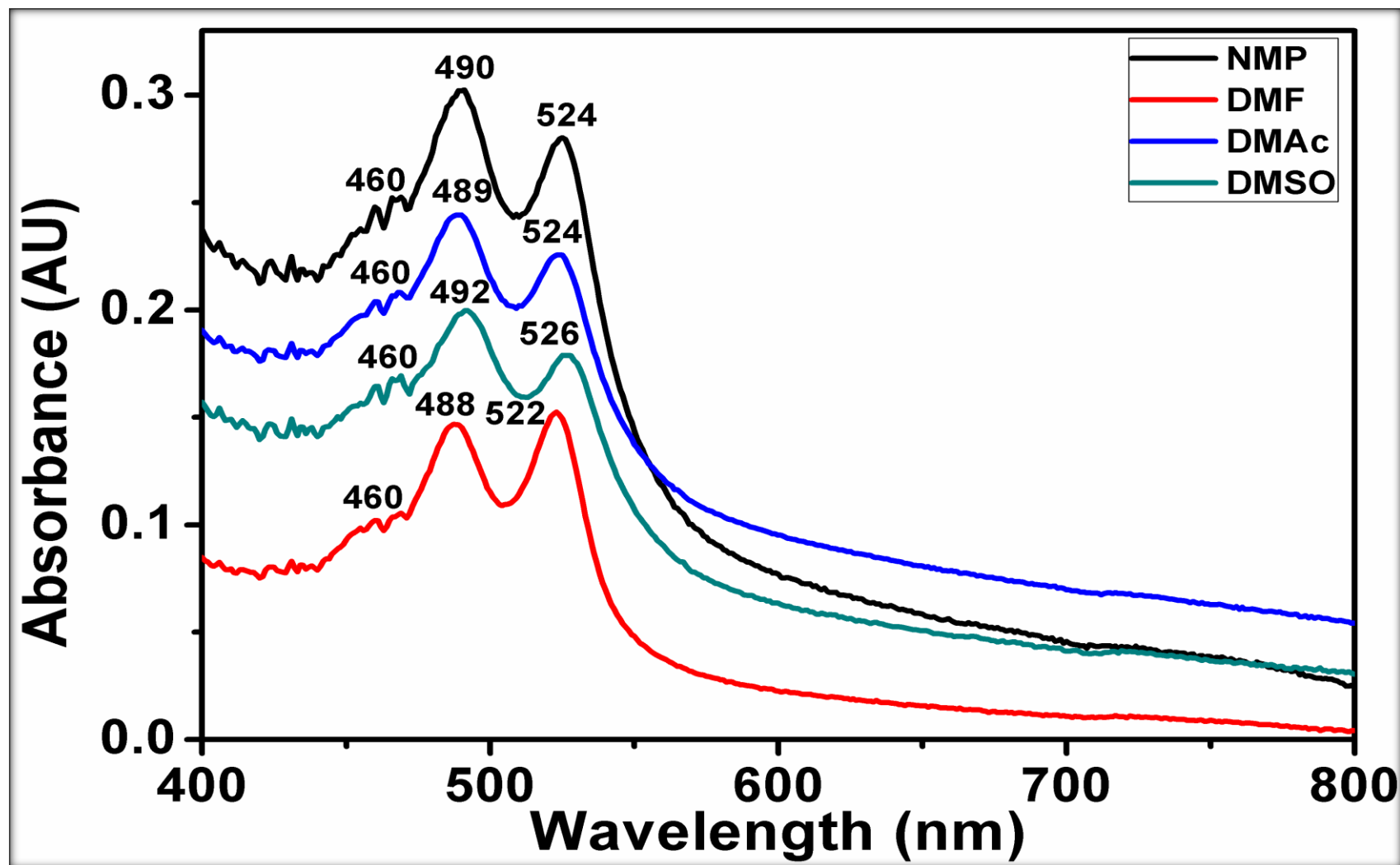


Figure 4.39: LCP3, Absorption Spectra (NMP, DMF, DMAc and DMSO)

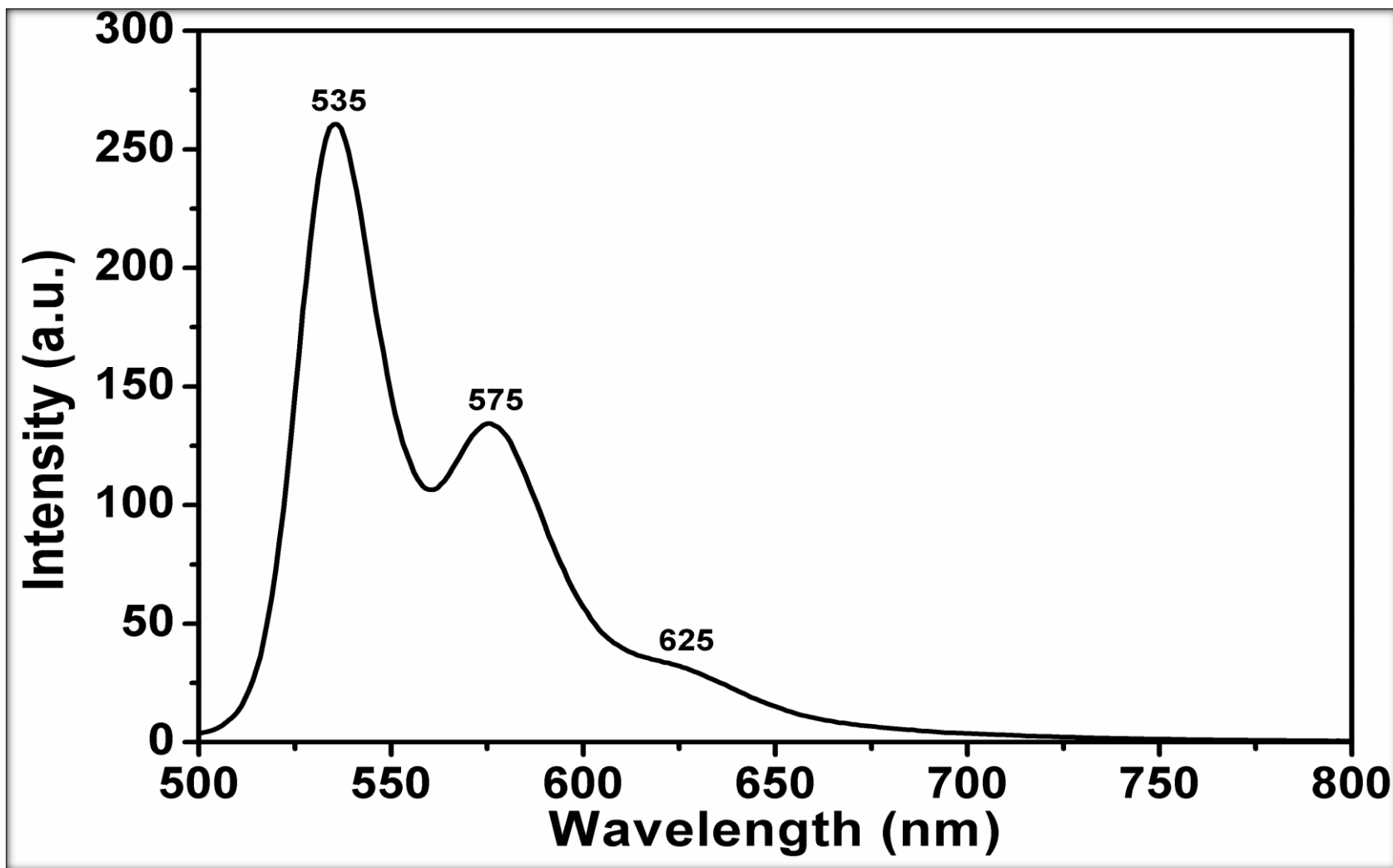


Figure 4.40: LCP3, Emission Spectrum (NMP)



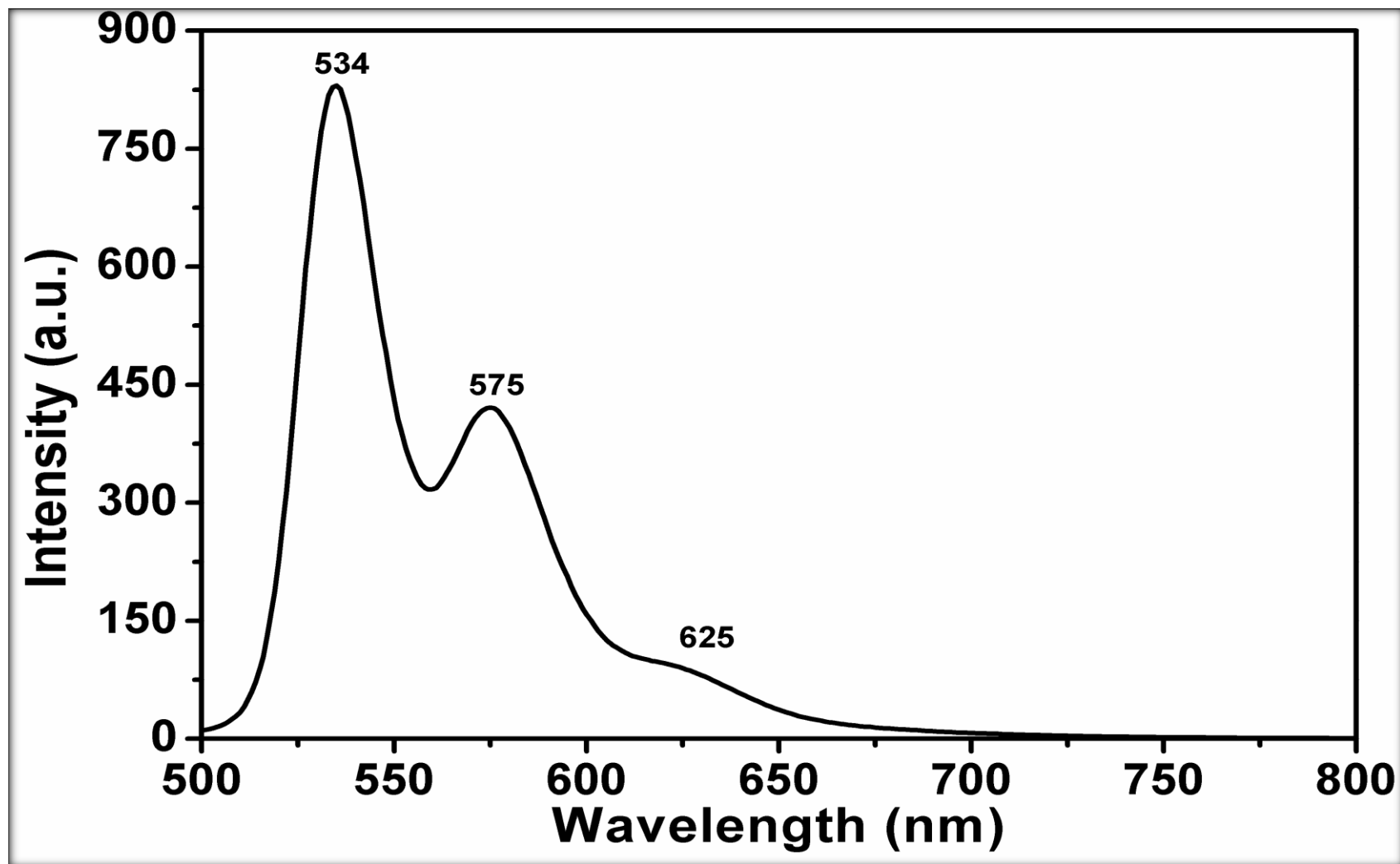


Figure 4.41: LCP3, Emission Spectrum (DMF)

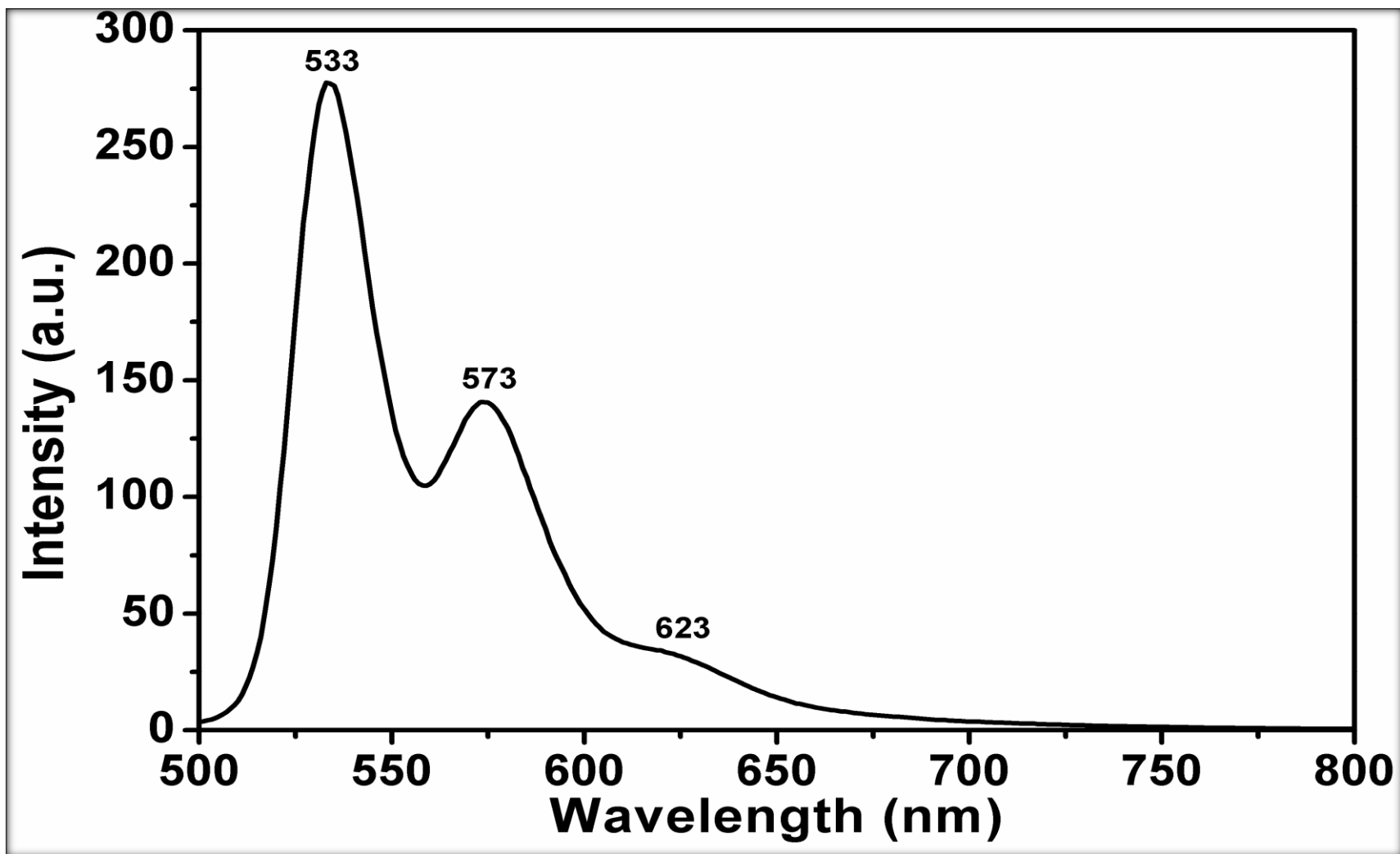


Figure 4.42: LCP3, Emission Spectrum (DMAc)

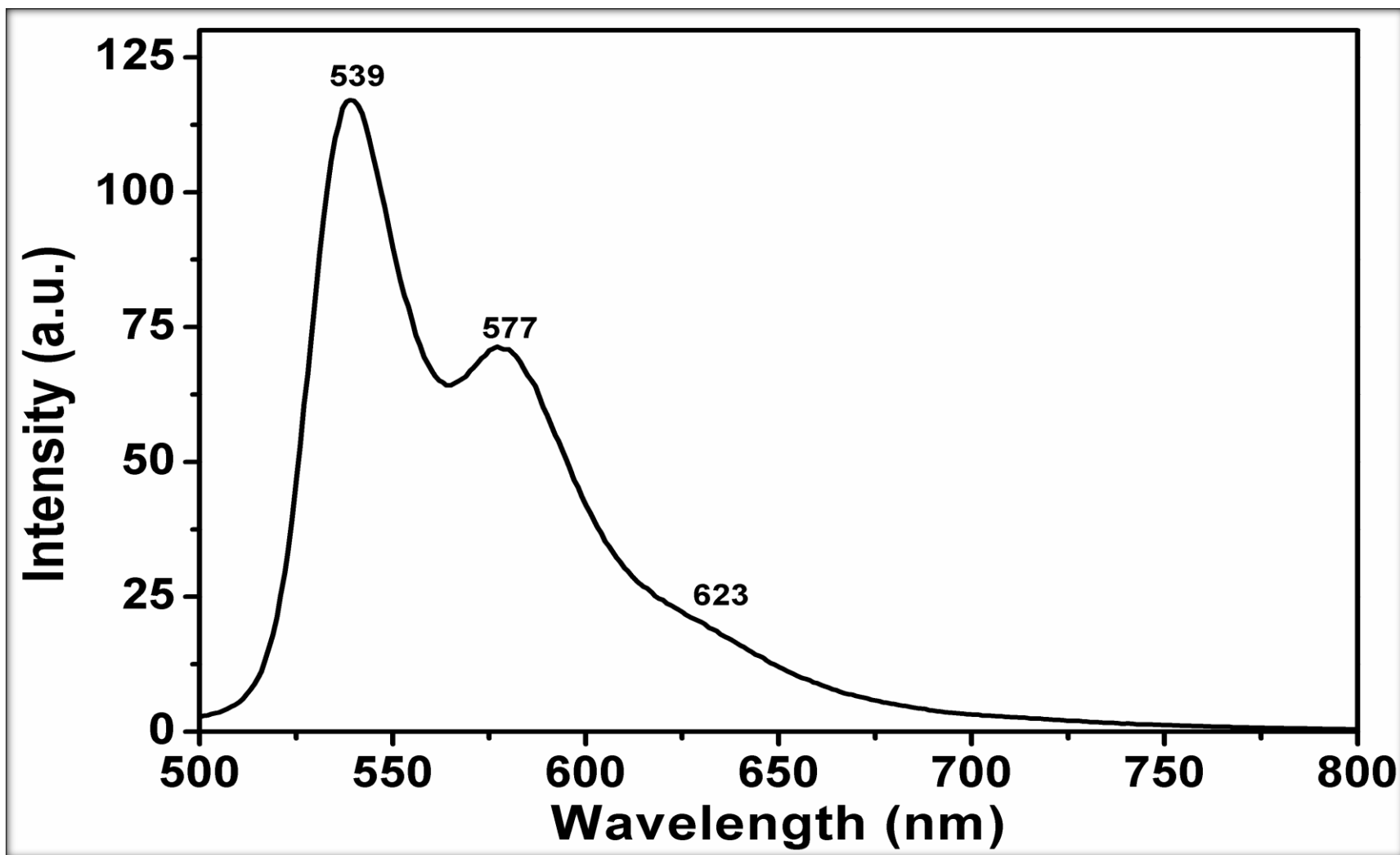


Figure 4.43: LCP3, Emission Spectrum DMSO

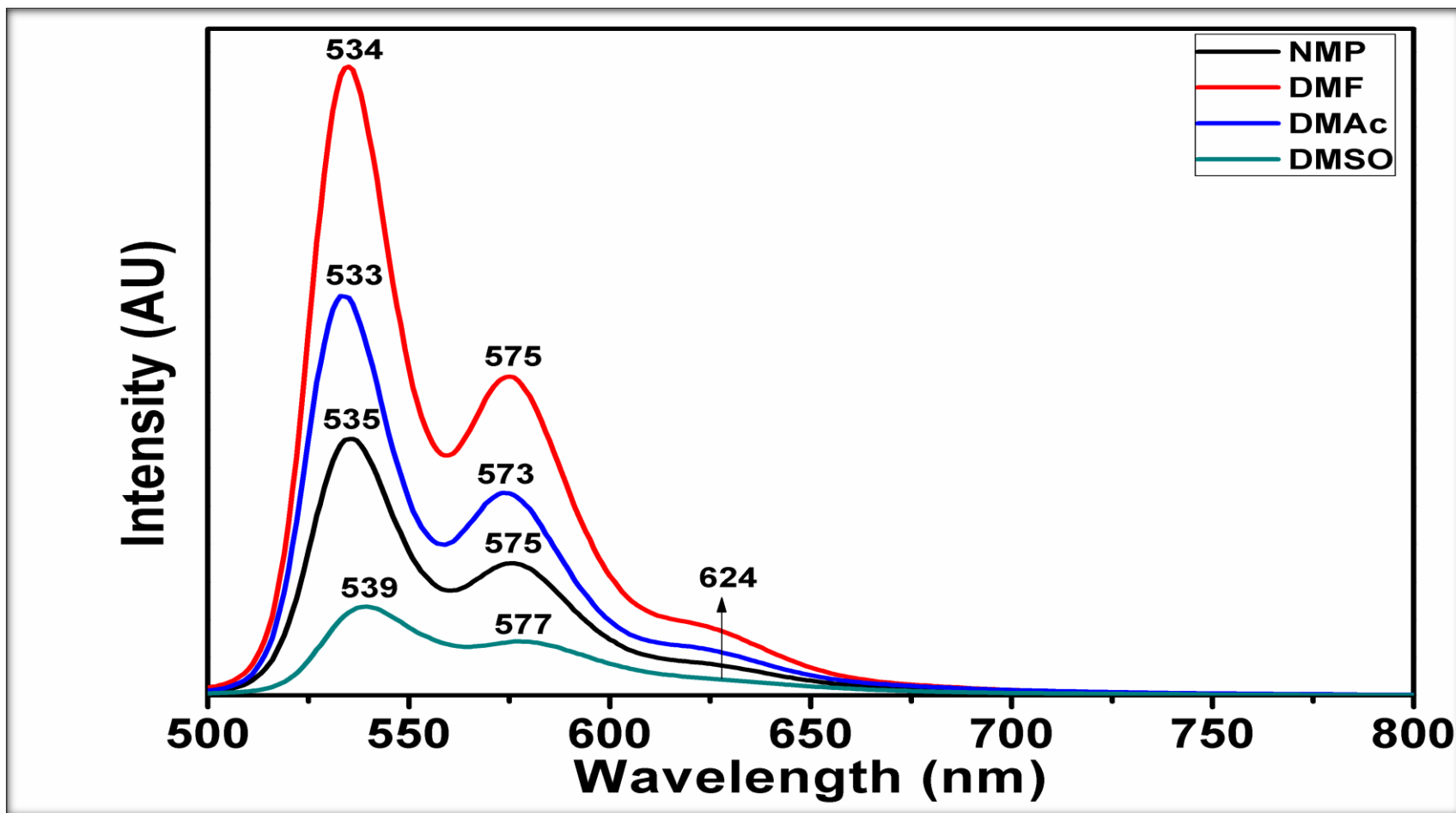


Figure 4.44: LCP3, Emission spectra (NMP, DMF, DMAc and DMSO)

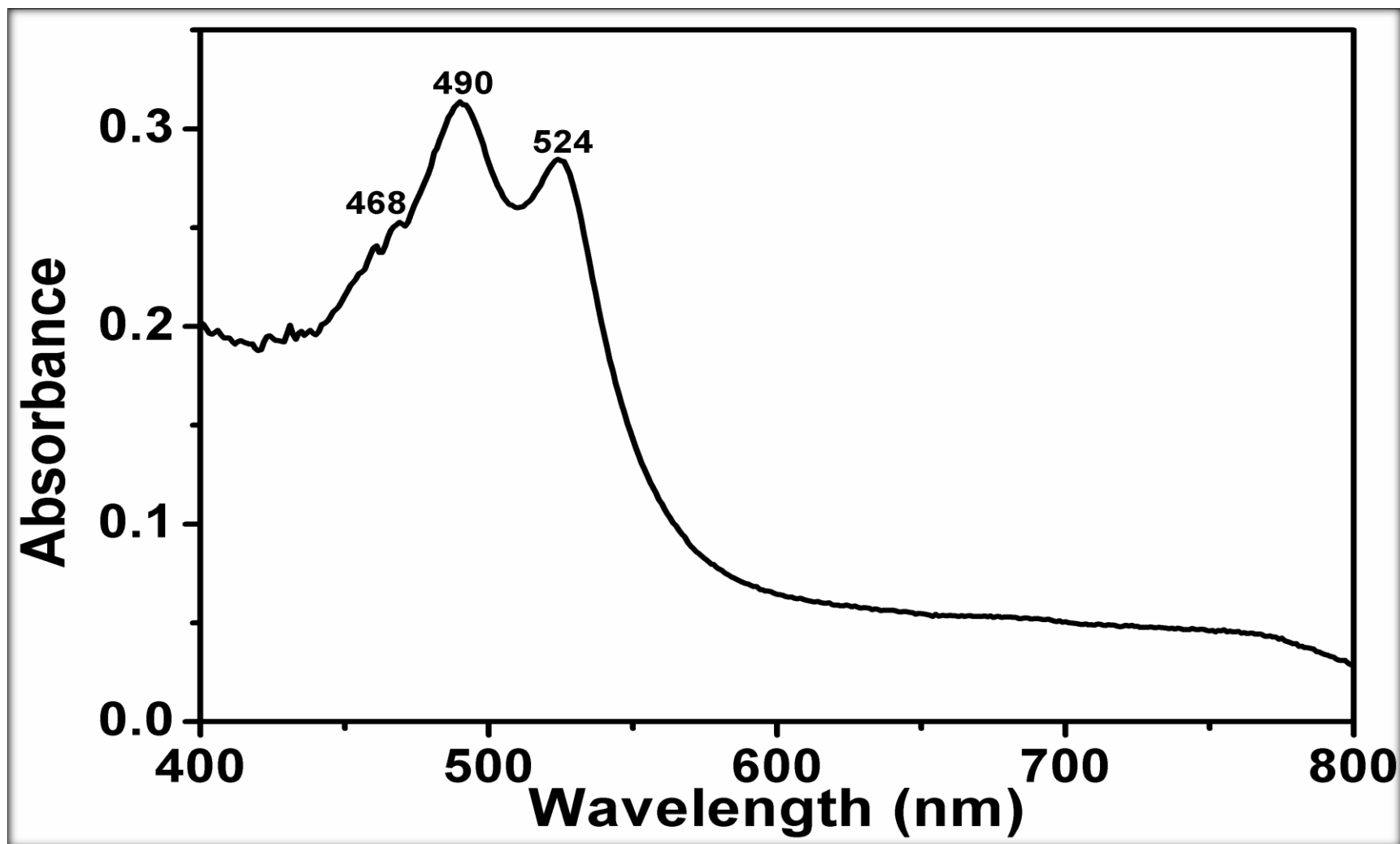


Figure 4.45: LCP4, Absorption Spectrum (NMP)

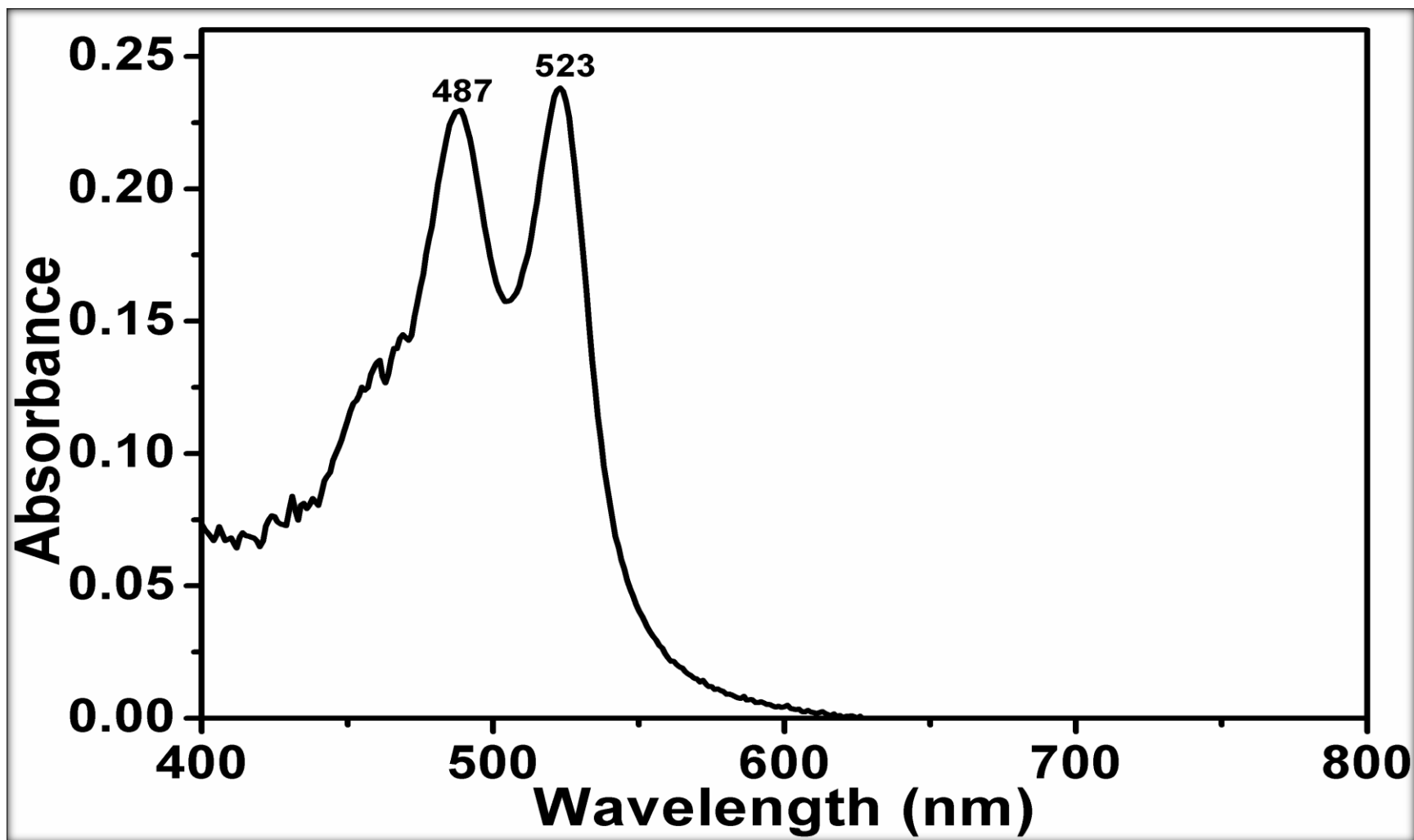


Figure 4.46: LCP4, Absorption Spectrum (DMF)

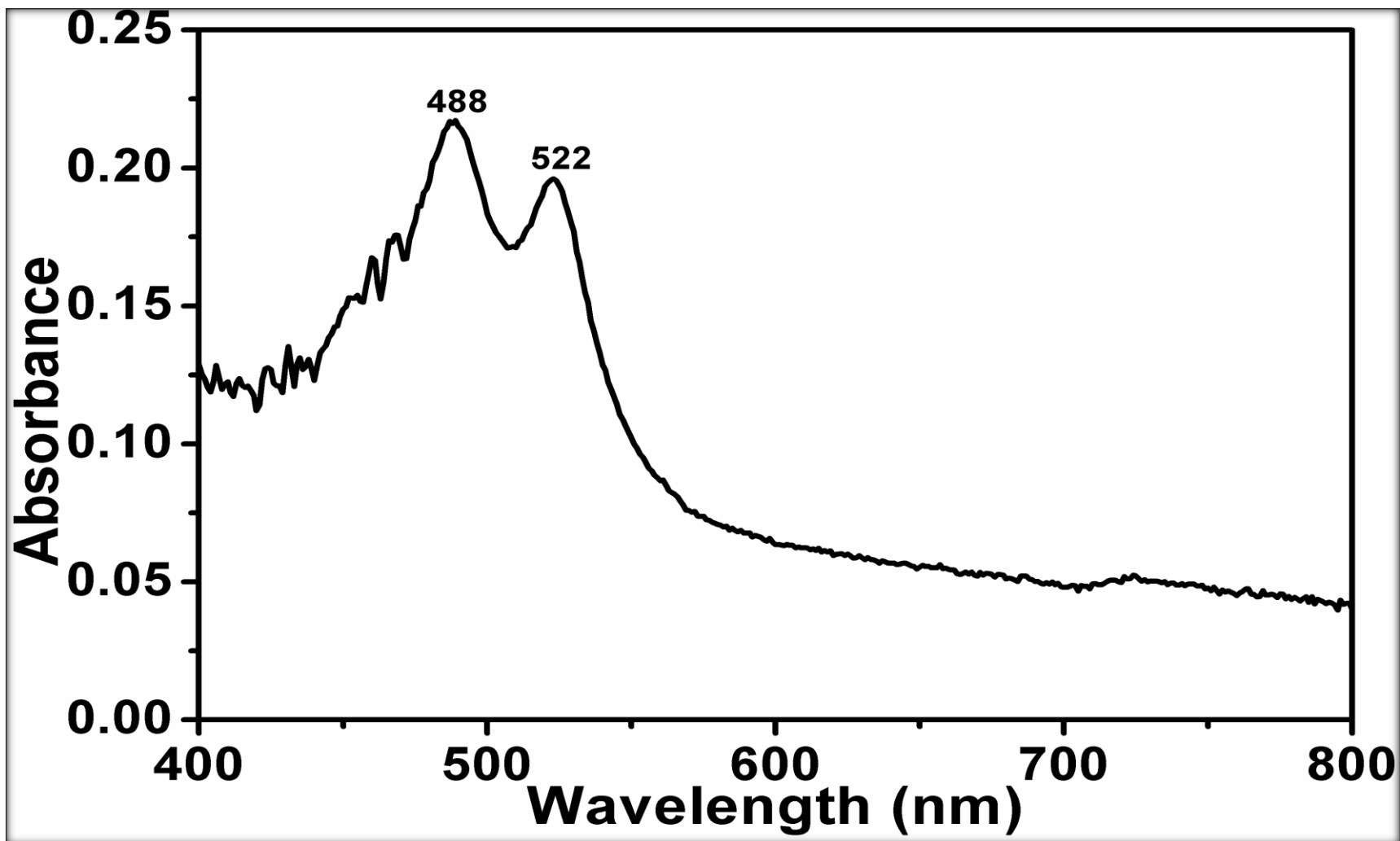


Figure 4.47: LCP4, Absorption Spectrum (DMAc)

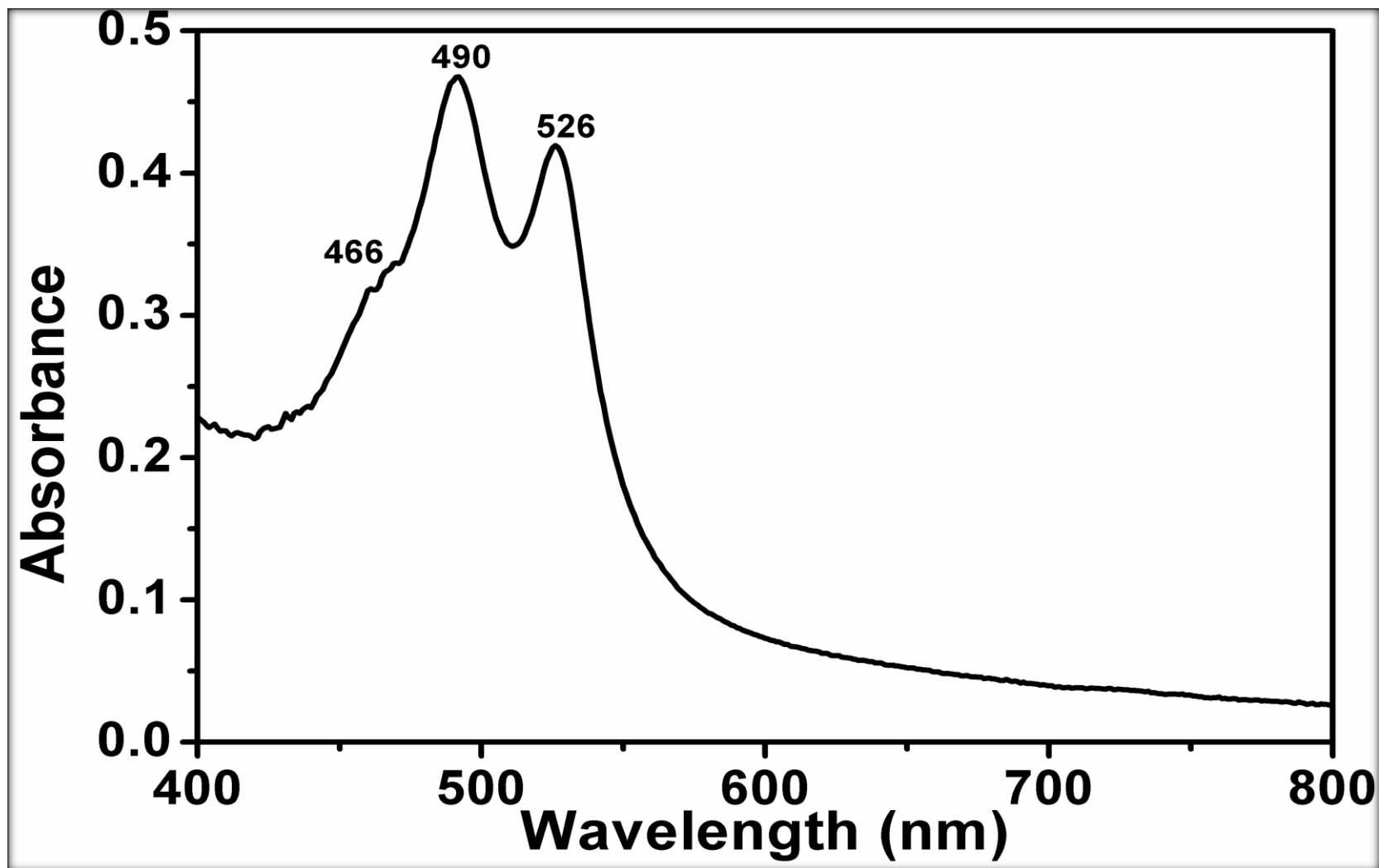


Figure 4.48: LCP4, Absorption Spectrum (DMSO)



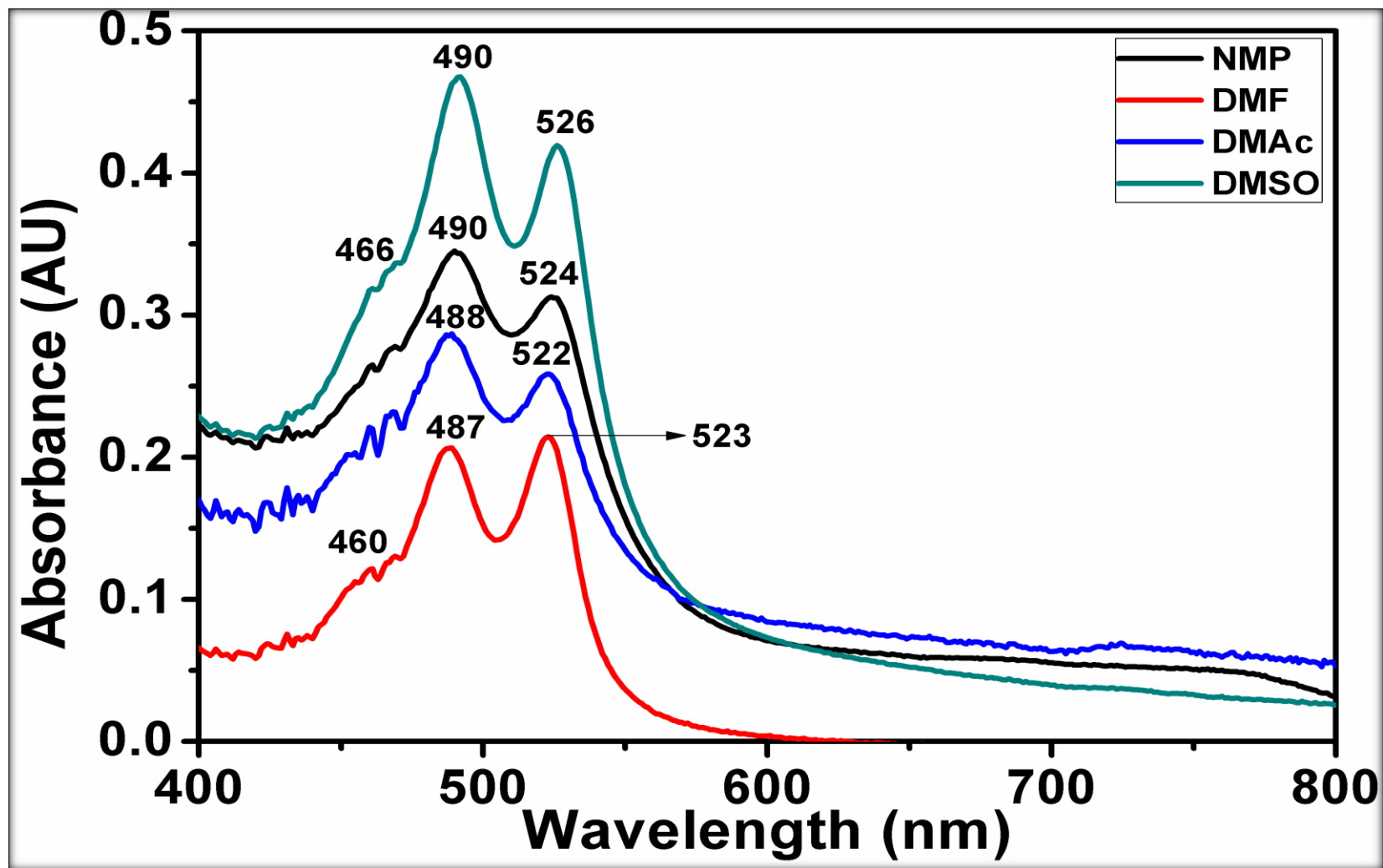


Figure 4.49: LCP4, Absorption Spectra (NMP, DMF, DMAc and DMSO)

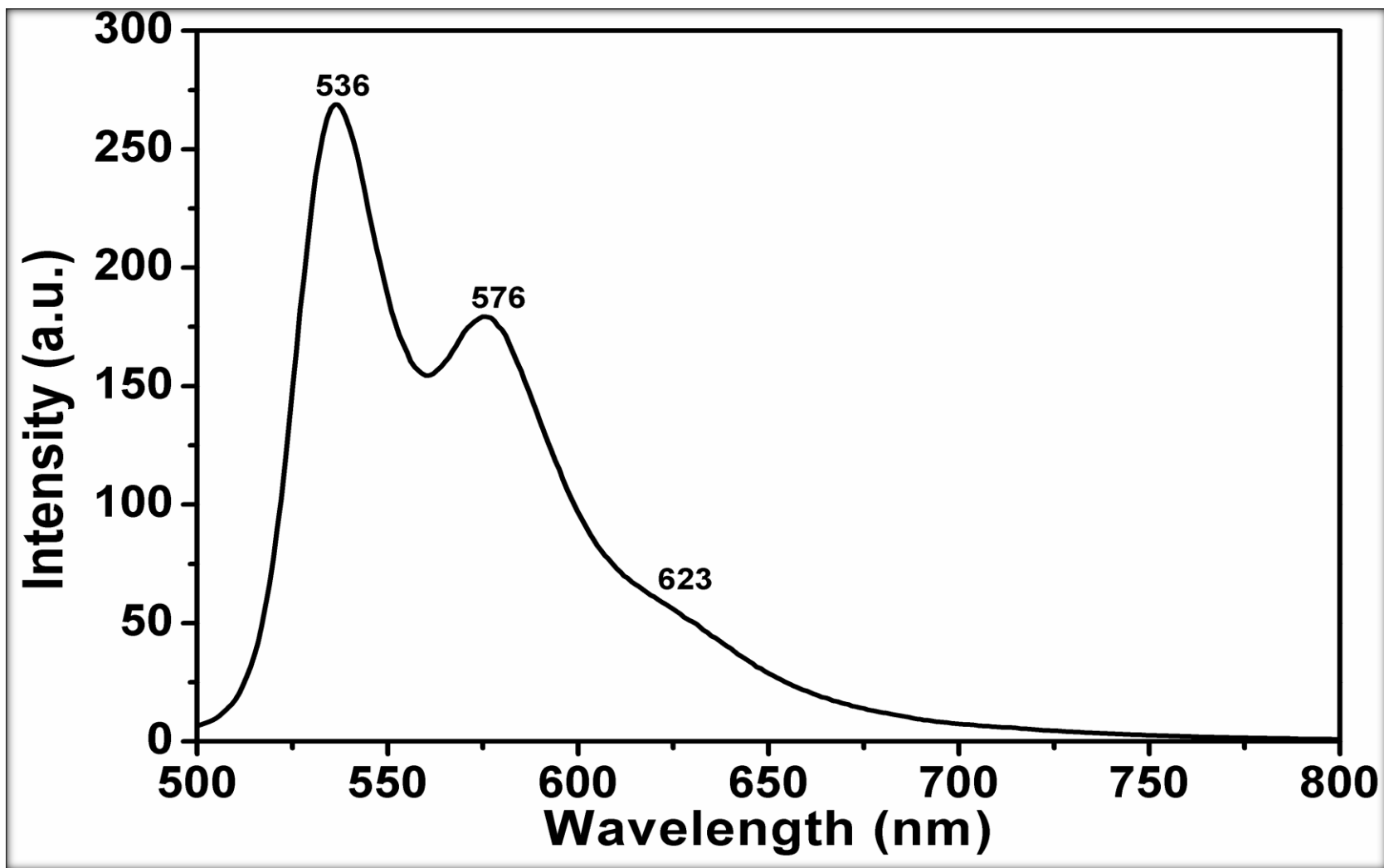


Figure 4.50: LCP4, Emission spectrum (NMP)

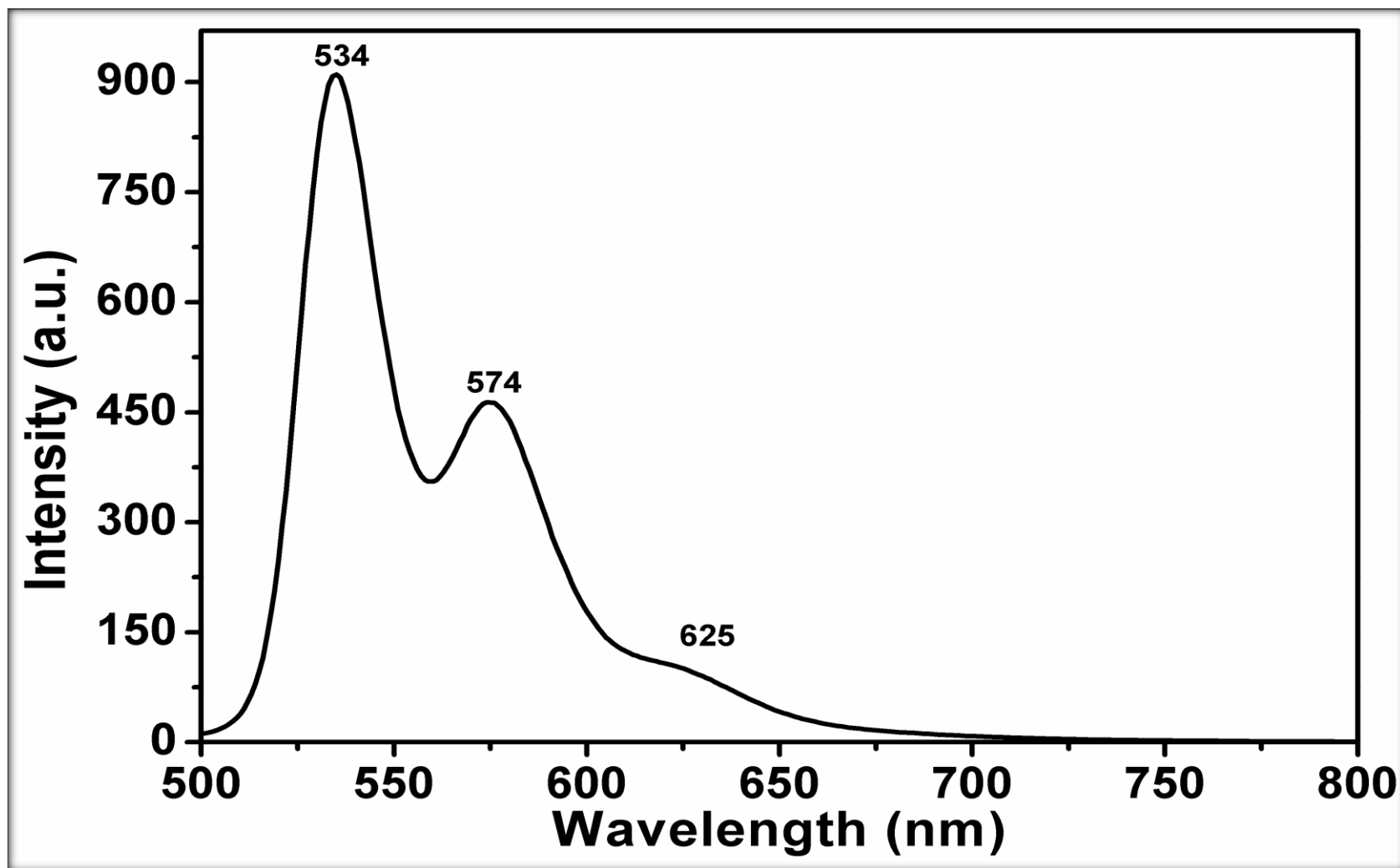


Figure 4.51: LCP4, Emission spectrum (DMF)

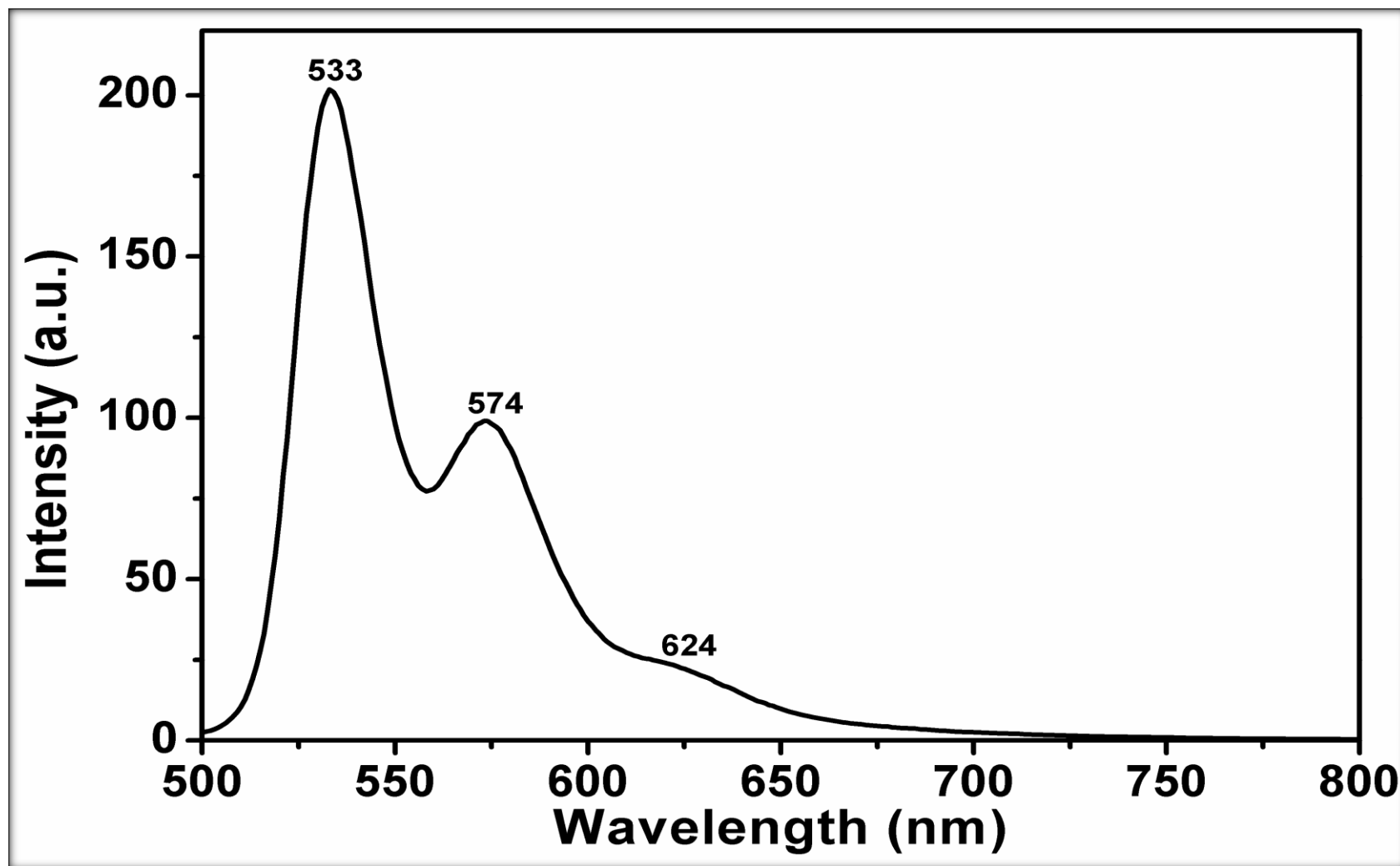


Figure 4.52: LCP4, Emission spectrum (DMAc)

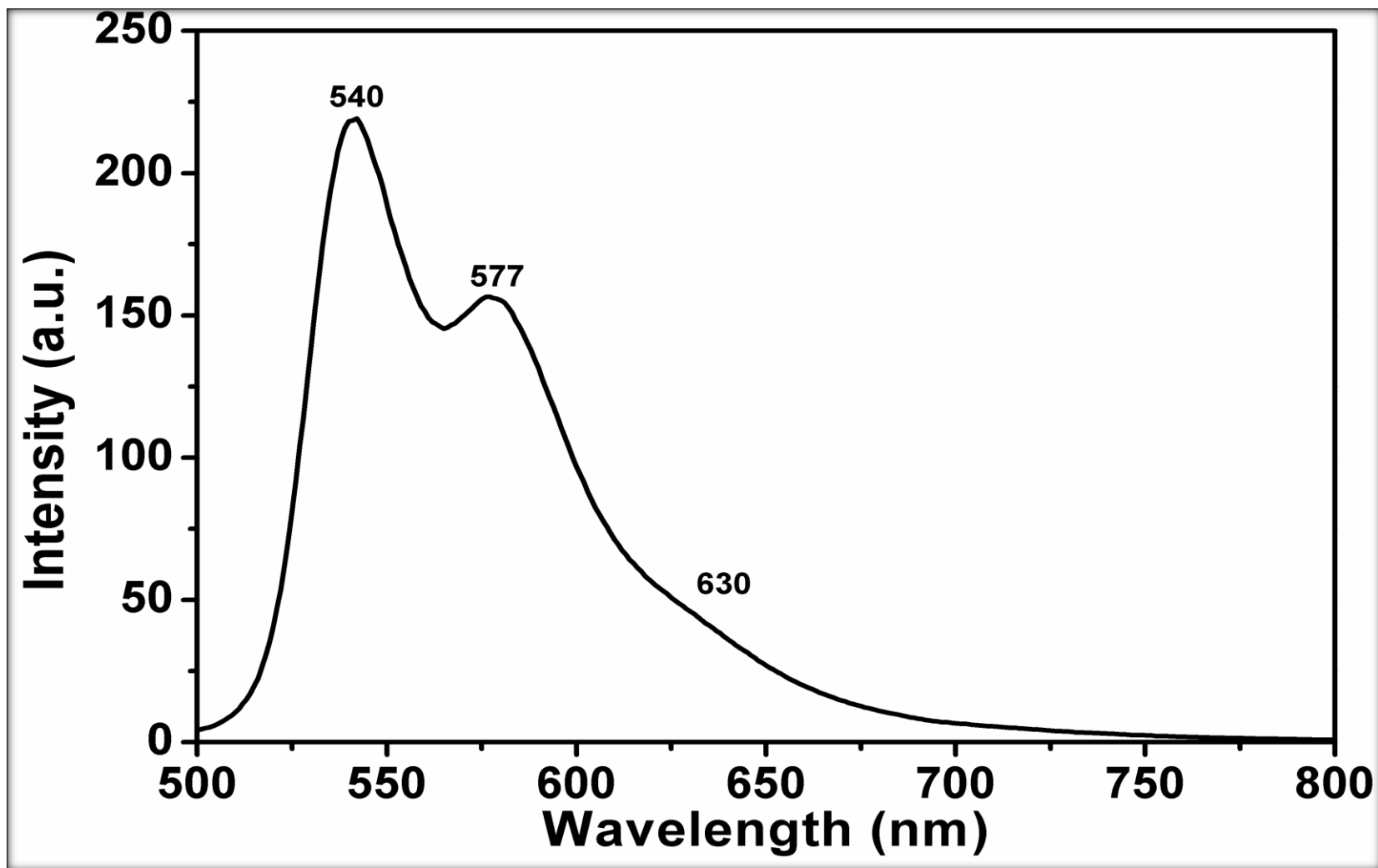


Figure 4.53: LCP4, Emission spectrum (DMSO)

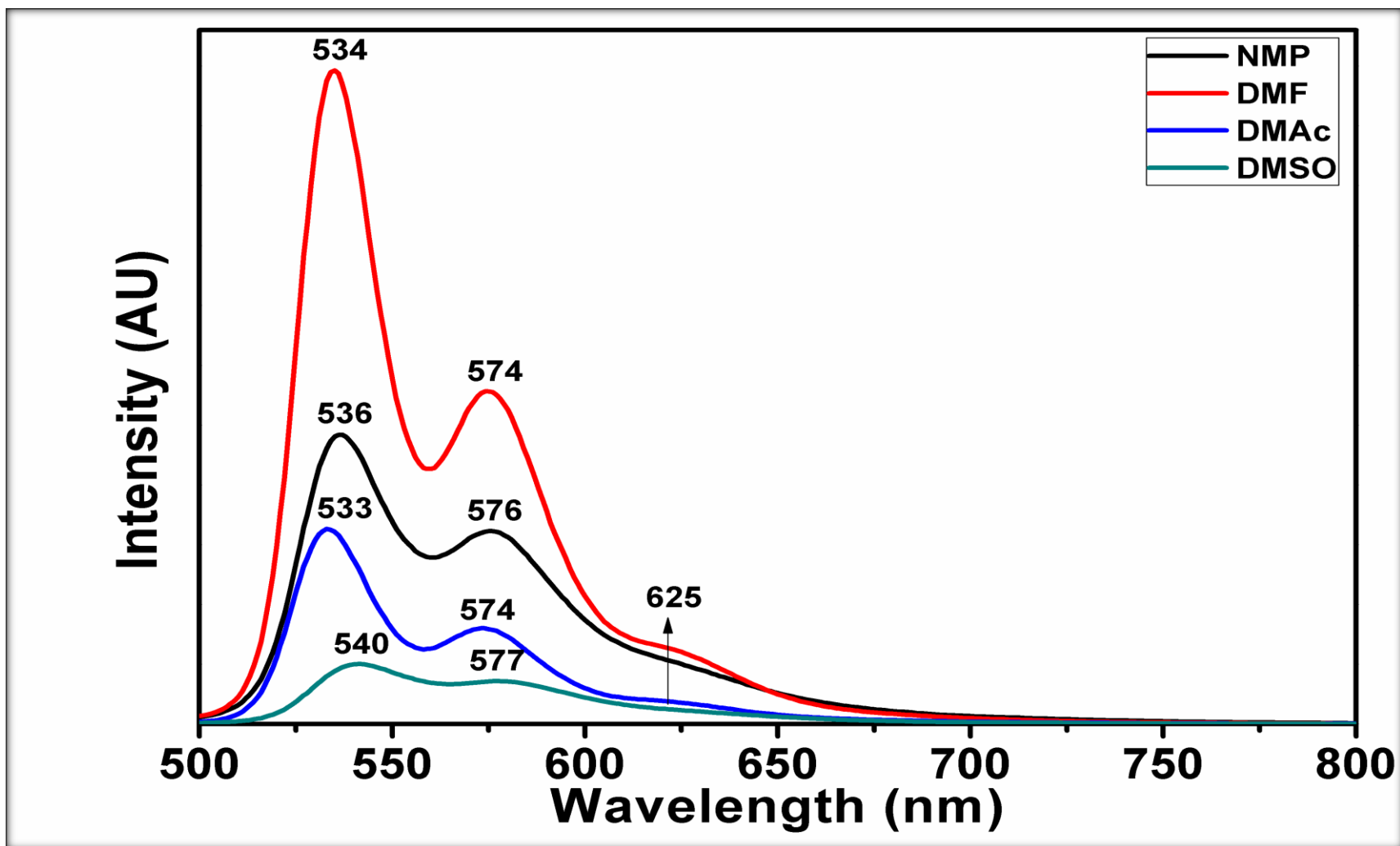


Figure 4.54: LCP4, Emission spectrum (NMP, DMF, DMAc and DMSO)

## Chapter 5

# RESULTS AND DISCUSSIONS

### 5.1 Synthesis and Characterization

The synthesis of chiral perylene diimides substituted chitosan LCPs were carried out through substitution reaction between an intermediate product *N*-((2*S*)-amino hexanoic acid)-3,4,9,10-perylene tetracarboxylic-3,4-anhydride-9,10-imide LPMI [10] and commercially existing chitosan (CH) under argon atmosphere. The LCP synthetic route is shown in Scheme 3.1. The mono anhydride part of LPMI molecules reacts with the amine groups of the CH backbone to synthesize LPCs. The structure and the properties of the LPCs have been well investigated by FT-IR, UV-vis and fluorescence spectroscopy.

### 5.2 Solubility of LCPs

Solubility details of LPMI, CH, LCP1, LCP2, LCP3 and LCP4 in common organic solvents are illustrated in Table 5.1 and Table 5.2. Chitosan polymer is insoluble in water or common solvent. However, it is soluble in aqueous dilute acids like 1 % HCl and 1 % CH<sub>3</sub>COOH and the solubility is good in low pH. LPMI is insoluble in polar and nonpolar organic solvents except NMP (N-methyl pyrrolidinone). The solubility of LPMI was limited because of the planarity and rigid structure of the monoimide.

Interestingly, Lysine perylene diimides conjugated chitosan polymers have shown better solubilities in polar aprotic solvents like dimethyl sulfoxide, N,N-dimethyl

formamide, dimethyl acetamide and N-methyl pyrrolidinone at the 60 °C in comparison with CH and LPMI. However, it is observed that, solubility increases from LCP1 toward LCP4.

Significant efforts have been spent to synthesize soluble fluorescent chitosan polymers which might be worthily applied in several biomedical applications.



Table 5.1: Solubility properties of LPMI\* and CH

Solvent	LPMI		CH	
	Solubility	Color	Solubility	Color
<b>CHCl<sub>3</sub></b>	(- -)	-	(- -)	-
<b>EtAc</b>	(- -)	-	(- -)	-
<b>CH<sub>2</sub>Cl<sub>2</sub></b>	(- -)	-	(- -)	-
<b>Acetone</b>	(- -)	-	(- -)	-
<b>EtOH</b>	(- -)	-	(- -)	-
<b>MeOH</b>	(- -)	-	(- -)	-
<b>NMP</b>	(+ +)	Orange	(- -)	-
<b>DMF</b>	(- -)	-	(- -)	-
<b>CH<sub>3</sub>CN</b>	(- -)	-	(- -)	-
<b>DMAc</b>	(- -)	-	(- -)	-
<b>DMSO</b>	(- -)	-	(- -)	-
<b>H<sub>2</sub>O</b>	(- -)	-	(- -)	-
<b>KOH (3%)</b>	(+ +)	Dark red	(- -)	-
<b>NaOH (5%)</b>	(- -)	-	(- -)	-
<b>Acetic acid (1%)</b>	(- -)	-	(+ +)	-

(+ +): Soluble, (- -): not soluble at room temperature, \*: [9].

Table 5.2: Solubility properties of LCP1, LCP2, LCP3 and LCP4

solvent	LCP1		LCP2		LCP3		LCP4	
	Solubility	Color	Solubility	Color	Solubility	Color	Solubility	Color
<b>CHCl<sub>3</sub></b>	(- -)	-	(- -)	-	(- -)	-	(- -)	-
<b>EtAc</b>	(- -)	-	(- -)	-	(- -)	-	(- -)	-
<b>CH<sub>2</sub>Cl<sub>2</sub></b>	(- -)	-	(- -)	-	(- -)	-	(- -)	-
<b>Acetone</b>	(- -)	-	(- -)	-	(- -)	-	(- -)	-
<b>EtOH</b>	(- -)	-	(- -)	-	(- -)	-	(- -)	-
<b>MeOH</b>	(- -)	-	(- -)	-	(- -)	-	(- +)*	PaleYellow
<b>NMP</b>	(- +)*	Pale Pink	(- +)	Pale Pink	(- +)	Pale Pink	(- +)	Pale Pink
<b>DMF</b>	(- +)*	Pale Pink	(- +)*	Pale Pink	(- +)	Pale Pink	(- +)	Pale Pink
<b>CH<sub>3</sub>CN</b>	(- -)	-	(- -)	-	(- -)	-	(- +)	-
<b>DMAc</b>	(- +)*	Pale Pink	(- +)*	Pale Pink	(- +)*	Pale Pink	(- +)*	Pale Pink
<b>DMSO</b>	(- +)*	Pale Pink	(- +)*	Pale Pink	(- +)	Pale Pink	(- +)	Pale Pink
<b>H<sub>2</sub>O</b>	(- -)	-	(- -)	-	(- -)	-	(- -)	-
<b>KOH (3%)</b>	(- +)*	Pale Pink	(- +)*	Pale Pink	(- +)*	Pale Pink	(- +)*	Pale Pink
<b>Acetic acid (1%)</b>	(- -)	-	(- -)	-	(- -)	-	(- -)	-

(- +): partially soluble, \* solubility increase upon heating at 60 ° C, (- -): insolub

### 5.3 Analysis of FTIR Spectra

Chemical structure of LPMI and CH were assigned and analyzed by using FTIR spectroscopy in terms of functional groups. As shown in Figure 4.5 and Figure 4.6, the FTIR spectrum of CH has distinctive band at  $3404\text{ cm}^{-1}$  ( $\text{NH}_2$  O-H stretch);  $2872\text{ cm}^{-1}$  (aliphatic C-H stretch);  $1658\text{ cm}^{-1}$  (Amide I C=O stretch);  $1599\text{ cm}^{-1}$  (Amide II. N-H stretch);  $1379$  (C-N stretch);  $1154$  and  $1081\text{ cm}^{-1}$  (pyranose). Also, as given in Figure 4.5, LPMI has a unique band at  $3407\text{ cm}^{-1}$  ( $\text{NH}_2$  O-H stretch);  $3072\text{ cm}^{-1}$  (aromatic C-H stretch);  $2862\text{ cm}^{-1}$  (aliphatic C-H stretch);  $1766\text{-}1729\text{ cm}^{-1}$  (anhydride C=O stretch);  $1692,1650\text{ cm}^{-1}$  (imide C=O stretch);  $1593\text{ cm}^{-1}$  (Ar C=C stretch);  $1342\text{ cm}^{-1}$  (C-N stretch);  $1017\text{ cm}^{-1}$  (C-O stretch);  $856, 809, 738\text{ cm}^{-1}$  (Ar C-H bend). The covalent bonding of the LPMI to chitosan back bone was demonstrated by FT-IR spectroscopy. Figure 4.7, 4.8, 4.9 and 4.10 presented FTIR spectra of synthesized compounds. It is clear that, new Polyimide formed. There are two significant characteristic changes of LPMI bands. Firstly, the disappearance of anhydride C=O stretching bands at around  $1766\text{ cm}^{-1}$ . Secondly, the distinctive peak of the C-O-C stretching at around  $1017\text{ cm}^{-1}$  had disappeared. On the Other hand O-H groups of chitosan has shifted to around  $3385\text{ cm}^{-1}$  from  $3407\text{ cm}^{-1}$ .

As shown in Figure 4.7, the FT-IR spectrum of LCP1 has distinctive bands at  $3384\text{ cm}^{-1}$  ( $\text{NH}_2$  O-H Stretch);  $2922\text{ cm}^{-1}$  (aromatic C-H stretch);  $2850\text{ cm}^{-1}$  (aliphatic C-H stretch);  $1687, 1656\text{ cm}^{-1}$  (imide C=O stretch);  $1597\text{ cm}^{-1}$  (conjugated C=C stretch) and  $1336\text{ cm}^{-1}$  (C-N stretch);  $1069\text{ cm}^{-1}$  (C-O stretch);  $827, 811, 739\text{ cm}^{-1}$  (Ar C-H bend).

The IR spectrum of LCP2, as given in Figure 4.8 has unique peaks at 3391  $\text{cm}^{-1}$  ( $\text{NH}_2$  O-H stretch); 2920  $\text{cm}^{-1}$  (aromatic C-H stretch); 2849  $\text{cm}^{-1}$  (aliphatic C-H stretch); 1689, 1654  $\text{cm}^{-1}$  (imide C=O stretch); 1597  $\text{cm}^{-1}$  (conjugated C=C stretch) and 1342  $\text{cm}^{-1}$  (C-N stretch); 1041  $\text{cm}^{-1}$  (C-O stretch); 811, 747  $\text{cm}^{-1}$  (Ar C-H bend).

As shown in Figure 4.9, the IR spectrum of LCP3 has distinctive bands at 3386  $\text{cm}^{-1}$  ( $\text{NH}_2$ O-H Stretch); 2920  $\text{cm}^{-1}$  (aromatic C-H stretch); 2851  $\text{cm}^{-1}$  (aliphatic C-H stretch); 1691, 1655  $\text{cm}^{-1}$  (imide C=O stretch); 1593  $\text{cm}^{-1}$  (conjugated C=C stretch) and 1342  $\text{cm}^{-1}$  (C-N stretch); 1064  $\text{cm}^{-1}$  (C-O stretch); 809, 746  $\text{cm}^{-1}$  (Ar C-H bend).

The IR spectrum of LCP4, as given in Figure 4.10 has unique peaks at 3386  $\text{cm}^{-1}$  ( $\text{NH}_2$  O-H stretch); 2922  $\text{cm}^{-1}$  (aromatic C-H stretch); 2852  $\text{cm}^{-1}$  (aliphatic C-H stretch); 1692, 1655  $\text{cm}^{-1}$  (imide C=O stretch); 1593  $\text{cm}^{-1}$  (conjugate C=C stretch) and 1342  $\text{cm}^{-1}$  (C-N stretch); 1066  $\text{cm}^{-1}$  (C-O stretch); 810, 746  $\text{cm}^{-1}$  (Ar C-H bend).

## 5.4 Absorption and Fluorescence Properties

Optical characteristics of LCPs were investigated in NMP, DMF, DMAc and DMSO through UV-vis absorption and emission spectroscopy. The absorption spectra of the LCP polymers in different solvents were shown in Figure 4.11- Figure 4.54.

LCP polymers exhibited red shifted peaks (bathochromic shift) in polar aprotic solvents. Also, it was observed that, the bathochromic shifts slightly increased with increasing solvent polarity. The absorption spectra of LCPs shown two characteristic peaks in the range of 485-525 nm which related respectively to 0-1 and 0-0 (vibronic transitions). On the other hand, the fluorescence spectra of LCPs exhibits two distinctive peaks at around 530 and 570 nm and one shoulder approximately at 625 nm. Small stokes shifts were noticed. Table 5.3-Table 5.6 represent the absorption and emission bands, Stokes shifts and intensity ratio of LCPs.

The emission spectrum of all LCPs was determined at  $\lambda_{exc} = 485$  nm and the related fluorescence quantum yield were measured in DMF using *N,N'*-didodecyl-3,4,9,10-perylenebis(dicarboximide) in CHL.

### 5.4.1 Optical properties of LCP1

Table 5.3: The maximum wavelengths of absorption and fluorescence of LCP1

<b>Solvent</b>	<b>Uv-vis (<math>\lambda_{\text{max}}</math>, nm)</b>	<b>Flu.Emis (<math>\lambda_{\text{max}}</math>, nm)</b>	<b>Stokes shift (<math>\Delta\lambda</math>, nm)</b>	<b>Intensity Ratio</b>
<b>NMP</b>	488, 524	535, 573	11	0.84
<b>DMF</b>	487, 522	534, 574, 625	12	1.02
<b>DMAc</b>	488, 523	533, 572, 624	10	0.97
<b>DMSO</b>	490, 526	538, 577, 627	12	1.0

The UV-vis spectrum of LCP1 in NMP (Figure 4.15) shows two characteristic bands at 524 nm ( $0 \rightarrow 0$ ) and 488 nm ( $0 \rightarrow 1$ ) which related to vibronic transition of  $\pi-\pi^*$  of perylene molecule. As well as, emission spectra was investigated in NMP, two characteristic fluorescence peaks were observed at 535 and 573 nm with a 11 nm Stokes shift as shown in Figure 4.20. The intensity ratio in NMP shows that it is weakly aggregated.

The UV-vis absorption spectrum of LCP1 in DMF, has two distinct peaks at 487 and 522 nm as represented in Figure 4.16. In the emission spectrum of LCP1 in DMF, two bands were observed at 534, 574 nm and 1 shoulder at 625 nm with 12 nm Stokes shift as shown in Figure 4.21.

In the DMAc, the UV-vis absorption of LCP1 represented two peaks at 488 and 523 nm with a weak aggregates as presented in Figure 4.17. The emission spectrum in DMAc shows two bands and a shoulder at 533, 572 and 624 nm, respectively. As shown in Figure 4.22 with 10 nm Stokes.

In DMSO, the absorption spectrum of LCP1 has two distinct peaks at 490 and 526 nm with slightly aggregated as represented in Figure 4.18. The fluorescence spectrum of LCP1 in DMSO, two bands and one shoulder peak were noticed at 538, 578 and 626 nm as represented in Figure 4.23 with 12 nm Stokes shift.

The comparison of absorption and fluorescence spectra and Stokes shift of LCP1 in NMP, DMF, DMAc and DMSO were demonstrated in Figure 4.15 and Figure 4.20.

### 5.4.2 Optical properties of LCP2

Table 5.4: The maximum wavelengths of UV-vis absorption and fluorescence of LCP2

<b>Solvent</b>	<b>Uv-vis (<math>\lambda_{\max}</math>, nm)</b>	<b>Flu.Emis (<math>\lambda_{\max}</math>, nm)</b>	<b>Stokes shift (<math>\Delta\lambda</math>, nm)</b>	<b>Intensity Ratio</b>
<b>NMP</b>	488, 522	536, 574, 624	14	0.97
<b>DMF</b>	456, 487, 522	534, 574, 624	12	1.08
<b>DMAc</b>	487, 522	533, 574, 625	11	0.94
<b>DMSO</b>	459, 490, 526	538, 578, 626	12	1.076

The UV-vis absorbance spectrum of LCP2 in NMP has two absorption peaks at 488 and 522 nm with slightly aggregated as shown in Figure 4.25. The fluorescence spectrum is obtained in NMP with the emission peaks at 536 and 574 nm and a shoulder at 624 nm. Stokes shift was found 14 nm as shown in Figure 4.30.

The UV-vis absorbance spectrum of LCP2 in DMF has three distinct absorption peaks at 456, 487 and 522 nm as shown in Figure 4.26. In the fluorescence spectrum,

three peaks at 534, 574 and 624 nm were indicated with 12 nm Stokes shift as shown in Figure 4.31.

The UV-vis absorption spectrum of LCP2 in DMAc, two peaks were obtained at 487 and 522 nm with slightly aggregated as indicated in Figure 4.27. The emission spectrum of LCP2 in DMAc, two band and a shoulder were noticed at 533, 574 and 625 nm respectively. Stokes shift was found 11 nm as show in Figure 4.32.

In DMSO, the UV-vis absorption spectrum of LCP2 has three characteristic band at 459, 490 and 526 nm with slightly aggregation as shown in Figure 4.28. The fluorescence spectra of LCP2 has three peaks at 533, 578 and 626 nm with 12 nm Stokes shift as defined in Figure 4.33.

The comparison of absorption and fluorescence spectra and Stokes shift of LCP2 in NMP, DMF, DMAc and DMSO were demonstrated in Figure 4.29 and Figure 4.34.

### 5.4.3 Optical properties of LCP3

Table 5.5: The maximum wavelengths of UV-vis absorption and fluorescence of LCP3

<b>Solvent</b>	<b>Uv-vis (<math>\lambda_{\max}</math>, nm)</b>	<b>Flu.Emis (<math>\lambda_{\max}</math>, nm)</b>	<b>Stokes shifts (<math>\Delta\lambda</math>, nm)</b>	<b>Intensity Ratio</b>
<b>NMP</b>	460, 490, 524	535, 575, 625	11	0.93
<b>DMF</b>	460, 488, 522	534, 575, 625	12	1.08
<b>DMAc</b>	460, 489, 524	533, 573, 623	9	0.91
<b>DMSO</b>	460, 492, 526	539, 577, 623	13	0.88



The UV-vis absorption spectrum taken in NMP, has three distinct absorption peaks at 460, 490 and 524 nm with a slight aggregate as shown in Figure 4.35. In the fluorescence spectrum of LCP3 in NMP, two bands and a shoulder were noticed at 535, 575 and 625 nm, as defined in Figure 4.40 with 11 nm Stokes shift.

The absorption spectrum of LCP3 in DMF has three characteristic bands at 460, 488 and 522 nm as represented in Figure 4.36. The emission spectrum of LCP3 in DMF, two bands and one shoulder were recognized at 533, 573 and 623 nm with 9 nm Stokes shift as defined in Figure 4.41.

The UV-vis absorption spectrum of LCP3 taken in DMAc has shown two absorbance peaks at 489 and 524 nm with a slight aggregates as shown in Figure 4.37. fluorescence spectrum of LCP3 in DMAc has three peaks at 533, 573 and 623 nm, respectively, as represented in Figure 4.42 with 9 nm Stokes shift.

In DMSO, the absorption peak at 492 and 526 nm were observed with aggregation (absorption ratio = 0.88) for LCP3 and specified in Figure 4.38. The fluorescence spectrum of LCP3 has three peaks at 534, 575 and 622 nm with 13 nm Stokes shift as defined in Figure 4.43.

The comparison of absorption and fluorescence spectra and Stokes shift of LCP3 in NMP, DMF, DMAc and DMSO were shown in Figure 4.39 and Figure 4.44.

#### 5.4.4 Optical Properties of LCP4

Table 5.6: The maximum wavelengths of UV-vis absorption and fluorescence of LCP4

<b>Solvent</b>	<b>Uv-vis (<math>\lambda_{\max}</math>, nm)</b>	<b>Flu.Emis (<math>\lambda_{\max}</math>, nm)</b>	<b>Stokes shifts (<math>\Delta\lambda</math>, nm)</b>	<b>Intensity Ratio</b>
<b>NMP</b>	468, 490, 524	536, 576, 623	12	0.858
<b>DMF</b>	487, 523	534, 574, 625	11	1.04
<b>DMAc</b>	488, 522	533, 574, 624	11	0.86
<b>DMSO</b>	466, 490, 526	540, 577, 630	14	0.889

Three characteristic bands at 468, 490 and 524 nm were observed with slightly aggregation in the UV-vis absorption spectrum of LCP4 in NMP as presented in Figure 4.45. In the emission spectra of LCP4 in NMP, two characteristic peaks were observed at 535 and 575 nm and a shoulder at 625 nm with 11 nm Stokes shift as represented in Figure 4.50.

The UV-vis absorption spectrum of LCP4 in DMF, two peaks were obtained at 487 and 523 nm with a slight aggregate as represented in Figure 4.46. The emission spectra of LCP4 in DMF, two peaks and a shoulder were observed at 534, 574 and 625 nm with 11 nm Stokes shift as represented in Figure 4.51.

LCP4 in DMAc, the UV-vis absorption spectrum of LCP4 has two distinctive bands at 488 and 522 nm with a slight aggregate as shown in Figure 4.47. The emission spectrum of LCP4 in DMAc, two bands and one shoulder were observed at 533, 574 and 624 nm, respectively, with 14 nm Stokes shift as defined in Figure 4.52.

In the UV-vis absorption spectra of LCP4 in DMSO. Three characteristic bands at 466, 490 and 526 nm were observed with slight aggregates as shown in Figure 4.48. Fluorescence spectrum of LCP4 in DMSO, two peaks and a shoulder peak were defined at 540,577 and 630 nm with 14 nm stoke shift as defined in Figure 4.53.

Absorption and fluorescence spectra and Stokes shifts of LCP4 in NMP, DMF, DMAc and DMSO were demonstrated in Figure 4.49 and Figure 4.54.

On the other hand, in chapter 4 maximum absorption wavelengths (nm), fluorescence quantum yield ( $\lambda_{exc} = 485$  nm), half-width ( $\text{cm}^{-1}$ ), singlet energy ( $\text{kcal.mol}^{-1}$ ), optical band gap energy (eV), absorption intensity ratios and Stokes shift (nm) data were determined for all synthesized compounds in various solvents and are summarized in the Table 5.7- Table 5.10.

All LPCs have low fluorescence quantum yield in NMP (0.21, 0.38, 0.25, 0.28, for LCP1 to LCP4 respectively) due to aggregation. The highest fluorescent quantum yield observed in DMF (0.50, 0.70, 0.73, 0.87 respectively).

Table 5.7: Optical and photochemical properties of LCP1

Solvent	$\lambda_{max}$ (nm)	$\Phi_f$	$\Delta\bar{\nu}_{1/2}$ ( $\text{cm}^{-1}$ )	$E_s$ ( $\text{kcal.mol}^{-1}$ )	$E_g$ (eV)	$A^{0\rightarrow 0}/A^{0\rightarrow 1}$	$\Delta\lambda$ (nm)
<b>NMP</b>	524	0.21	1480.7	54.58	2.094	0.84	11
<b>DMF</b>	522	0.50	1391.1	54.79	2.214	1.02	12
<b>DMAc</b>	523	0.12	2126.7	54.68	2.067	0.97	10
<b>DMSO</b>	526	0.1	1503.2	54.37	2.145	1.0	12

Table 5.8: Optical and photochemical properties of LCP2

<b>Solvent</b>	$\lambda_{\max}$ (nm)	$\Phi_f$	$\Delta\bar{\nu}_{1/2}$ ( $\text{cm}^{-1}$ )	$E_s$ ( $\text{kcal.mol}^{-1}$ )	$E_g$ (eV)	$A^{0\rightarrow 0}/A^{0\rightarrow 1}$	$\Delta\lambda$ (nm)
<b>NMP</b>	522	0.38	1593.09	54.79	2.160	0.93	11
<b>DMF</b>	522	0.70	1253.9	54.79	2.230	1.08	12
<b>DMAc</b>	522	0.23	1536.25	54.79	2.138	0.91	9
<b>DMSO</b>	526	0.2	1601.07	54.37	2.305	0.88	13

Table 5.9: Optical and photochemical properties of LCP3

<b>Solvent</b>	$\lambda_{\max}$ (nm)	$\Phi_f$	$\Delta\bar{\nu}_{1/2}$ ( $\text{cm}^{-1}$ )	$E_s$ ( $\text{kcal.mol}^{-1}$ )	$E_g$ (eV)	$A^{0\rightarrow 0}/A^{0\rightarrow 1}$	$\Delta\lambda$ (nm)
<b>NMP</b>	524	0.25	1581.03	54.58	2.160	0.93	11
<b>DMF</b>	522	0.73	1322.75	54.79	2.230	1.08	12
<b>DMAc</b>	524	0.12	1503.22	54.58	2.138	0.91	9
<b>DMSO</b>	526	0.09	1349.44	54.37	2.305	0.88	13

Table 5.10: Optical and photochemical properties of LCP4

<b>Solvent</b>	$\lambda_{\max}$ (nm)	$\Phi_f$	$\Delta\bar{\nu}_{1/2}$ ( $\text{cm}^{-1}$ )	$E_s$ ( $\text{kcal.mol}^{-1}$ )	$E_g$ (eV)	$A^{0\rightarrow 0}/A^{0\rightarrow 1}$	$\Delta\lambda$ (nm)
<b>NMP</b>	524	0.22	1302.68	54.58	2.175	0.858	12
<b>DMF</b>	523	0.87	1184.55	54.68	2.263	1.04	11
<b>DMAc</b>	522	0.26	1447.83	54.79	2.168	0.86	11
<b>DMSO</b>	526	0.18	1292.8	54.37	2.206	0.889	14

## Chapter 6

### CONCLUSION

In this thesis, four novel comb shaped chiral amphiphilic polymers were synthesized successfully by substitution reaction between low molecular weight chitosan (CH) and different amounts of *N*-((2*S*)-amino hexanoic acid)-3,4,9,10-perylene tetracarboxylic-3,4-anhydride-9,10-imide (LPMI). The structure and optical properties of fluorescent chiral chitosan polymers (LCPs) were characterized by FTIR, UV-vis and emission spectroscopy.

Chitosan suffer from limited solubility in either water or organic solvents which limits its processability in various fields. However, the synthesized fluorescent chiral amphiphilic polymers (LCP1, LCP2, LCP3 and LCP4) showed to some extent good solubility in aprotic polar solvents such as NMP, DMF, DMAc and DMSO that could be important in biomedical applications.

A novel comb shaped and chiral amphiphilic polymer is prepared for pharmaceutical applications including hydrophobic drug solubilisation due to the property of amphiphilic polymer to form micelles.

Spectroscopic properties of LCPs were investigated by UV-vis absorption and emission spectroscopy. Interestingly, unlike chitosan which has no UV absorption, the combination of hydrophilic chitosan with hydrophobic LPMI which have comb

shaped structure showed optical and photochemical properties because of extension of  $\pi$ - $\pi$  conjugations. Generally, the UV spectra of lysine perylene mono imide (LPMI) substituted chitosan polymer represented three characteristic peaks with slightly aggregation in aprotic polar solvents such as NMP, DMF, DMAc and DMSO. The absorption bands were shown a red shifted (bathochromically shift) with increasing solvent polarity. As well as, the fluorescence spectra of compound show three emission peaks of  $0 \rightarrow 0$ ,  $0 \rightarrow 1$  and  $0 \rightarrow 2$  transitions with small Stokes shifts.

Optical and photochemical properties of the four amphiphilic chitosan polymers have been investigated. It was noticed the differences between the polymers owing to the differences in the intermolecular interaction for each polymer.

In conclusion, four novel comb shaped chiral amphiphilic chitosan polymers having fluorescent properties could be useful compounds for drug delivery system.

## REFERENCES

- [1] Gade, L., Galka, C., Williams, R., Cola, L., Partlin, M., Dong, B., & Chi, L. (2003). Synthesis, Photophysical properties, and NanoCrystal Formation of a New Class of Tetra-N-Substituted Perylenes. *Angew Chem. Int.Ed* 42, 2677-2681.
- [2] Sun, Y., He, C., Sun, K., Li, Y., Dong, H., Wang, Z., & Li, Z. (2011). Fine-Tuned Nanostructures Assembled from L-Lysine-Functionalized Perylene Bisimides. *Langmuir*. 27, 11364-11371.
- [3] Heek, T., Nikolaus, J., Schwarzer, R., Fasting, C., Welker, P., & Haag, R. (2013). An Amphiphilic Perylene Imido Diester for Selective Cellular Imaging. *Bioconjugate Chem*. 24, 153-158.
- [4] Li, C., & Wonneberger, H. (2012). Perylene Imides for Organic Photovoltaics: Yesterday, Today, and Tomorrow. *Materials. Advanced* 24, 613-636.
- [5] Würthner, F., Möller, C., Fimmel, B., Ogi, S., Leowanawat, P., & Schmidt, D. (2015). Perylene Bisimide Dye Assemblies as Archetype Functional Supramolecular Materials. *Chemical Reviews*. 116, 962-1052.
- [6] Bodapati, J., & Icil, H. (2008). Highly Soluble Perylene Diimide and Oligomeric Diimide Dyes Combining Perylene and Hexacethylene glycol Units: Synthesis, Characterization, Optical and Electrochemical Properties. *Dyes and Pigments*. 79, 224, 224-235.

- [7] Bugnicourt, L., & Ladaviere, C. (2016). Interests of Chitosan nanoparticles Ionically Cross-Linked with Tripolyphosphate for Biomedical Applications. <http://dx.doi.org/10.1016/j.prog> *polym sci.*2016.06.002.
- [8] Kohl, C., Weil, T., Qu, J., & Müllen, K.(2004). Towards Highly Fluorescent and Water-Soluble Perylene Dyes. *Chem. Eur. J.* 10, 5297-5310
- [9] Asir, A., Zanardi, C., Seeber, R., & Icil, H. (2016). A novel unsymmetrically Substituted Chiral Amphiphilic Perylene Diimide: Synthesis, photophysical and electrochemical properties both in Solution and Solid state. *Journal of Photochemistry and Photobiology A: Chemistry.* 318, 104-113
- [10] Refiker, H., & Icil, H. (2011). Amphiphilic and Chiral unsymmetrical Perylene Dye for Solid-state Dye-Sensitized Solar Cells. *Turk J Chem.* 35, 847-859.
- [11] Kozma, E., Kotowski, D., Catellani, M., Luzzati, S., Famulari, A., & Bertini, F. (2013). Synthesis and Characterization of New electron Acceptor perylene diimide molecules for photovoltaic application. *Dyes and pigments.* 99, 329-338.
- [12] Berger, J., Reist, M., Mayer, J., Felt, O., Peppas, N., & Gurny, R. (2004). Structure and Interactions in Covalently and Ionically Crosslinked Chitosan Hydrogels for Biomedical Application. *European Journal of Pharmaceutics and Biopharmaceutics,* 57, 19-34.



- [13] Rinaudo, M.(2006). Chitin and Chitosan: Properties and Applications. *Prog. Poly. Sci.* 31, 603-632.
- [14] Kurita, K.(2001). Controlled Functionalization of The Polysaccharide chitin. *Prog. Polym.Sci* 26, 1921-1971.
- [15] Domard, A.(2011). A perspective On 30 Years research On Chitin and Chitosan. *Carbohydrate Polymers.* 84, 696-703.
- [16] Thakur, V., & Thakur, M.(2014). Recent Advances in Graft Copolymerization and Applications of Chitosan: A Review. *Acs Sustainable Chem. Eng.* 2, 2637-2652.
- [17] Pillai, C., Paul, W., & Sharma, C.(2009). Chitin and Chitosan Polymers: Chemistry, Solubility and Fiber Formation. *Progress in Polymer Science.* 34, 641-678.
- [18] Temürlü, S. Ms. Thesis (2016). Eastren Mediterranean University.
- [19] Jonassen, H., Kjøni Ksen, A., & Hiorth, M.(2012). Stability of Chitosan Nanoparticles Cross-Linked with Tripolyphosphate. *Biomacromolecules.*13, 3747-3756.
- [20] Torchilin, V. (2001). Structure and Design of Polymeric Surfacta Based Drug Delivery System. *Journal of Controlled Release.* 73, 137-172

- [21] Hoskins, C., Lin, P., & Cheng, W. (2012). A review On Comb-Shaped Amphiphilic Polymers for Hydrophobic Drug Solubilization. *Therapeutic Delivery*. <http://www.ncbi.nlm.nih.gov/pubmed/2283393>.
- [22] Bigot, J., Charleux, B., Cooke, G., Delattre, F., Fournier, D., Lyskawa, J., Sambe, L., Stoffelbach, F & Woisel, P.(2010). Tetrathiafulvalene End-Functionalized Poly (N-Isopropylacrylamide): A New Class of Amphiphilic Polymer for the Creation of Multistimuli Responsive Micelles. *Am. Chem. Soc.* 132, 10796-10801.
- [23] Liaw, D., Wang, Y., Lee, K., Lai, J., & Sikha, C. (2012). Advanced Polyimide Materials: Syntheses, Physical Properties and Applications. *Progress in Polymer Science*. 37, 907-974.
- [24] Huang, C., Barlow, S., & Marder, S.(2011). Perylene-3,4,9,10-Tetracarboxylic Acid Diimides: Synthesis, Physical Properties, and Use in Organic Electronics. *J. Org. Chem.* 76, 2386-2407.
- [25] Qu, J., Zhang, J., Crimdale, A., & Müllen, K.(2004). Dendronized Perylene Diimide Diimide Emitters: Synthesis, Luminescence and Electron and Energy Transfer Studies. *Macromolecules*. 27, 8297-8306.
- [26] Aleshinloye, A., Bodapati, J., & Icil, H.(2015). Synthesis, Characterization, Optical and Electrochemical Properties of A New Chiral Multichromophoric System Based On Perylene and Naphthalene Diimides. *Journal of Photochemistry and Photobiology A: Chemistry*. 300, 27-37.

- [27] Icil, H., & Arslan, E. (2001). Synthesis and Spectroscopic Properties of Highly Pure Perylene Fluorescent Dyes. *Spectroscopy Letters*. 34(3), 355-363.
- [28] Walsh, J., Lee, J., Draper, E., King, S., Jackel, F., Zwijnenburg, M., Adams, D., & Cowan, A. (2016). Controlling Visible Light Driven Photoconductivity in Self-Assembled Perylene Bisimide Structures. *J. Phys. Chem.* 120, 18479-18486.
- [29] Kozma, E., Grisci, G., Mroz, W., Catellani, M., Andicsova, A., Pagano, K., & Galeotti, F. (2016). Water-Soluble Aminoacid Functionalized Perylene Diimides: The Effect of Aggregation On The Optical Properties in Organic and Aqueous Media. *Dyes and Pigments*. 125, 201-209.
- [30] Bellich, B., Agostino, I., Semeraro, S., Gamini, A., & Cesaro, A. (2016). “The Good, The Bad and The Ugly” of Chitosans. *Mar. Drugs*. 14, 99.
- [31] Özdal, D. Ms. Thesis (2009). Eastern Mediterranean University.
- [32] Rafique, A., Zia, K., Zuber, M., Tabasum, S., & Rehman, S. (2016). Chitosan Functionalized Poly (Vinyl Alcohol) For Prospects Biomedical and Industrial Applications: A review. *International Journal of Biological Macromolecules*. 87, 141-154.
- [33] Cheung, R., Ng, T., Wong, J., & Chan, W. (2015). Chitosan: An Update On Potential Biomedical and Pharmaceutical Applications. *Mar. Drugs*. 13, 5156-5186.

- [34] Xiao, y., & Zhou, X. (2008). Synthesis and Properties of A novel Cross Linked Chitosan Resin Modified By L-lysine. *Reactive & Functional Polymers*. 68, 1281-1289.
- [35] Barata, J., Pinto, R., Serra, V., Silvestre, A., Trindade, T., Neves, M., Cavaleiro, J., Daine, S., Sadocco, P., & Freire, C. (2016). Fluorescent Bioactive Corrole Grafted-Chitosan Films. *Biomacromolecules*. 17, 1395-1403.
- [36] Liu, H., Du, Y., Yang, J., & Zhu, H. (2004). Structural Characterization and Antimicrobial Activity of Chitosan / Betaine Derivatives Complex. *Carbohydrate Polymers*. 55, 291-297.
- [37] Jayakumar, R., Menon, D, Manzoor, K., Nair, S., & Tamura, H. (2010). Bio-medical Applications of Chitin and Chitosan Based Nanomaterials-A short Review. *Carbohydrate Polymers*. 82, 227-232.
- [38] Kong, M., Chen, X., Xing, K., & Park, H.(2010). Antimicrobial Properties of Chitosan and Mode of Action: A State of The Art Review. *International Journal of Food Microbiology*. 144, 51-63.
- [39] Zhao, K., Zhang, & Xi., Zhang, L.(2009). The First Biolbased Solar Cells. *Electrochemistry Communications*. 11, 612-615.
- [40] Kadir, M., Majid, S., & Arof, A. (2010). Plasticized Chitosan-PVA blend Polymer electrolyte Based Proton battery. *Electrochimica Acta*. 55, 1475-1482.

- [41] Thompsor, C., Ding, C., Qu, X., Yang, Z., Uchegbu, I., Tetley, L., & Cheng, W. (2008). The Effect of Polymer Architecture On The Hano Self-Assemblies Based On Novel Comb Shaped Amphiphilic Poly (Allylamine). *Colloid Polym Sci.* 286, 1151-1526.
- [42] Ali, S., Phd. Thesis (2009). Eastern Mediterranean University.
- [43] Nuopponen, M., Ojala, J., & Tenhu, H.(2004). Aggregation Behaviour Of Well Defined Amphiphilic Diblock Copolymers With Poly (N-Isopropylacrylamide) and Hydrophobic Blocks. *Polymer.* 45, 3643-3650.
- [44] Matsumoto, K., Terashima, T., Sugita, T., Takenaka, M., & Sawamoto, M. (2016). Amphiphilic Random Copolymers with Hydrophobic/ Hydrogen-Bonding Urea Pendants: Self-Folding Polymers in Aqueous and Organic media. *Macromolecules.* 49, 7917-7927.
- [45] Nagarajan, R. (2011). Amphiphilic Surfactants and Amphiphilic Polymers: Principles of Molecular Assembly. American Chemical Society: *Washington, DC*, 2011.
- [46] Fernandez, A., Edler, K., Arnold, T., Heenan, R., Porcar, L., Terry, A., & Jackson, A. (2016). Micelle Structure In A Deep Eutectic Solvent: A Small-Angle Scattering Study. *Phys. Chem.* 18, 14063-14073.
- [47] Assa, F., Malmiri, H., Ajamein, H., Vaghari, H., Anarjan, N., Ahmadi, O., & Berenjion, A. (2016). Chitosan Magnetic Nanoparticles for drug delivery Sys-

tems. *Reviews in Biotechnology Critical*: [Http://dx.doi.org/10.1080/07388551.2016.1185389](http://dx.doi.org/10.1080/07388551.2016.1185389).

- [48] Cheug, R., Ng, T., Wong, J., & Chen, W. (2015). Chitosan: An Update On Potential Biomedical and Pharmaceutical Applications. *Mar. Drugs*. 13, 5156-5186.
- [49] Rijcken, C., Soga, O., Hennink, W., & Nostrum, C. (2007). Triggered Destabilisation of Polymeric Micelles and Vesicles By Changing Polymers Polarity: An Attractive Tool For Drug Delivery. *Journal of Controlled Release*. 120, 131-148.
- [50] Jana, A., Devi, K., Maiti, T., & Singh, N. (2012). Perylene-3-Ylmethanol: Fluorescent Organic Nanoparticles As A Single-Component Photoresponsive Nanocarrier With Real-time Monitoring of Anticancer Drug Release. *J. Am. Chem. Soc.* 134, 7656-7659.
- [51] Icil, S., Icil. H. (1996). A Thermal and Photostable Reference Probe for Qf Measurements: Chloroform Soluble Perylene-3,4,9,10-tetracarboxylic acid-bis-*N,N'*-dodecyl diimide. *Spectroscopy letters*. 29, 1253-1257.
- [52] Bodapati, J., Phd thesis (2011). Eastern Mediterranean University.

## **APPENDIX**

## **Appendix A: Curriculum Vitae**

### **Personal Information**

Name	Nura
Surname	Ageel
Adress	Sakarya, Famagusta- TRNC Mersin 10 Turkey
Phone	Mobile: 05428725067
e-mail	<a href="mailto:nura_ageel@yahoo.com">nura_ageel@yahoo.com</a>
Date of Birth	03/08/1985
Citizenship	Libyan
Marital	Married, 3 Child

### **Education**

<b>1990-1996</b>	Aeen Zara Primary School, Tripoli/ Libya
<b>1996-2003</b>	Abn Alhaitm Secondry School, Tripoli/ Libya
<b>2003-2008</b>	Tripoli University Faculty of Science Depart ment of Chemistry (BS), Tripoli / Libya
<b>2014-2015</b>	Atilim University, Prep English School, Ankara/ Turkey
<b>2015-Present</b>	Eastern Mediterranean University Faculty of Art & Science, Department of Chemistry/ Organic Chemistry (MS).



## **Work Experience**

**2009-2014**

Tripoli University Faculty of Education, Department of Chemistry (Assistant), Tripoli/ Libya

## **Skills**

**Language**

Arabic, English